CHALMERS
UNIVERSITY OF TECHNOLOGY

Machinability of Crankshaft Steel: On the Influence of Batch-to-Batch Material Variations

Master's thesis in Production Engineering

TYRONE JULIUS MACHADO

Department of Industrial and Material Science
CHALMERS UNIVERSITY OF TECHNOLOGY
Gothenburg, Sweden 2019

Master's thesis 2019

Machinability of Crankshaft Steel: On the Influence of Batch-to-Batch Material Variations

TYRONE JULIUS MACHADO

CHALMERS
UNIVERSITY OF TECHNOLOGY

Department of Industrial and Material Science
Division of Materials and Manufacture
Chalmers University of Technology
Gothenburg, Sweden 2019

Machinability of Crankshaft Steel: On the Influence of Batch-to-Batch Material Variations

TYRONE JULIUS MACHADO

Supervisors:
Amir Malakizadi, Chalmers University of Technology
Niklas Helsing, Volvo Car Corporation
Goran Ljustina, Volvo Car Corporation

Examiner: Uta Klement, Chalmers University of Technology

Master's Thesis 2019
Department of Industrial and Material Science
Division of Materials and Manufacture
Chalmers University of Technology
SE-412 96 Gothenburg
Telephone +46 31 772 1000

Typeset in LaTeX
Printed by
Gothenburg, Sweden 2019

Acknowledgements

I would like to thank my thesis supervisor at Chalmers, Amir Malakizadi, who has tremendously supported me and a few other students during our thesis work. His constant efforts to keep us on track ensured that we performed to the best of our abilities while also building a healthy friendship with each other. He went out of his way to ensure that we, the student thesis workers, were not stressed. Over and above all, he taught me to believe in myself and that sometimes, the impossible is only impossible because we limit ourselves to the choices that we can make.

I am very grateful to Yiming Yao from Chalmers for constantly providing training and support with the characterization equipment in the materials laboratory. I would also like to thank my thesis examiner at Chalmers, Uta Klement, for being very flexible with the thesis schedule as well as for providing very useful feedback, which I can even use going forward in life.

I would like to thank Niklas Helsing and Goran Ljustina from Volvo Car Corporation for providing this amazing opportunity to perform this thesis. Their co-operation, timely responses, and continual support have ensured that the thesis work proceeded as planned.

Lastly, I would like to thank my parents Julius Machado and Ursella Machado, and my brother Romit Machado, who have constantly supported my decisions in life, especially when I decided to move to Sweden.

Tyrone Machado, Gothenburg, July 2019

Abstract

Steel produced in different batches generally have similar macro-mechanical properties due to small variations in the alloying elements – within the standard specifications – and stringent control on post-process treatments such as rolling and subsequent heat treatments. Despite the small variations in macro-mechanical properties, the variations in type, amount, and size distribution of non-metallic inclusions (NMIs) present within the steel can lead to inconsistent behaviour of material batches during machining. Thus, process planners face a big challenge in achieving a high quality of machined components at low costs due to such production disturbances.

This study examines the tool wear during the semi-finishing operation of 5 different batches of crankshafts. Initially, the influence of NMIs and microstructural differences on machinability of different steels reported in the literature was reviewed. Later, an in-depth metallographic analysis was performed on one crankshaft from each batch using optical and electron microscopy to determine the composition, distribution, morphology, size, and type of NMIs along with microstructural differences. Cutting tool inserts from each batch were analysed to determine the wear and layer formation on the cutting surfaces of the inserts.

MnS inclusions were the most prominent inclusions followed by complex oxy-sulphide inclusions in smaller numbers with varying morphologies, size, and distribution. The inserts exhibited small differences in the flank and nose wear. However, the topography of the worn surfaces on the rake face was different in some cases. This perhaps indicates the beneficial protective and lubricative effects of layers formed on the tool surfaces due to the presence of soft and chemico-physically stable inclusions.

Keywords: Machinability, Flank wear, Nose wear, Scanning electron microscopy, Non-Metallic Inclusions (NMIs), Crankshaft.

Abbreviation List

Al_2O_3	Alumina or Corundum
BSE	Backscattered Electrons
CAS	Calcia-Alumina-Silicate
EDS	Energy Dispersive X-ray Spectroscopy
FeS	Iron Sulphide
IC	Internal Combustion
ISO	International Standards Organization
HV	Hardness Vickers
LOM	Light Optical Microscopy
MnS	Manganese Sulphide
NMI	Non-Metallic Inclusion
PCBN	Polycrystalline Cubic Boron Nitride
REM	Rare Earth Metals
SE	Secondary Electrons
SEM	Scanning Electron Microscopy
TiC	Titanium Carbide
VB_{BMax}	Flank Wear
VB_C	Nose Wear
VCC	Volvo Car Corporation

Contents

List of Figures

List of Tables

1 Introduction

Machinability can be defined as the ease of material removal during machining to attain a particular fit, form, and/or function. In metals, there are 6 ISO standard material groups with different material properties, thus having different machinability (Sandvik, 2017). Machinability can be quantified using various parameters such as tool life, tool wear, material removal rate during the metal cutting process. The metal cutting process is governed by various cutting parameters, the most important ones being cutting speed, depth of cut, and feed. For specific metals belonging to particular ISO standard material group, the machinability should be identical in terms of tool life and tool wear for constant cutting parameters. Therefore, data regarding tool life and tool wear is readily available from tool suppliers for specific cutting conditions for specific ISO material groups.
Crankshafts are an integral component of every automobile with an Internal Combustion (IC) engine. The crankshafts are usually manufactured from steel (ISO P) which is forged and subsequently machined using different metal cutting operations. Crankshafts are components with high volume batch production and hence production planners use the data from tool suppliers to plan and schedule machining activities on the production line such as batch sizes, machine maintenance, tool changeovers, etc. Thus, the material arrives in different batches as per the production plans. However, when a material batch is changed, it has been observed that while the physical and chemical properties of the different batches of materials remain practically unchanged, there can be a drastic change in the machinability of the material, leading to deviation of the tool wear behaviour from general specifications. This leads to unplanned downtime with increased machining times, thereby increasing the overall costs of production. Such batch-to-batch material variations affecting the machinability of crankshafts at the Engine Plant of Volvo Car Corporations in Skövde have been the focus of this study.

1.1 Goals

The aim of this thesis is to investigate the influence of inclusions within the materials which cause the batch-to-batch variations, thereby influencing the tool performance while machining crankshaft steel. Since the material batches conform to the prevalent manufacturing standards with consistent macro-mechanical properties for different batches, the basic process monitoring methods would not always provide timely indications for tool change, which poses a big challenge for process planners to maintain the high quality of machined parts. Thus, the main focus of the the-

sis would thus be to identify the differences in the type, distribution, and size of the inclusions by material characterization. The results of this investigation will be used to correlate the cutting parameters such as tool wear to the material properties for the semi-finishing turning operation performed on crankshaft steel using coated cutting tools.
To conduct this investigation efficiently, two major questions need to be answered:

1. What does the literature say about the relation of inclusions and machinability of different steels? Which properties of inclusions are worth investigating?

2. Can the method developed in this thesis be used to correlate the tool wear to the inclusion type, size, distribution within the different batches?

1.2 Limitations

The investigations were conducted on the crankshaft and tools from one machining process only i.e. Operation 30 or semi-finishing operation using the V shaped insert with tool grade 4315 (Sandvik Coromant). The total number of material batches investigated were limited to 5 batches i.e. 2 to 4 inserts per batch and 1 crankshaft per batch. In total, 14 inserts and 5 crankshafts from 5 different batches were provided by Volvo Car Corporation (VCC). The crankshaft material and insert samples were obtained from a regular production process, without any special setup for dedicated tool life tests. However, it should be noted that one crankshaft sample was delivered in the fully finished condition along with surface hardening. The level of investigation was decided at Chalmers University of Technology based on the available time and resources such as Light Optical Microscopy (LOM) and Scanning Electron Microscopy (SEM) along with EDS. If a batch performed inconsistently in terms of tool life after the first 5 batches had been delivered, the tools and crankshaft could have been sent for characterisation at Chalmers University of Technology. This additional possibility did not occur during the time period of investigation. Thus, the investigations were limited to 5 material batches. Due to the confidential nature of this thesis work, certain specific details about the material specifications, chemical certificates, and supplier information cannot be disclosed without the approval of Volvo Car Corporation.

2

Background

This section contains background information that will be useful in understanding concepts such as machinability, material composition, etc.

2.1 Steelmaking practices

Some knowledge about the different steel making practices is required to understand the origin and possible sources of different inclusions. The steel making practices are only described briefly to get an overview of the different steel making processes. The different alloying elements in steel have different effects on the final properties of steel (Bryson, 2015) (Mandal, 2015). Table 2.1. shows the effect of the different alloying elements of steel.

Table 2.1: Alloying elements affecting steel characteristics. Modified from (Bryson, 2005)

Alloying Elements	**Effects**
Aluminium (Al)	Used as a deoxidizer in steelmaking. Restricts grain growth and promotes a finer grain structure in steels.
Boron (B)	Increases hardenability in low-carbon steels.
Calcium (Ca)	Improves machinability and does not dissolve in the steel melt. It may form stringers, voids, and inclusions which enhance machinability but reduce the overall strength of the steel.
Carbon (C)	Addition of C to Iron leads to the formation of steel. Higher C content is linked to higher hardness and wear resistance of steel.
Chromium (Cr)	Can form chromium carbides when iron and carbon are present. Increases wear resistance, toughness, and corrosion resistance.
Cobalt (Co)	Forms cobalt carbide and improves heat resistance properties of steel.
Lead (Pb)	Improves machinability but may form voids on the surface of steel during heat treatment. Environmental issues limit the use of Lead.

Manganese (Mn)	Increases hardenability and improves steel transformation phases. It may form stringers, voids, and inclusions which enhance machinability but reduce the overall strength.
Molybdenum (Mo)	Forms molybdenum carbide when the right amount of carbon is present. Improves corrosion and wear resistance and adds hardenability and heat resistance.
Nickel (Ni)	Adds strength, toughness, and wear resistance while decreasing hardenability.
Niobium (Nb)	Restricts/reduces grain growth and promotes a fine grain structure while decreasing hardenability. Improves creep resistance at higher operating temperatures.
Phosphorous (P)	Does not dissolve in the steel melt but improves machinability. It may form stringers, voids, and inclusions which enhance machinability but reduce the overall strength.
Silicon (Si)	Used as a deoxidizer in steel making. Improves the strength and toughness but decreases machinability and surface roughness of the steel when present in higher concentrations.
Sulphur (S)	It does not dissolve in the steel melt but improves machinability. It may form stringers, voids, and inclusions which enhance machinability but reduce the overall strength.
Titanium (Ti)	Forms titanium carbide (TiC) but may not improve hardenability. Reduces grain growth and can be used as a deoxidizer.
Tungsten (W)	Adds wear resistance.
Vanadium (V)	Forms vanadium carbide. Leads to a finer grain structure in steel and restricts grain growth. Improves hardenability of steel.
Zirconium (Zr)	Used as a deoxidizer. Inhibits grain growth.

Steel making involves melting, treatment or purification, and alloying of the metal to obtain the desired properties of the steel. These particular processes can either take place simultaneously, interfering with other processes, or in a sequence, depending on the manufacturer of the steel (Wente et al., 2017). The processes involved in steel making from raw material to finished steel are: Primary Steelmaking, Secondary Steelmaking, Continuous Casting, and Finishing Operations (NPTEL, 2011). The knowledge of these processes may enable better understanding discussions related to non-metallic inclusions and have been described in detail by Wente et al (2017) as well as in the notes available on NPTEL (2011). Usually, the Secondary Steelmaking process is used to control the alloying elements and to reduce the impurities within the steels (Mandal, 2015). Of particular interest are the slag modification, oxidation reactions and removal of elements such as sulphur, carbon, and oxygen, resulting in cleaner steels with improved performance. For example, rimmed steel, killed steel, and semi-killed steel along with the solidification processes such as vacuum arc remelting (VAR) and electroslag remelting (ESR) are of interest to understand the formation of non-metallic inclusion formations in steel, from a wider perspective.

2.2 Non-Metallic Inclusions (NMIs) and Carbides

NMIs are non-metallic phases within the steel matrix which influence the behaviour of steel due to their type, size, and distribution in the steel matrix (Silva, 2018). The Non-Metallic Inclusions (NMIs) and their influence on the properties of steel have been studied extensively by Kiessling and Lange (1964). The knowledge of various processes within steel making can provide a good understanding about the properties and origins of NMIs during various manufacturing operations such as machining, forming, welding, etc (Silva, 2018) (Ånmark, Karasev and Jönsson, 2015) (Kiessling and Lange, 1964). Carbides are chemical compounds formed by the combination of metallic or semi-metallic elements with carbon (Zumdahl, 2009), usually when the carbon content exceeds 0.025 % (Mandal, 2015). Sometimes, the carbides are intentionally produced in the steel to increase the wear resistance of the steel (Mandal, 2015). However, carbides can also exist in the form of inclusions within the steel matrix. Elements such as iron, chromium, titanium, vanadium can form different carbides, with iron carbides being considered as important constituents within the steel.

2.3 Microstructure

Steels have a variety of microstructures due to different solid-state transformations and processing operations which enables steels to exhibit a variety of properties (Bhadeshia and Honeycombe, 2017). For example, forging operations can reduce grain sizes while the heat treatment will determine the final microstructure of the material (Hagberg and Malm, 2010). Additionally, different steel specimens with the same chemical properties can have different microstructures and thereby different mechanical properties (Dovebro, 2012). Thus, it becomes useful to understand the behaviour of iron, iron-carbon alloys, and the various alloying elements. The effect of the different alloying elements in steel have already been described in Table 1. The most common crankshaft material in cars is forged medium-carbon or micro-alloyed steel due to their superior mechanical properties (Alessandro and Millefanti, 2017). Generally, such steels with ferritic-pearlitic microstructure give a good combination of toughness and strength, fulfilling the design requirements of the high performance IC engines. Additional surface treatments e.g. induction hardening would be necessary to improve the wear resistance and fatigue properties (Scurria et al., 2017).

2.4 Machining processes and machinability

The final shape in almost all metallic components is achieved by the means of a machining process (Hagberg and Malm, 2010). Thus, the forged or rolled steels are further expected to meet acceptable surface finish requirements and dimensional tolerances as per the design and assembly specifications. These specifications are achieved by means of various machining processes such as turning, milling, drilling, grinding, and polishing. Hence machining is considered as a very important process within manufacturing, which influences the overall functionality, quality, and cost of the manufactured products (Malazikadi et al., 2019).

Machinability depends on these main factors: Workpiece material, tool material, cutting parameters, and tool geometry (Klocke, 2011). Machinability can also be classified using three factors i.e. tool life, chip breakability, and geometrical accuracy (Hashimura et al., 2009). Within geometrical accuracy, surface roughness of a finished component is considered as the most significant property as it influences the joints and sliding contacts with other components in order to ensure proper functionality (Hashimura et al., 2008), especially in a component such as a crankshaft.

Depending on the workpiece material, a particular tool grade and tool geometry is chosen for the turning operation. The most important cutting parameters in turning operation are the cutting speed, feed, and depth of cut (Sandvik, 2017) (Klocke, 2011) which are influenced by the workpiece material and the cutting tools. The productivity of turning operations depend on the cutting parameters and can be measured using different parameters such as material removal rate, specific material removal rate, tool life, and tool wear (Klocke, 2011) (Sandvik, 2017). The tool life is the time taken by the tool from the first cut until it becomes unusable under specific tool life criterion such as a width of flank wear or unacceptable surface finish on the final component during machining conditions (Klocke, 2011). The tool life is related to the tool wear and is the most significant parameter used to characterize the machinability of the material (Klocke, 2011). The different wear on the flank and rake surfaces of the tool as shown in Figure 2.1, are used as an indicator to characterize the tool life until a specific tool life criterion has been reached (Klocke, 2011). Sometimes the surface finish of machined component is also used as a tool life criterion wherein the geometrical tolerances and surface finish requirements govern the acceptable or allowable tool life limits (ASM Handbook, 1990).

The tool life is given by the Taylor equation $VT^n = C$, where V is the cutting speed, T is the tool life, and n and C are constants which depend on the cutting parameters, workpiece materials and tool wear criterion (Sinha, 2011). Figure 2.2 shows the effect of cutting speed on the flank wear for a tool life criterion of 0.5 mm flank wear. According to the ISO standard (ISO 3685), an average flank wear width between 0.3 mm to maximum of 0.6 mm is recommended as tool life criterion during machining tests.

The workpiece material and its complexity governs the type and number of machining operations required to complete a given part ("Machining Success," n.d.). For example, given that the same crankshaft is produced in the entire batch, the workpiece material, tool material, tool geometry, and cutting parameters remain unchanged throughout the machining operations. Thus, theoretically, the cutting forces and the tool wear/tool life should remain constant. However, it has been commonly noticed that the tool life reduces drastically for a specific batch of crankshaft material. This reduction in tool life occurs in all the machines which are performing different processes such as turning and milling. The reduction in tool life leads to an addition of extra tools which increases the indexing and tool change times, thus longer overall production time and higher costs ("Machining Success," n.d.).

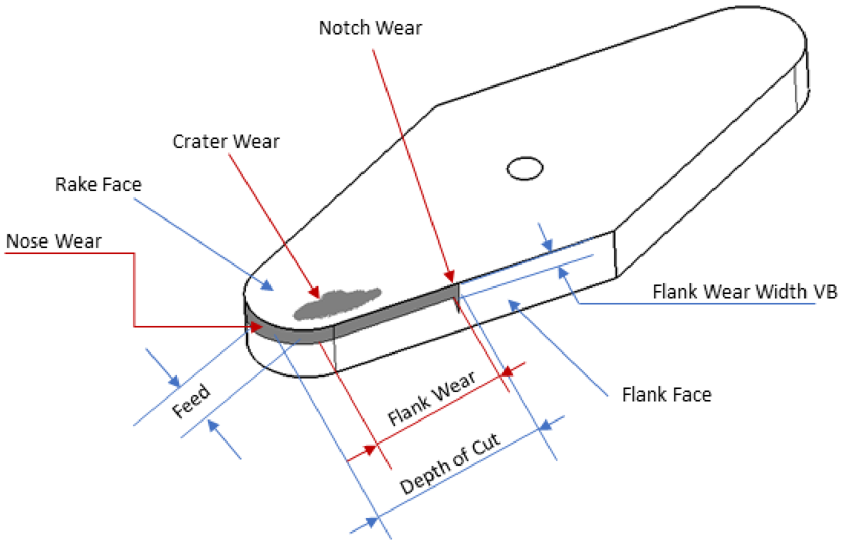

Figure 2.1: Worn cutting tools with simplified wear locations. Adapted from (Sinha, 2011)

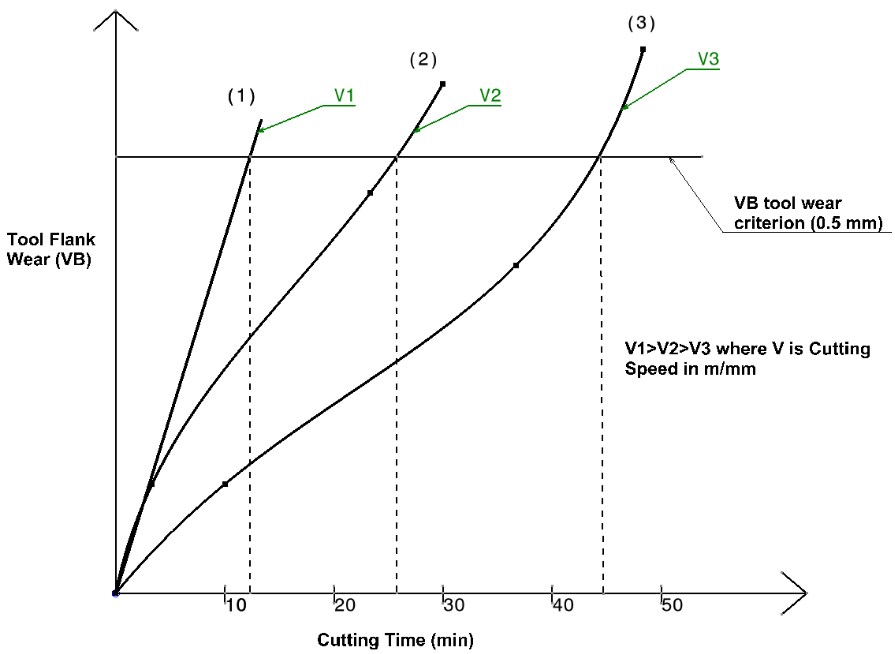

Figure 2.2: Effect of cutting speed for tool life criterion of 0.5mm flank wear. Adapted from (Sinha, 2011)

2.5 Batch variations

The standards for the chemical composition of steel such as the USN and EN standards, allow a wide range of alloying elements which enables different steel manufacturers to produce steel conforming to these standards ("CHEMICAL COMPOSITION," n.d.). Thus, different batches of steel with the same chemical properties but containing some variations in alloying elements can still be certified as a specific grade of steel. Such grades of steel are then used for different purposes which may include operations such as forging, machining, welding, etc. The variations in such alloying elements do not necessarily affect the macro-mechanical properties but will behave inconsistently from batch-to-batch during machining or welding ("CHEMICAL COMPOSITION," n.d.). Various machine operators have also reported unusual vibrations and noises from the machines while machining different batches of the same materials (Jamshidi et al., 2014) in addition to increased or faster tool wear and reduced chip breakability (Surreddi et al., 2013). Such batch-to-batch inconsistency makes it difficult for process planners to standardize the machining process leading to a non-robust process and unplanned downtime due to additional setup time from readjusting of the machine, thereby leading to an overall loss of productivity (Surreddi et al., 2013).

2.6 Crankshaft

The crankshaft is an integral component in the transmission system of an internal combustion automobile. An image of a machined and finished crankshaft is shown in Figure 2.3.

Figure 2.3: A fully machined crankshaft. (Copyright © Volvo Car Corporation)

The crankshaft converts the linear motion of a piston into rotational motion(torque), which in turn is used to power the wheels by a series of different mechanical connections. The bearing surfaces on the crankshaft act as an interface for components such as the piston rod and the crankshaft. These bearing surfaces ensure that the linear motion of the pistons are efficiently converted into the rotational motion of the crankshaft. Moreover, certain cylindrical surfaces on the crankshaft may have an eccentric centre of rotation which makes it a complex component for machining. It can also be observed from Figure 2.3 that the front part of the crankshaft has splines. Thus, the finished crankshaft components have very tight requirements on the surface roughness and tolerances, which are achieved through a series of machining processes.

3

Methodology

The methodology followed in this thesis is mentioned in Figure 3.1 below. Since one of the main goals of the thesis was to find out the most relevant and interesting properties of NMIs, the thesis began with a literature study to give an overview of the NMIs present in steels. As mentioned earlier, the experimental study was limited to 5 batches of crankshafts. Thus, one crankshaft and between 2 to 4 inserts from each batch were delivered by VCC for experimental studies. Further, the inserts were examined at low magnification using Scanning Electron Microscopy (SEM) to get an overview on the rake and flank face of the inserts. A few minor differences were observed among the inserts, in terms of the topography on the rake face and the wear on the flank face of the inserts. Based on these observations, the material from each batch was examined to determine the inclusion composition, distribution, size, type, and morphology, as well as the microstructure and hardness of the steel at different depths from the cutting surface. A few differences were observed in the properties of the NMIs between different batches. Subsequently, high magnification imaging and analysis of the inserts was performed using SEM to identify and understand the wear patterns and layer formation on the inserts from different batches.

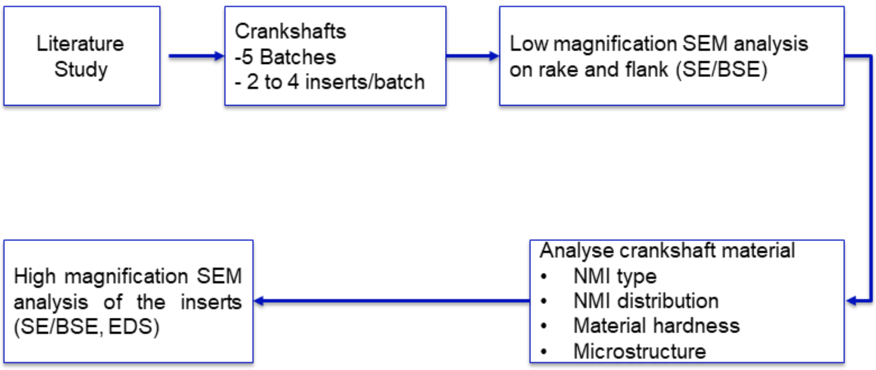

Figure 3.1: Methodology used in the thesis

4
Literature Study

4.1 Inclusion systems

The concept of "Clean Steels" which are free of inclusions or having very less amount of inclusions are assumed to be the most ideal steels (Nordberg and Sandström, 1981). However, the concept of cleanness as the preferred quality in steel depends on the functionality or the operations performed on the steel according to Nordberg and Sandström (1981). For example, a clean steel which is considered good for metal forming operations may not be considered as a good steel for machining operations. While many of the high cleanliness steels have good macro-mechanical properties and corrosion resistance, they exhibit lower machinability in terms of difficult chip breaking and reduced tool life, and are also associated with higher machining costs, higher energy consumptions and increased tool wear (Ånmark, Karasev and Jönsson, 2015). Thus, certain inclusions are necessary within the steel to ensure good machinability properties while maintaining high performance macro-mechanical properties of steel (Ånmark, Karasev and Jönsson, 2015). The modification of inclusion properties within steels to obtain desirable properties of steel for different purposes is known as "Inclusion Engineering" (Hoier et al., 2019). For example, microalloying stainless steel with Tellurium or Zirconium significantly modifies MnS inclusions for improved machinability while maintaining mechanical properties of the material as per the standards (Mahmutović et al. 2017).

The various inclusion systems were studied by Kiessling and Lange and published from 1964 to 1978 in the 4-part series of books called Non-metallic inclusions in steel (Kiessling and Lange, 1978). These studies give a good overview of the different types on inclusions with steel. The studies focused primarily on the following inclusion systems: MnO-SiO_2-Al_2O_3, $Fe_xMn_{1\text{-}x}O$-SiO_2-Al_2O_3, MgO-SiO_2-Al_2O_3, CaO-SiO_2-Al_2O_3, oxide inclusions with Rare Earth Metals (REM) and transition metals, sulphide inclusions, and iron oxides. The type of steel, method of steelmaking, casting and deoxidation all have an effect on the type, size, number, and distribution of the inclusions in steel (Kiessling and Lange, 1964). Experimental methods were used for the microscopic study of the samples to derive these inclusion systems.

Inclusions can enter from indigenous or exogenous sources (Kiessling and Lange, 1964) (Silva, 2018). The correct identification and comparison of the inclusion composition to the chemical composition of the steel can give a good estimate about the origin of the inclusions. This is necessary for inclusion control. For example, Al_2O_3 or corundum as an inclusion should be avoided as they are usually hard

inclusions which lead to abrasion between the material and the tool edges (Nordberg and Sandström, 1981). Since aluminium is used for deoxidation of steel, such aluminium acts as a source of corundum (Kiessling and Lange, 1964). Thus, if corundum was identified in the steels- with low concentration of aluminium in the liquid steel and in the absence of aluminium deoxidation- it would be beneficial to investigate the source of corundum such as the slag or refractory materials. In case of MgO, magnesium compounds are a part of the refractories and hence act as a major source of MgO (Kiessling and Lange, 1966). In modern steels, it is also possible that Mg is added as a deoxidant or to modify certain inclusions (Verma et al., 2012) (Jung et al., 2004). The temperature transformations make it difficult to identify the exact phases of (MgO.SiO) and hence a direct phase analysis is required for such identification (Kiessling and Lange, 1966). The phase analysis and precise chemical composition of the inclusions are often necessary for understanding the inclusion formation mechanisms (Thunman, 2009). Pure (Al,Mg)O inclusions- which are believed to be extremely hard, have also been found in carburized steel which increase the tool wear during machining due to abrasion (Ånmark, Karasev and Jönsson, 2016). Calcium is not soluble in iron and hence in most cases the calcium inclusions are considered as exogenous especially if MgO is detected in the inclusion (Kiessling and Lange, 1966). Note that in modern steels, Ca may be added to modify the properties of Al_2O_3 oxides, this process is called Calcium Treatment of steels (Ånmark and Björk, 2016) (Ruppi et al., 1998) (Nordberg and Sandström, 1981). Oxides such as CaO and MgO are relatively softer and globular in shape compared to pure Al_2O_3 inclusions which are hard, brittle, and irregularly shaped thereby adversely affecting machinability (Mandal, 2015). Anorthite and gehlenite which are Calcia-Alumina-Silicate (CAS) inclusions are of metallurgical interest especially during the calcium treatment of steels and can enter the steel as reaction products from slags and refractories(Kiessling and Lange, 1966) (Nordberg and Sandström, 1981). Titanium and zirconium are of interest as deoxidizers because titanium and zirconium are present in refractories and slag which can form oxide inclusions. Modifications of inclusions using zirconium and tellurium in stainless steel have shown to improve the machinability by about 25% in comparison to unmodified stainless steel (Mahmutović et al. 2017).
Sulphur has low solubility in the solid steel phase but is soluble in liquid steel and therefore forms sulphide inclusions in the steel. However, the presence of sulphur in steel also leads to hot-shortness (Silva, 2018) (Kiessling and Lange, 1966). Hot shortness is the phenomenon in which sulphur forms FeS, which is a low melting point constituent along the grain boundaries. When the steel is being worked at higher temperatures, the FeS melts and may cause transgranular fracture due to decohesion of grain boundaries (Silva, 2018) (Mandal, 2015). This can be avoided by the formation of MnS inclusions which have a higher melting point that FeS (Mandal, 2015) The sulphides such as MnS increase the machinability of steel because they precipitate out during the solidification of liquid steel (Ånmark, Karasev and Jönsson, 2015) thus forming voids and/or lubricating layers between the materials and the cutting tools. It has been observed that elements with low solubility in iron and REMs, form sulphides at the molten steel temperatures (Silva, 2018). According to Kiessling and Lange (1966), those regions in the steel ingots which are

rich in sulphur tend to form oxide inclusions containing an outer rim of sulphide. Furthermore, the sulphide inclusions in rimmed steels are often observed at the centre of the steel ingots whereas in killed steels, the sulphide inclusions are generally concentrated in the outer regions near the surface of the ingot. This is because of the inherent differences in rimming and killing methods applied during steelmaking process (Kiessling and Lange, 1966). While Metal-sulphur systems can have great number of intermediate phases with varying homogeneity, a knowledge of sulphide inclusions would be necessary to assess the deformation mechanisms of sulphides under e.g. shear loading. The formability of inclusions would potentially influence the tool wear and chip breakability when machining, and thus the machinability of steel (Kiessling and Lange, 1966).

Kiessling and Lange (1966) observed that FeS exists in the grain boundaries of oxide scales on steels. If such steel is not completely freed from oxide scales, the oxide scales may get worked into the steel during forging or rolling which would lead to exogenous inclusions in the steel containing iron oxides, FeS and Fayalite-Fe_2SiO_4 (Kiessling and Lange, 1966). The MnS sulphide phases may be described as type-I, type-II, and type-III sulphides respectively, all of which differ in their shape and size. Type-I sulphides are usually globular, duplex with oxygen compounds (i.e. oxide inclusions), and are common in rimmed or semi-killed steel where silicon has been used as a deoxidant (Kiessling and Lange, 1966). Type-II sulphides are dendritic and spread in the form of chains or as thin precipitates within the grain boundaries and are more likely to be found in aluminium deoxidized killed steels. Since aluminium is used as deoxidizer, corundum is also formed which acts as a nucleus for the sulphide phase but is always found as a separate phase (Kiessling and Lange, 1966). Type-III sulphides are similar to type-I sulphides except that they are monophase inclusions which are irregular, randomly distributed, and found in deoxidized steels with excess of aluminum as deoxidant (Kiessling and Lange, 1966). Additions of aluminium can promote the formation of type-I and type-III sulphides and are also known to affect the MnS morphology, changing type-II sulphides to either type-I or type-III sulphides (Brandaleze et al., 2013).

REM additions to steels change the morphology of the sulphide inclusions from elongated strings to globular and shorter sulphide inclusions in worked steels (Ånmark, Karasev and Jönsson, 2015) (Kiessling and Lange, 1966). The addition of such REM to steel have been reported to increase the machinability of steel. MnS inclusions are good for machinability as they act as inner lubrication during machining due to their plasticity (Ånmark, Karasev and Jönsson, 2015). However, different amounts and types of metal (M:Ti,V,Cr,Fe,Co,Ni) in solid solutions can influence the plastic properties of (M,Mn)S, which makes it complex to understand the exact influence of sulphide inclusions on the machinability of steel (Kiessling and Lange, 1966). Among REM, Lanthanides(La, Ce, Lu, and Y) are of special interest in steelmaking due to their high affinity for oxygen and sulphur. For example, the addition of lanthanum to steels causes the α-MnS sulphides to change from type-II and type-III inclusions to type-I inclusions. This type of sulphide is globular and smaller in size, thus improving the machinability of steel (Kiessling and Lange, 1966). MgS and CaS have a wide range of mutual solid solubility with MnS and sulphides containing different amounts of Ca, Mg, and Mn found in steels. These mixed sulphides

generally have lower formability that MnS (Kiessling and Lange, 1966), thus might have different influence on the machinability of steels.
Inclusions which are large are considered harmful for machinability, however the size of the inclusion at which it becomes harmful is not exactly known (Nordberg and Sandström, 1981). For example, the shape, composition, and distribution of sulphide inclusions are very important in free machining steels with a major difference being observed in the behaviour of such steels for different oxide and sulphide inclusions (Kiessling and Lange, 1966). Machinability changes depending on the inclusion shape especially with MnS inclusions (Mahmutović et al. 2017). In addition to shape, size, and distribution of inclusions (Xia et al., 2015), the chemical and mechanical properties of the inclusions can exhibit detrimental properties on the materials too (Mahmutović et al. 2017).

4.2 Inclusion aspects of batch variations

Much of the literature on the influence of inclusions on machinability is focussed towards the machinability of free-machining or free-cutting steels. Free machining steels have additions of elements such as sulphur, phosphorous, lead, calcium, etc. which improve the cutting characteristics of the steel (Xia et al., 2015). The presence of sulphur in free machining steels thus leads to the formation of MnS inclusions which are known to improve the machinability by forming lubricating layers and protective slag deposits on the cutting tool edges, thereby reducing the flank wear and crater wear rate (Ånmark, Karasev and Jönsson, 2016) (Xia et al., 2015). Various types of sulphur inclusions such as (Mn,Ca)S and oxy-sulphide inclusions such as (Al,Mg)O-(Mn,Ca)S - not to be confused with pure (Al,Mg)O inclusions, can protect the cutting tool at the cutting edge-chip interface by forming protective layers (Ånmark, Karasev and Jönsson, 2016) (Helle, 1995). Ideally, such protective layers formed by non-metallic inclusions should completely prevent crater wear on the rake face and reduce the flank wear (Helle, 1995).
The distribution and shape of MnS inclusions affect the surface roughness of machined surfaces (Hashimura et al., 2009). The deformability of sulphide inclusions depends on the composition of the inclusions and thus directly affects the behaviour of such inclusions during machining. With higher deformability of MnS inclusions, the cutting forces required are lower (Jiang et al., 1996). Such deformability of sulphide inclusions also leads to the formation of microcracks and microvoids in the steel matrix, which is believed to reduce the flank wear on the cutting tools (Jiang et al., 1996). While deformable inclusions are certainly good for machinability, certain inclusions with relatively low formability such as Ca-inclusions would also form protective layers on the cutting tool surface, thus protecting the cutting edge when machining (Helle, 1995). It is not exactly clear why only certain inclusions form protective layers though. Additionally, a few machinability studies performed on Boron Nitride (BN) free cutting steels (Chen et al., 2016) (Chen et al., 2014) (Tanaka et al., 2007) demonstrated the beneficial properties of BN inclusions in steel. The BN and MnS inclusions tend to envelop the harder inclusions such as Al_2O_3 and TiN, thereby reducing the abrasive wear on the cutting tools during metal cutting (Wang

et al., 2014).
The tool life and tool wear during machining depends on the volume fraction and the aspect (length to width) ratio of non-metallic inclusions (Ånmark, Karasev and Jönsson, 2016). Liu and Chen (2012) showed that an increase in the oxygen content upto 0.0105 wt % of SAE 1215 steel reduces the aspect ratio of MnS inclusions without affecting the volume fraction, thereby improving the machinability. Helle (1995) also found that NMIs (e.g. oxides) with the right composition and in small quantities would be needed for the formation of protective layers on the tool surfaces. The chip breakability of different steel grades has also been correlated to the chemical composition of the steel and thereby to the content of non-metallic inclusions in the steel (Ånmark, Lövquist et al., 2015). The proportion of Rare Earth Metals to the sulphur compositions has an effect on the deformability of sulphide inclusions with increasing REM:S ratio leading to reduced flank wear (Jiang et al., 1996).
In a study on the machinability of low carbon free cutting steels, Hashimura et al. (2009) found that with coarse MnS inclusions and non-homogeneous distribution of such inclusions, the chips broke away at a location away from the tool-chip interface leading to the formation of a built-up edge, a similar result also being reported by Helle (1995). It was also found that the smaller and homogeneously distributed MnS inclusions led to a very small built-up edge on the tool which enabled a better surface roughness on the machined surface compared to the steel having coarser and non-homogeneously distributed inclusions (Hashimura et al., 2009). Zhang et al. (2009) found that bigger sulphide inclusions led to a bigger built-up edge at relatively low cutting speeds leading to higher surface roughness in free cutting steels while spindle shaped inclusions led to lesser tool wear. However, while studying the effect of MnS inclusion size on low-carbon, leaded, re-sulfurized free-machining steel, it was found that an increase in the size of sulphide inclusions led to a decrease in the built-up edge size in addition to a decrease in the heat generation at a given cutting speed (Yaguchi, 1986). In a study on free-machining steels, Jiang et al. (1996) showed that increasing the area fraction (dependent on the spacing between sulphide inclusions) and shape factor of sulphide inclusions led to a decrease in the cutting forces. The flank wear of the cutting tools was also reduced by increasing the area fraction of the sulphide inclusions but with a decreased shape factor (Jiang et al., 1996). Thus, even though it is known that the presence of MnS improves the machinability of steels, there is still no consensus on the mechanism with which the sulphide inclusions improve the machinability (Yaguchi, 1986) (ASM Handbook, 1990).
An increase in oxygen content, especially above 0.0125 wt % drastically deteriorates the machinability of steel due to the formation of harder and larger oxide inclusions which may also be wrapped around by the MnS inclusions (Liu and Chen, 2012). Some of the oxide inclusions reported with increasing oxygen content are as follows: MnO-Al_2O_3, MnO-SiO and 2MnO-SiO. These oxide inclusions lead to faster tool wear and thus the improved machinability is obtained only when the increase in total oxygen content is less than 0.0105 wt % of the steel.
Xia et al. (2015) has shown that the machinability of low carbon resulfurized free cutting steel improves when Mn:S ratio increases, with the best machinability obtained at a Mn:S ratio of 3.33:1. This ratio of Mn:S also reduced the main cutting

force in the steel along with improving the surface roughness for values below 3.33:1 (Xia et al., 2015). Another study also found that increasing the sulphur content in steel from 0.02-0.04% to 0.3% led to the formation of MnS inclusions rather than hard silicate inclusions (Helle, 1995). The MnS inclusions tend to form protective layers whereas the silicate and alumina inclusions promote crater wear on the tool rake surface (Helle, 1995). The iron in solid solution is also known to influence the type of sulphide inclusions as follows: MnS type I is formed with 21% Fe, type II with 93% Fe, and type III with 84% Fe (Brandaleze et al., 2013). In a separate investigation on the effect of non-metallic inclusions on hard part turning of carburizing steels using PCBN cutting tools, it was reported that the calcium-treated carburized steels exhibited better machinability than clean carburized steels (Ånmark, Björk et al., 2015). The findings of this investigation were that the composition of inclusions and the number and size of inclusions are equally important for an improved machinability. Larger inclusions tend to be detrimental for machinability (Nordberg and Sandström, 1981) (Helle, 1995), while smaller inclusions seem to be more favourable to form protective layers on the tools thereby reducing tool wear and improving machinability (Helle, 1995). However, as mentioned before, the composition of these inclusions do play an important role for the formation of the stable protective layer on the cutting edge.

The presence of transferred materials from the steel, especially Fe, on the cutting tools is an indication of the absence of NMIs associated with sulphur, which minimizes material transfer tendency (Ånmark, Lövquist et al., 2015). Additionally, during the hard turning of steels it was found that a lower content of non-metallic inclusions in clean and ultra clean steel led to a transfer of iron (Fe) onto the tools from the workpiece materials (Ånmark and Björk, 2016), believed to be a sign of chemical degradation of the tools while machining. This material transfer contributes to diffusion induced wear on the tool rake surface. Ånmark and Björk (2016) also found that the presence of calcium enriched non-metallic inclusions formed a lubricating layer on the tool-workpiece interface, thereby reducing the abrasive wear on the cutting edges of the PCBN tool during hard turning. During the turning operation test of different carburizing steels, it was found that the calcium-rich inclusion depositions on the PCBN tool surface reduced the chemical induced wear on the PCBN tool from the passing steel (Ånmark, Björk et al., 2015).

Helle (1995) found that the coatings on the tool played an important part in how non-metallic inclusions affected the tool wear in the machining of steel. For example, carbide tools with 20 % TiC showed better layer formation than carbide tools containing only 8 % TiC. Additionally, some oxide inclusions had a tendency to react with the Al_2O_3 coatings while the CaS inclusions showed a tendency to interact with the TiC coatings thereby changing the wear characteristics of the cutting tools (Helle, 1995). Certain tool coatings also reduced the chip-tool contact surfaces thereby reducing the heat generated on the tool surface wherein a relation was also found between the cutting temperature and the optimum inclusion melting point which enabled a longer tool life (Helle, 1995). However, small differences in the compositions of inclusions led to layer formation in one case but an absence in the layer formation in another case (Helle, 1995). Helle (1995) also found that layer formation on the tools would not be possible if oxidation happened in phases which were not stable with respect to the FeO or high concentration solute elements in the steel. The absence of such protective/lubricating layers may also lead to the Fe-rich compounds penetrating the tool surface, thereby leading to premature tool chipping (Ånmark and Björk, 2016).

4.3 Microstructure aspects of batch variations

Despite having the same chemical compositions of steel as per standards, varying phase constituents and phase distributions can be utilised to obtain different microstructures (Surreddi et al., 2013). For example, Doverbro (2012) examined crankshafts from two different suppliers which, ideally should have had a ferritic-pearlitic microstructure. Small variations in the quantity and distribution of inclusions within the two samples were found despite having a similar chemical composition. However, the microstructure of the crankshafts from different suppliers were quite similar except for minor differences in the impurity distribution (Dovebro, 2012).

In an investigation of different steel grades, Ånmark, Karasev and Jönsson (2016) found that the carbon equivalent of the steel can be used to determine the grain size and the number of grains, which in turn affect the surface area of grain boundaries. The higher strength and ductility imparted by finer grains - which have higher boundary areas, may be considered bad for machinability, due to difficulties in chip breakability (Mandal, 2015). The hardenability of a steel grade improved with a higher equivalent carbon content, thereby reducing the machinability of such steel grades due to higher hardness values (Ånmark, Karasev and Jönsson, 2016). Steels with lower average grain size values exhibited relatively poor machinability attributed to grain boundary strengthening, thereby requiring higher critical stresses to cause grain fracture during machining (Ånmark, Karasev and Jönsson, 2016).

During the machining of superalloy Inconel 718, it was found that smaller grains resulted in increased hardness and also increased surface stresses in the material which causes surface defects in the machined components (Jamshidi et al., 2014). Another study by (Ånmark, Lövquist et al., 2015) found that the microhardness of steels influences the machinability especially in carburized steel where a decrease in the microhardness increases the soft part machinability. Such decrease in microhardness is attributed to the lower fraction of pearlitic phase in the ferritic-pearlitic microstructure (Ånmark, Lövquist et al., 2015). Pearlite which is harder than ferrite increases the tool wear especially when the pearlite spacing is low (ASM Handbook, 1990). Surreddi et al. (2013) reports that machinability improves when the microstructure contains equal proportions of ferrite and pearlite as opposed to steel exhibiting either larger amounts of ferritic or pearlitic microstructure. A larger pearlite nodular structure in case hardened steels increases the chip breakability but also increases the tool wear (Surreddi et al., 2013).

5 Experimental Methods

This section provides an overview of the methods used during the thesis to perform the experimental work such as characterization of the crankshaft material and cutting inserts, along with the analyses performed to generate the results.

5.1 Machining

The crankshafts used in this study are delivered to VCC by the same supplier. The crankshafts are forged from continuous cast steel. The material composition of these crankshafts corresponds to medium-carbon steel exhibiting a pearlitic-ferritic microstructure, according to the Volvo VCC Standard. These forged crankshafts undergo a series of machining and subsequent hardening processes to achieve the final fit, form, and function at the engine plant of Volvo Car Corporation in Skövde. The manufacturing operations on the crankshafts remains identical regardless of the different material batches.

As mentioned in the limitations earlier, only the semi-finishing operation has been considered for this study to maintain consistency in the results. The semi-finishing process is a part of the turning operation performed on the cylindrical portions of the crankshaft. The main reason for choosing the semi-finishing operation in this study is due to the close control on the cutting parameters such as depth of cut and feed when compared to the rough machining operations. It should be noted that all the analysed inserts reached their intended tool life of a specific number of machined crankshafts per insert. Additionally, no difficulties were encountered during the machining of these crankshafts.

The 5 different batches of crankshafts manufactured on different dates had the following notations: G8, P8, S8, W2, and Z2. The material composition and mechanical properties were reported in a chemical certificate for each batch based on the Volvo VCS Standard. The front portion of the crankshafts were the focus of the thesis study. The samples of the crankshafts and related cutting tool inserts were obtained from the semi-finishing operation also known as operation 30 at VCC. The crankshafts from batches G8, P8, S8, and W2 were delivered in the semi-finished condition while the crankshaft from batch Z2 was delivered in the surface hardened condition. 4 inserts each were delivered from batches G8 and P8 respectively, while 2 inserts each were delivered from S8, W2, and Z2 respectively. Since the semi-finishing operation takes place before the surface hardening process, the inserts for Z2 were delivered from the same process as the remaining batches, thereby ensuring consistency. The inserts from each batch are denoted with batch name followed by a number such as 30:1 or 30:2 where, 30 stands for Operation 30 while 1 and 2 represent machine 1 and machine 2 respectively. For example, S8 30:1 would correspond to an insert from batch S8, Operation 30, Machine 1. While batches S8, W2, and Z2 had 1 insert delivered from each machine, batches G8 and P8 had 2 inserts each, delivered from machine 1 and machine 2 respectively. Thus, the notations of inserts for batch G8 and P8 have an additional number. For example, G8 30:1-1 would indicate an insert from batch G8, Operation 30, Machine 1, Insert number 1.

5.2 Sample preparation

5.2.1 Inserts

V shaped inserts of type 4315 (Sandvik Coromant grade) were used in the semi-finishing operation. The worn-out inserts were collectively submerged in an acetone solution and placed in an ultrasonic bath for 10 minutes. Subsequently, each insert was cleaned under flowing water by thoroughly rubbing the cutting surfaces of the inserts. This was followed by cleaning the inserts with isopropanol, and finally ethanol. The inserts were then placed on mounting pins for examination in the scanning electron microscope (SEM).

5.2.2 Crankshaft

5.2.2.1 Sectioning

The samples of interest were extracted from the front end of the crankshaft as shown in Figure 5.1. The front end was cut off from the crankshaft using a combination of Wire-EDM and a semi-automatic bandsaw. The front end was further sectioned into a disc of 12 $\pm$1 mm thickness using consumable abrasive cutting on a Struers Discotom 2 with a resin-bound consumable Al_2O_3 abrasive disc. The cut of samples was further sectioned in the radial as well as transverse direction as shown in Figure 5.2, according to the minimum surface area requirement for inclusion mapping given in ASTM E45-18a standard. Five radial and five transverse cross-sections corresponding to each batch of material were obtained.

5.2.2.2 Mounting

The cross-section of the specimen was mounted using polyfast as a resin on a Struers Citopress- 20 machine. Each cross-section was mounted individually using the 30 mm mount and 20 ml of polyfast, with a pre-set heating time of 3 minutes and cooling time of 2 minutes.

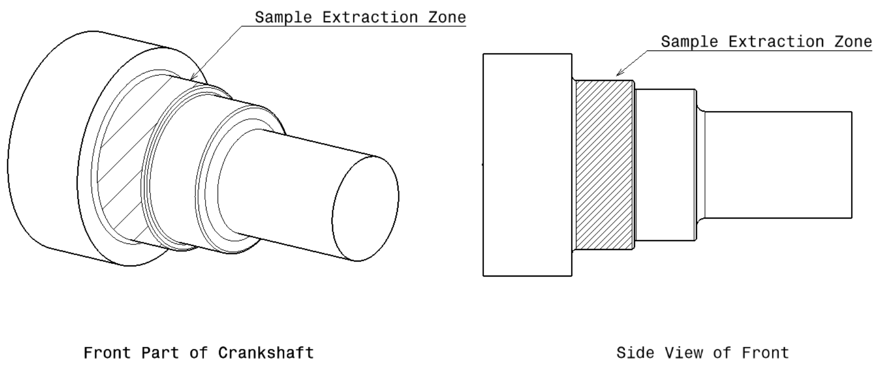

Figure 5.1: Simplified views of the front end of the crankshaft

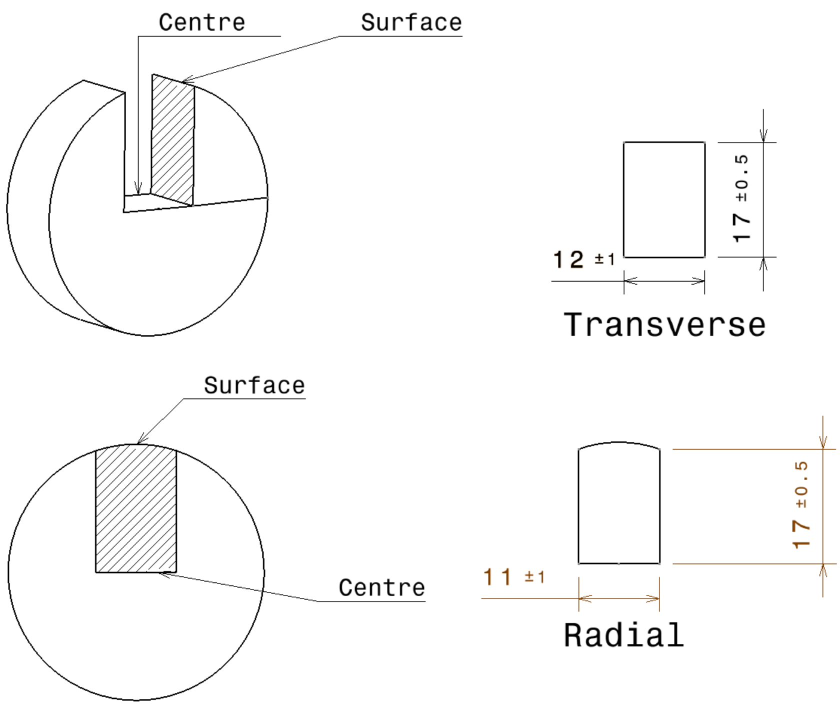

Figure 5.2: Cross-section of crankshafts for metallography

5.2.2.3 Grinding and polishing

The mounted specimens were prepared for microscopy using the standard procedures for mechanical grinding and polishing of alloyed carbon steels on a Struers Tegraforce-5 machine. Grinding was performed using grit sizes #120, #320, and #800 in the same order as mentioned. Fine grinding and polishing were performed in 3 steps using 9 µm MD-Largo fine grinding, 3 µm DP-Dac and 1 µm Nap polishing discs in the same order as mentioned. The 3 µm and 1 µm polishing steps were repeated on the etched samples to prepare the materials for hardness testing. After each polishing step, the samples were cleaned with ethanol to prevent oxidation of the material. Certain phases of sulphide inclusions may disintegrate on reaction with water; thus, ethanol should be used during the grinding and polishing operations for preparation of microsections (Kiessling and Lange, 1966). The fully polished samples after the 1µm step were immersed in isopropanol and placed in an ultrasonic bath for 10 minutes and were subsequently cleaned with ethanol and cotton swabs to obtain the highly reflective mirror finish required for optical and electron microscopy.

5.3 Scanning Electron Microscopy

The crankshaft material and inserts were examined using a Philips XL-30 Environmental Scanning Electron Microscope (SEM) equipped with an Oxford INCA Energy Dispersive X-ray Spectroscopy (EDS) system. Both secondary electron (SE) and backscattered electron (BSE) imaging were used to obtain images with different properties. SE images were used to obtain topographic images of the inserts as well as a few non-metallic inclusions. BSE images were used to obtain elemental contrasts which enabled easy identification of the wear and layer formations on the inserts as well as to acquire images required for quantitative analysis of inclusions in steels.
SE and BSE images of the inserts were obtained from the top view (rake) and the isometric view showing the primary cutting edge (rake and flank surfaces and tool nose). Only BSE images were obtained for the side view (primary flank) and the front view (nose). EDS elemental mapping was performed on the rake face of all inserts along with several point analyses on the flank face.
The images of the inclusions in the crankshaft samples were obtained according to ASTM E45-18a standard for determination of inclusions in steel. BSE imaging was used to obtain 25 images of each sample at 500X magnification in both the radial and transverse directions. The location of the 25 images was based on the pattern shown in Figure 5.3, corresponding to an equivalent sampling area of 6.0492 mm^2 which is greater than the total area of 4mm^2 recommended in ASTM E45-18a.

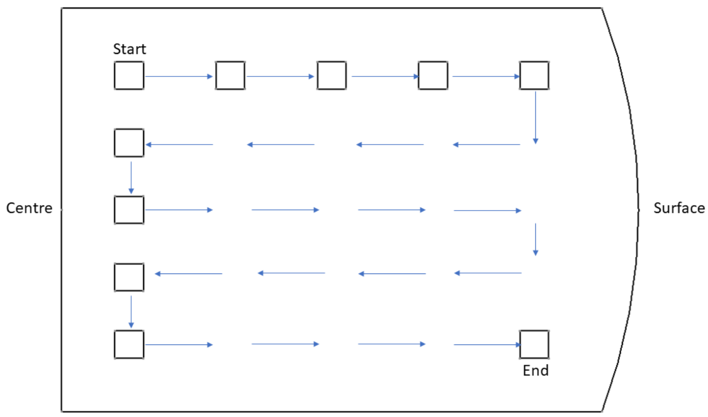

Figure 5.3: Pattern for inclusion mapping of 25 zones

The first image, regardless of the sample orientation (radial/transverse) was always captured at the centre end and the last image was always at the surface end. The BSE micrographs of the inclusions were further analysed using the open-source image processing software Image-J. EDS elemental mapping was performed on 20 most interesting NMIs per batch, identified visually, in the radial samples only. The same pattern of inclusion mapping shown in Figure 5.3 was used to find these NMIs to avoid mapping the same inclusion again.

5.4 Image analysis

The image analysis was performed using the open source software Image J, to obtain statistics about the inclusion type, numbers, distribution, and the area fraction. The image threshold was adjusted individually for each image regardless of the sample orientation (radial/transverse). The analysis, however, was performed using different settings available in Image-J, for the radial and transverse samples. For example, each image from the radial sample was analysed individually while the images from the transverse samples were analysed as a sequence of images. The different settings were used to avoid/eliminate the noise in the images.

5.5 Light Optical Microscopy

Only the radial crankshaft samples were etched using 3 % Nital for approximately 5 seconds. These samples were then examined using a Leica LEITZ DMRX optical microscope equipped with a Zeiss AxioCam MRc 5 to get an overview of the microstructure of the samples. Images at 10X, 20X, 50X, and 100X magnifications were obtained for each sample from the centre end and the surface end and were processed using the AxioVision image processing software.

5.6 Hardness testing

The hardness testing was done using a Struers DuraScan-70 G5 hardness testing instrument. The etched radial samples were re-polished using 3 µm and 1 µm polishing steps to prepare the samples based on the ASTM E92 standard for Vickers Hardness of Metallic Materials. All the samples had three rows of 15 indents each under a load of 1kgf, in the pattern shown in Figure 5.4. The first indent in each row was always made on the surface end of the sample, and the distance between indents was set at 10 times the length of the diagonal impression. Automatic settings available on the hardness testing instrument were used to maintain the pattern of indents by user specified spacing of 10 times the diagonal length of the indent. The loading time and diagonal measurement was performed using the automatic settings.

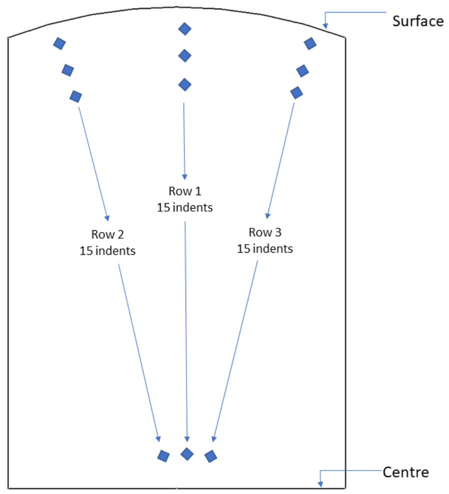

Figure 5.4: Hardness pattern with 45 (15 X 3) indents

6
Results

This section contains brief discussion of the results obtained from the experimental methods.

6.1 Inserts

As mentioned in section 3, low magnification imaging using SEM provided an overview of the topography and wear on all the inserts. The results have been briefly discussed below.

6.1.1 Topography

The topography of the inserts was obtained primarily by using low magnification SE imaging at 12 kV accelerating voltage. The representative topographic images of the worn-out tools are shown in Figure 6.1 and Figure 6.2.

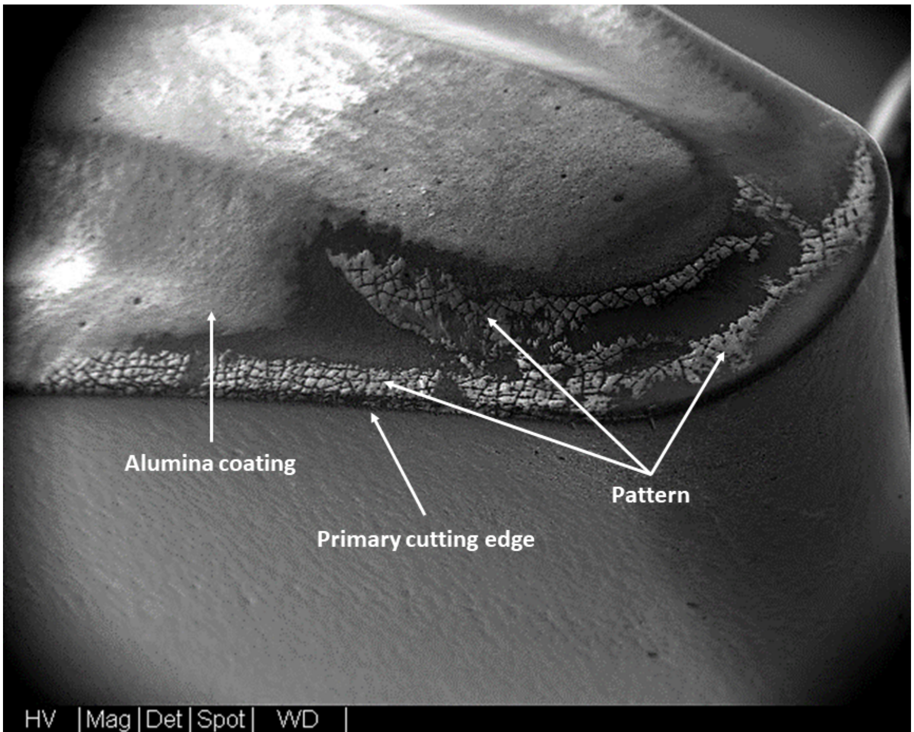

Figure 6.1: W2 30:2, SE 65X, isometric view

As it can be observed in Figure 6.1 and Figure 6.2, a pattern (higher contrast regions) exists on the surfaces of all the inserts. The same pattern is observed on all the cutting inserts (see also APPENDIX A).

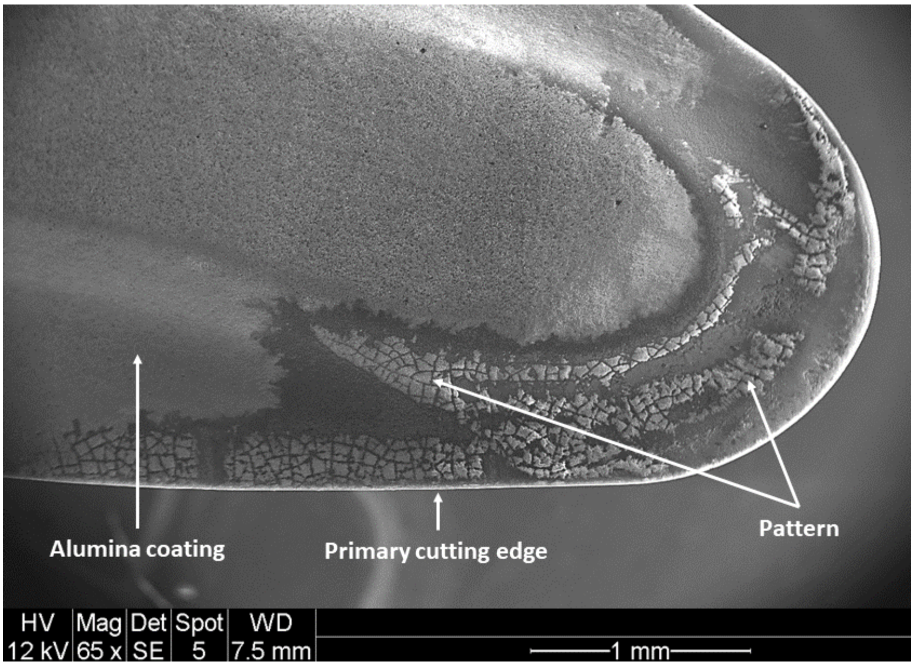

Figure 6.2: Z2 30:2, SE 65X, top view

A similar pattern on the inserts was also observed by (Gassner et al., 2019) who suggested the presence of a crack network between the TiCN layer and Al_2O_3 layer of the tool coating on the insert. However, this layer as shown in the high magnification image in Figure 6.3 below, was not observed in BSE images shown in Figure 6.3b, and both the EDS map and point analysis indicate the strong intensities for Al and O existing in the alumina coating. Thus, it is not possible to determine the reasons for occurrence of these patterns on the tool rake surface using the SEM/EDS characterisation techniques followed in the present study. Two possible reasons for occurring of such patterns on the rake face of the tool can be given:

1. The coating comprises of a very thin Al_2O_3 layer – perhaps with different properties and functions, deposited on the main thicker alumina layer. In this case, determination of this layer using elemental contrast e.g. BSE and/or EDS analysis would not be possible, see Figure 6.3b. Thus, the patterns shown in Figure 6.3a are perhaps the network of cracks of this top thin coated layer.
2. A very thin layer of calcium and silicon is deposited on the rake face during the machining process. Note the EDS point analysis occasionally indicates the presence of small amounts of Ca and Si in the high contrast regions of Figure 6.3a apart from Al and O coming from the coating. However, due to very weak EDS intensities associated with the low resolution of the adopted technique, it is not possible to utterly confirm the presence of such tribo-layers.

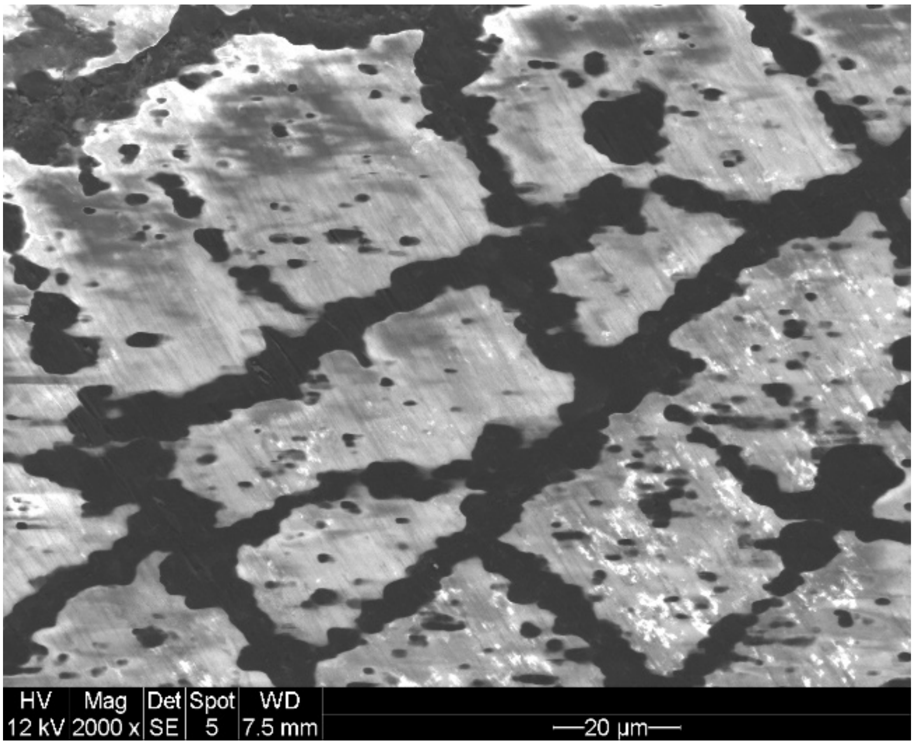

(a) SE, top view, 2000X

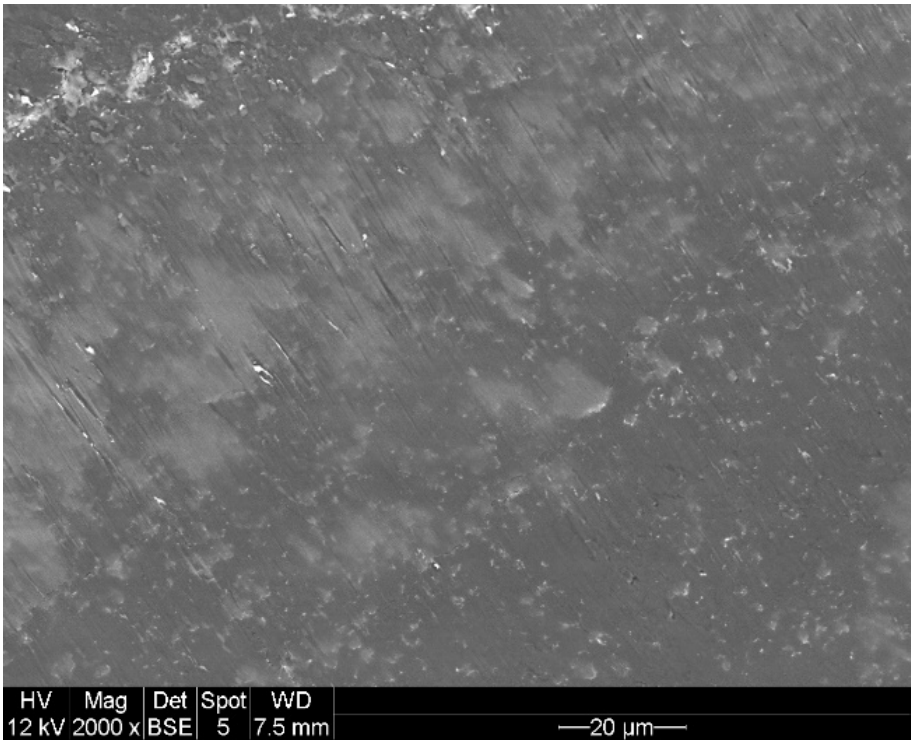

(b) BSE, top view, 2000X

Figure 6.3: P8 30:1-2, High magnification SE/BSE images of a zone within the pattern

6.1.2 Flank wear and nose wear

The flank wear on the primary cutting edge has been documented by measuring the wear for all the inserts from the BSE micrographs, a summary of which is shown in Figure 6.4. The average flank wear (VB_{BMax}) for the batches are: G8= 40.4 µm, P8= 41.6 µm, S8= 45.7µm, W2= 50.7µm, and Z2=39.7 µm. Similarly, the wear on the nose of the insert has also been documented for all the inserts, a summary of which is shown in 6.5. The average nose wear (VB_C) for the batches are: G8= 89.7 µm, P8= 93 µm, S8= 82.3 µm (only one measurement), W2= 94.8 µm, and Z2=85.3 µm. It should be noted that both the values for batch Z2 shown in 6.5 are the same.

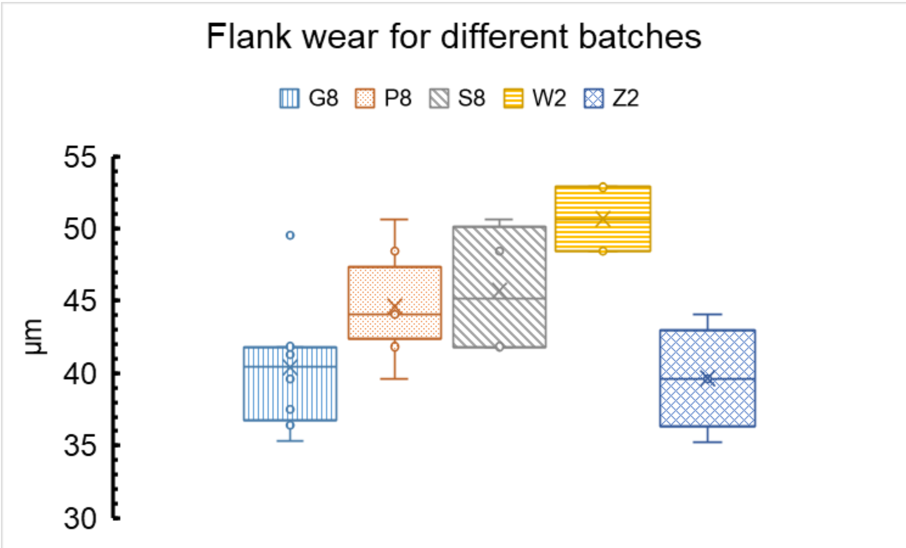

Figure 6.4: Flank wear VB_{BMax} for different batches in µm

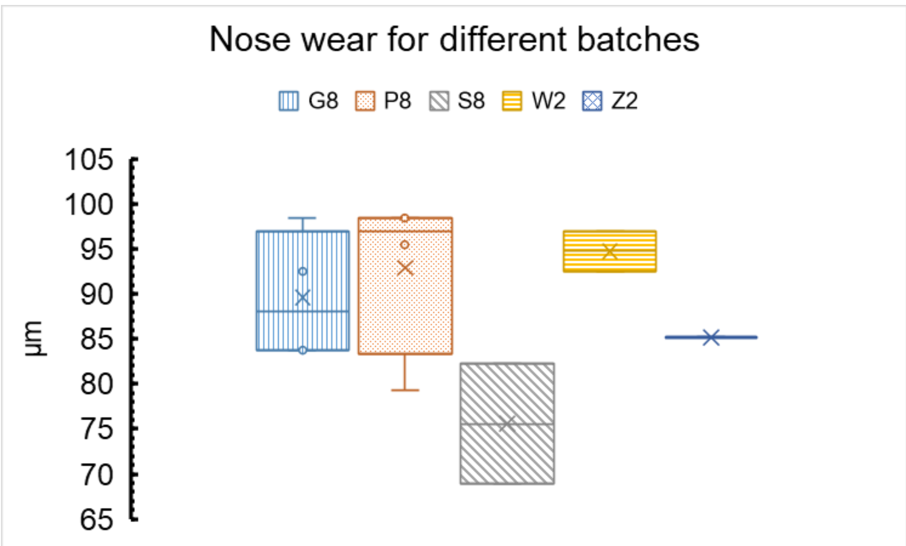

Figure 6.5: Nose wear VB_C for different batches in µm

Since the images of the flank and nose wear look identical only a few representative images are shown in Figure 6.6 and Figure 6.7 (see also Appendix B). An unused cutting edge has also been shown in Figure 6.8 for reference.

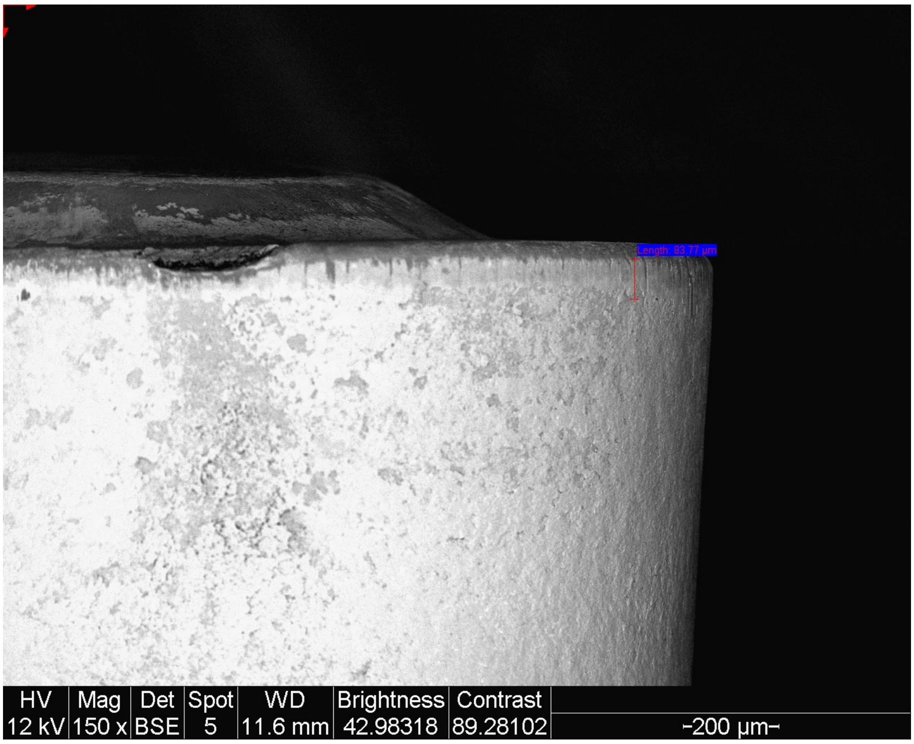

Figure 6.6: Nose wear for G8 30:2-1, VB_C=84µm

The flank wear on the inserts is quite low compared to the flank wear criteria mentioned in ISO 3685 standard for tool life tests during turning. The inserts from batch W2 exhibited the highest flank wear while inserts from Z2 exhibited the lowest flank wear. The difference between the average maximum and minimum flank wear was approximately 11 µm. However, this minor difference in the wear is understandable since the current wear criterion at VCC is the surface roughness of the machined component. Thus, the tools are changed on a predefined schedule before the machined surfaces are damaged due to excessive tool wear. Moreover, the edge radius of the unused inserts, as can be seen in Figure 6.8, was approximately 25 µm. Thus, the actual flank wear progression is much lower than the absolute values shown in Figure 6.4 and Figure 6.5. The nose wear, however, was relatively larger than the flank wear. This observation was consistent with the tool path during the semi-finishing operation since the nose of the insert was probably engaged longer during the machining process and performed the major part of the cutting. Again, inserts from different batches exhibited minor differences in the nose wear. The difference between the average maximum and minimum nose wear was approximately 12.3 µm.

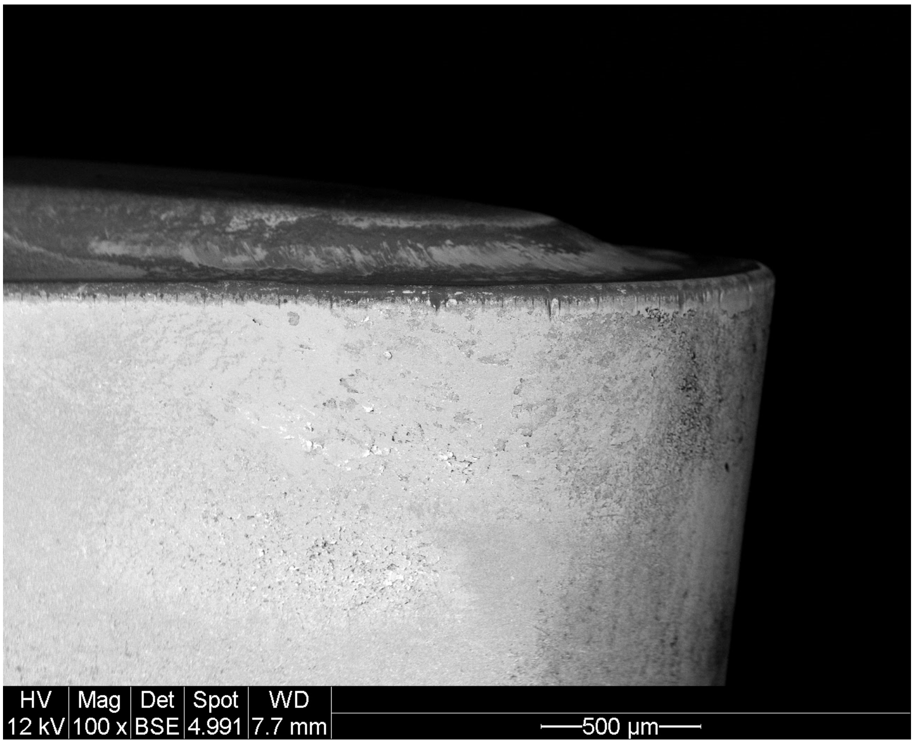

Figure 6.7: Flank wear for S8 30:1, VB_{BMax}= 49.6 µm VB_C=82.3µm

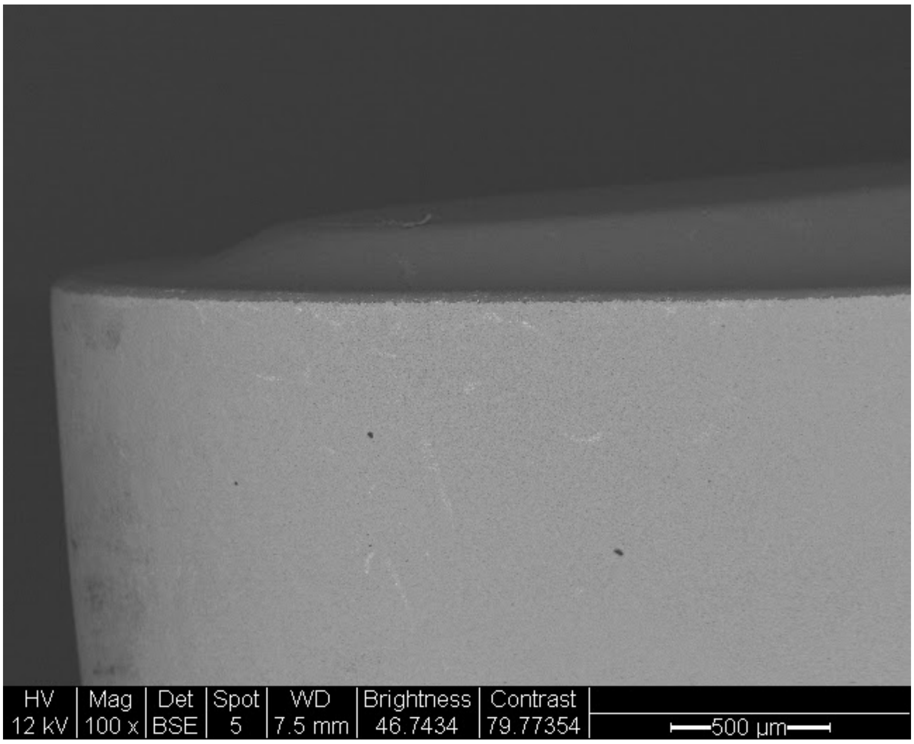

Figure 6.8: Cutting edge of an unused insert, edge preparation= 28 µm

Note that the depth of cut slightly varied during the machining experiments due to the dimensional tolerances allowed from previous machining operations. This variation is random in nature and could not be monitored during an automated machining operation. Thus, these small differences between the flank and nose wear among the inserts of different batches cannot be solely related to the variations in the micro-properties of the work material and could be a result of changes in cutting process itself.

6.2 Crankshaft

As mentioned in section 3, the crankshafts were examined after observing the wear on the inserts. Each batch of the crankshaft was examined to determine the size, type, composition, and morphology of the inclusions. These results have been discussed in this subsection.

6.2.1 Inclusion maps

Inclusion mapping were performed for both the radial cross-section as well as the transverse cross-section of the crankshafts. An example each from the inclusion maps of the radial and transverse cross-sections have been shown in Figure 6.9 and Figure 6.10.

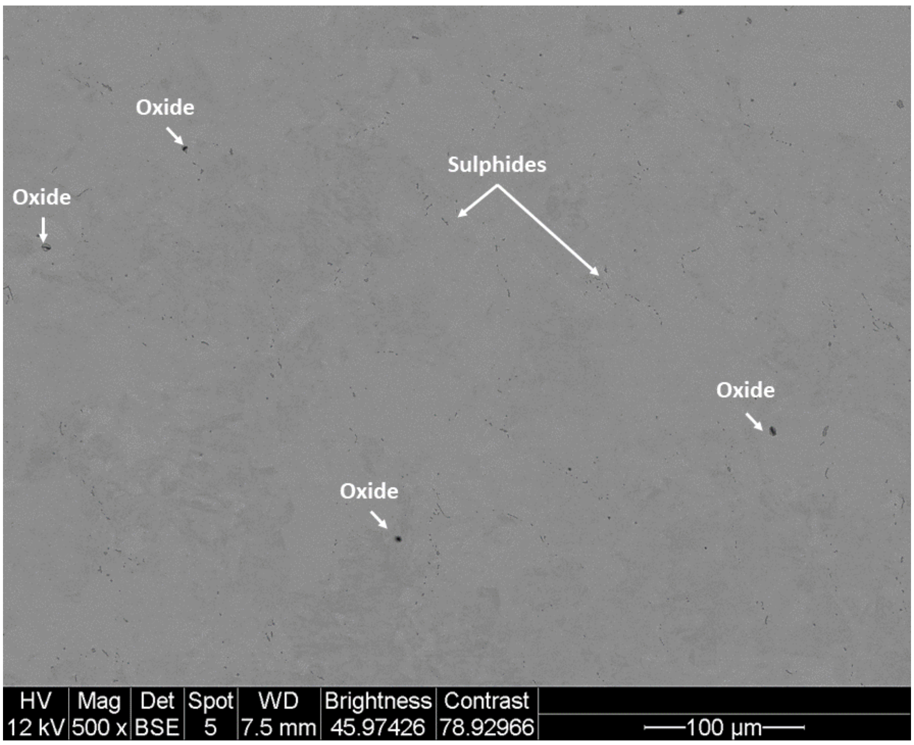

Figure 6.9: An inclusion map zone within P8-Radial

A visible difference can be observed in the size/length of the MnS inclusions between the radial and transverse position in all the batches. This is because the softer inclusions which are elongated along the rolling and forging direction- i.e. transverse direction in this case, would be larger in size and resulting in higher area fractions. As per the recommendations in ASTM E45-18a, the inclusion distribution in terms of area fraction and size, should be calculated/approximated from a sample extracted from a plane parallel to the rolling direction. In this case, the transverse direction is the rolling direction and hence the results for the area fraction of inclusions have been displayed for samples from the transverse cross section.
The different contrasts as seen in Figure 6.9 and Figure 6.10 indicate the different type of inclusions. For example, the darker and relatively circular inclusions are usually oxide inclusions, while the lighter and elongated inclusions are sulphides. The oxide inclusions found in the different batches are undeformed in the rolling direction and hence their appearance and size in the radial and transverse directions are the usually the same.

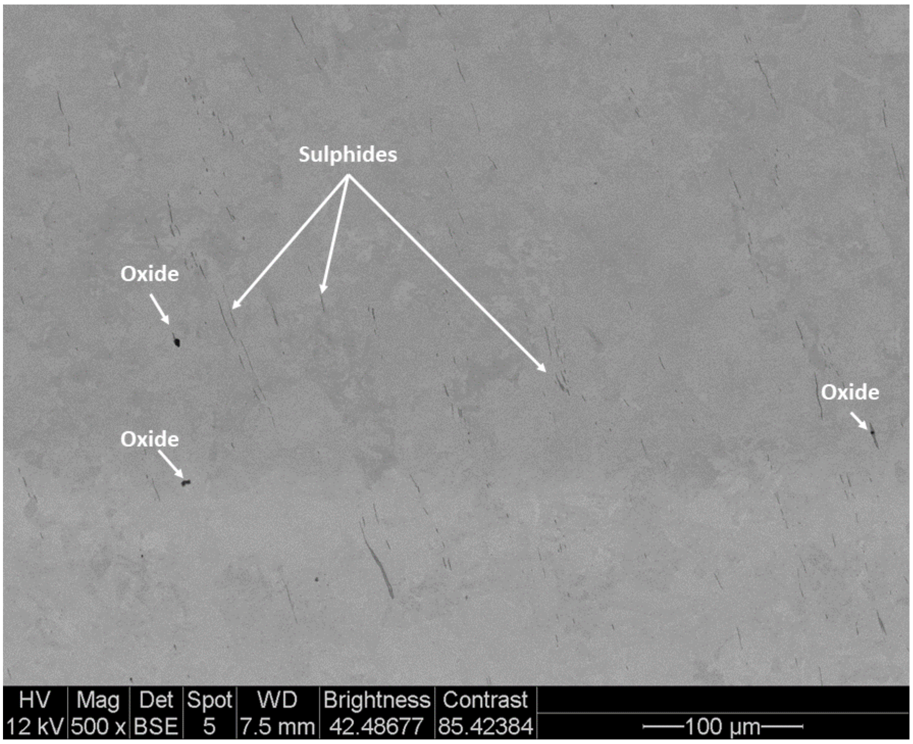

Figure 6.10: An inclusion map zone within P8-Transverse

The basic type (sulphide or oxide) of NMI was identified based on visual identification of the inclusions based on the image contrast generated by BSE imaging. The images obtained at 25 locations on each sample were analysed in ImageJ, and subsequently certain statistics of the inclusion size and distribution were generated as shown graphically in Figure 6.11 and Figure 6.12 (see also Appendix E).
A summary of the NMI distribution, area fraction, and basic NMI types identified in the crankshafts are shown graphically in Figure 6.11. It can be observed that the total number of inclusions per mm^2 is different for each batch. However, when doc-

umenting the effect of NMIs, both their number per unit area and the area fraction of inclusions should be analysed to provide a better understanding of their effects. For example, although batch S8 has the highest number of inclusions per mm^2 as shown in Figure 6.11a , the batch W2 has the highest area fraction of sulphide inclusions as observed in Figure 6.11b. This is because the size/area of the inclusions are different for different batches.
Since oxide-rich inclusions could be considered detrimental for machinability (depending on their type: hardness and formability), the results of the size distribution of only oxide-rich inclusions per batch of the transverse samples are shown in Figure 6.12. However, the total size distribution of the NMIs and the normal distribution of NMIs based on size are also shown in Appendix E. The maximum size of the oxide-rich inclusions identified among all the 120 inclusions identified, exceeded 13 µm in the largest dimension only once.

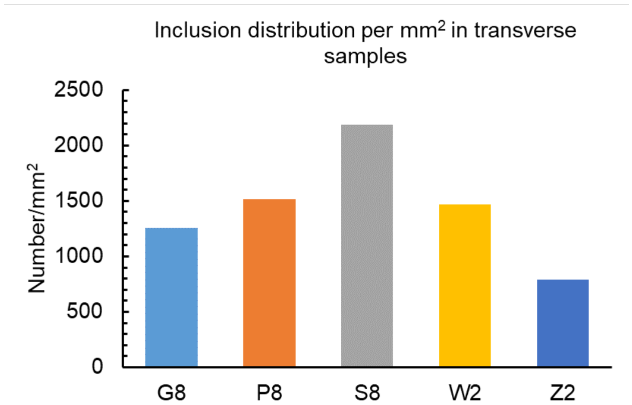

(a) Total NMI (oxides and sulphides) distribution in different batches- Transverse

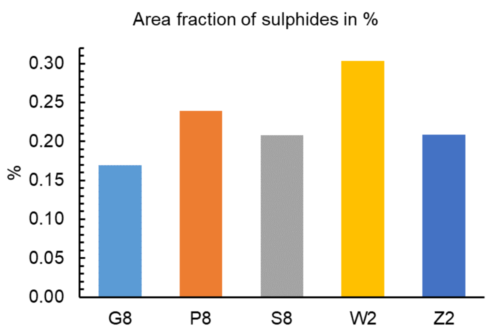

(b) Area fraction of sulphide inclusions in different batches- Transverse

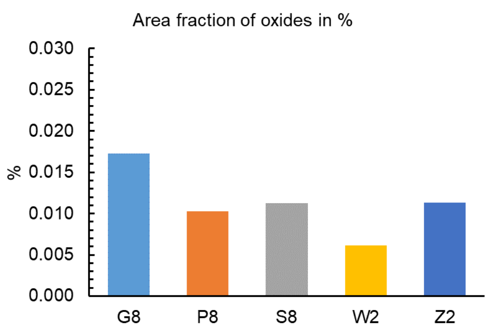

(c) Area fraction of oxide inclusions in different batches- Transverse

Figure 6.11: Inclusion distribution in different batches

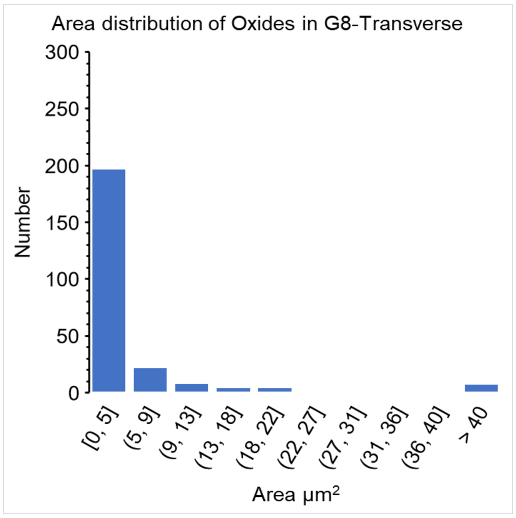

(a) G8

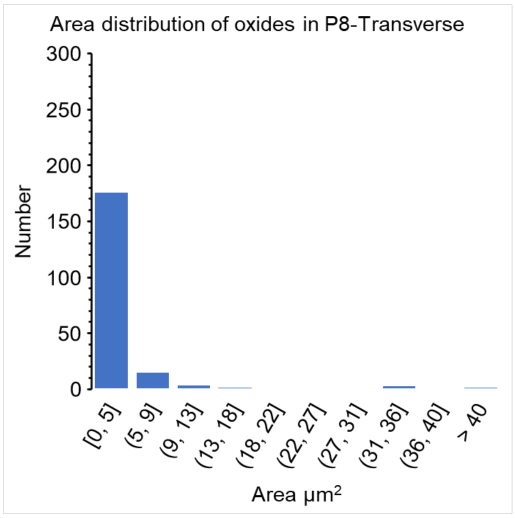

(b) P8

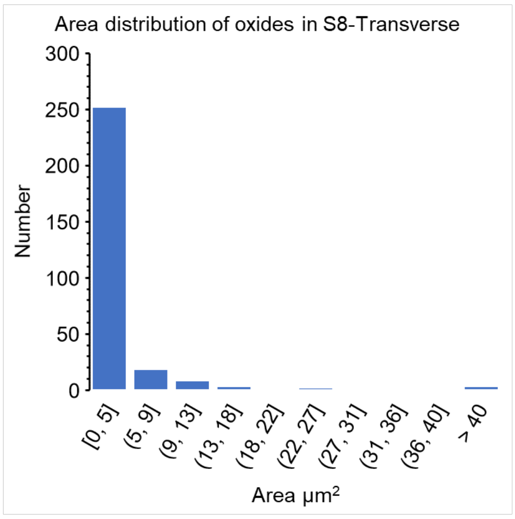

(c) S8

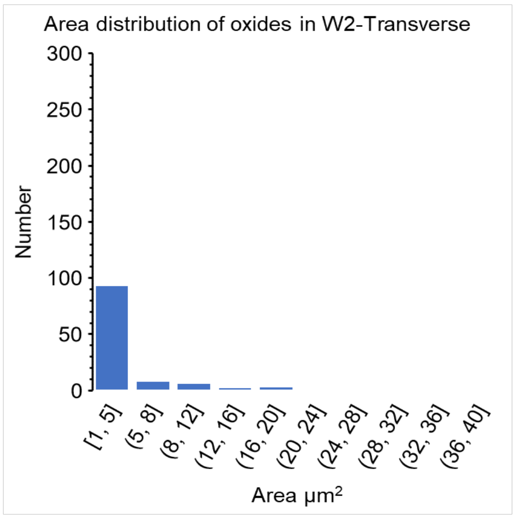

(d) W2

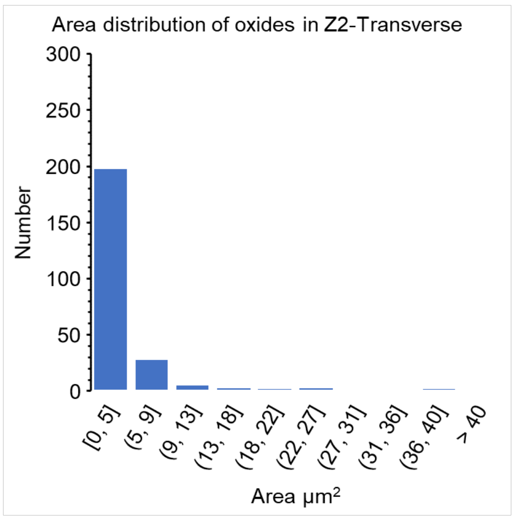

(e) Z2

Figure 6.12: Area distribution of oxide inclusions in different batches- Transverse

The oxide-rich inclusions in batch G8 had relatively larger sizes as shown in Figure 6.12a, while the oxide-rich inclusions in S8 had smaller sizes despite being in higher numbers as shown in Figure 6.12c. Thus, the area fraction of the oxide-rich inclusions for G8 was relatively higher than that of the other batches. The batch W2 on the other hand had relatively lower number and smaller oxide-rich inclusions as shown in Figure 6.12d, thereby having a smaller area fraction of oxide inclusions.
It should be noted that since the inclusions are mapped using the pattern already described in section 5.3, the area fraction, distribution, and size of NMIs are dependent on the probability of finding inclusions at that particular mapping location. Thus, the results shown in Figure 6.11 and Figure 6.12 are representative of only one inclusion map of 25 images per batch. It should also be noted that inclusions are not affected by heat treatment and thus the influence of the surface hardened condition of the crankshaft from batch Z2 can be ignored for inclusion mapping.

6.2.2 Inclusion type, composition, and morphology

A total of 20 oxide-rich inclusions per batch were mapped using EDS to determine the composition of the NMIs. The total number of a particular type of inclusion within the oxide-rich NMI per batch are shown in Figure 6.13 as well as summarized in Table 6.1 (see also Appendix F for graphical representations).

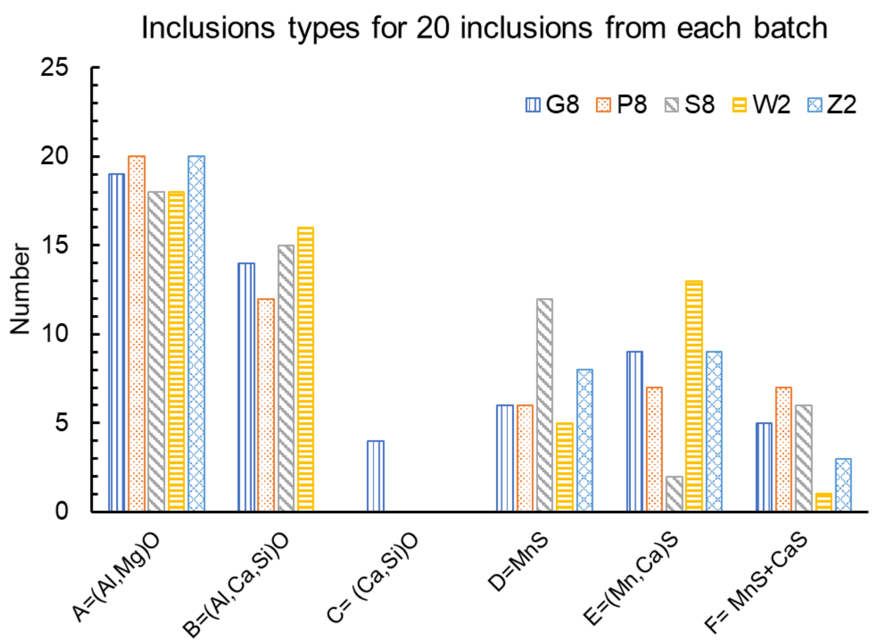

Figure 6.13: Composition of oxides among 20 inclusions per Batch

The different types of combinations of oxide-rich inclusions for each batch are shown in Figure 6.14, wherein the nomenclature A, B, C, D, E, and F are the same as those in Figure 6.13. Thus, the inclusions could be a combination of any type of these compounds. For example, the most frequent type of inclusion found in batch G8 was a complex oxide containing (Al,Mg)O+(Al, Ca, Si)O+(Mn,Ca)S. However, as Figure 6.13 and Figure 6.14 indicate, a complex compound containing (Al,Mg)O+(Al,Ca,Si)O+(Ca,Si)O+(Mn,Ca)S was also observed. The sulphide compounds in these inclusions surrounds the oxide-rich inclusions (MnS Type-I) and should not be confused with individual sulphide (MnS Type-III) inclusions.

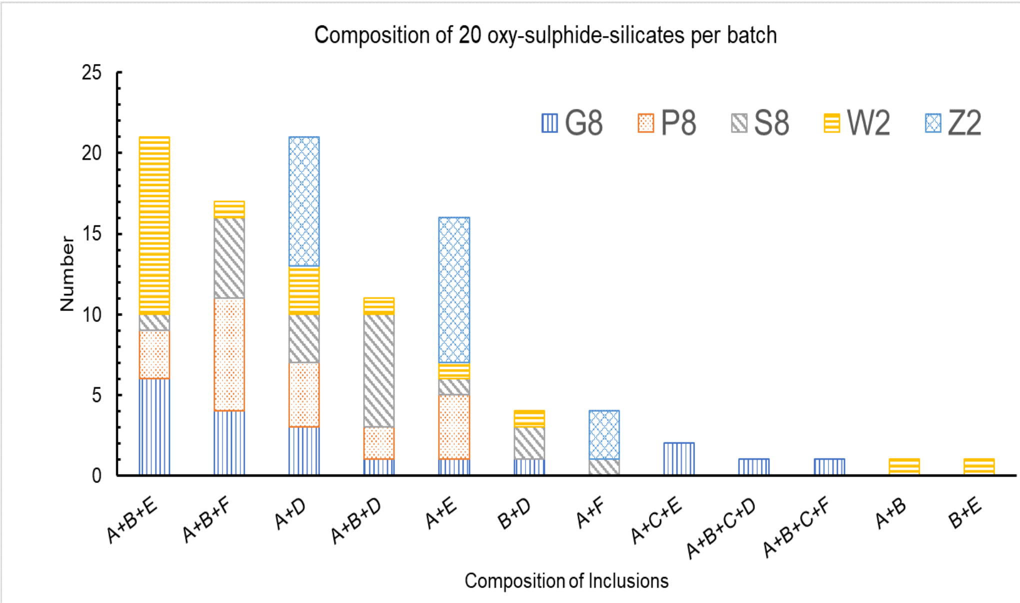

Figure 6.14: Approximate chemical composition of NMIs (Oxides)

Table 6.1: Composition of 20 oxide-rich inclusions per Batch

	A (Al,Mg)O	B (Al,Ca,Si)O	C (Ca,Si)O	D MnS	E (Mn,Ca)S	F MnS+CaS
G8	19	14	4	6	9	5
P8	20	12	0	6	7	7
S8	18	15	0	12	2	6
W2	18	16	0	5	13	1
Z2	20	0	0	8	9	3
Total	95	57	4	37	40	22

The chemical composition of the NMIs mentioned earlier in this section, including the majority inclusion type (sulphides) were initially confirmed using EDS point analysis. After a few point analyses, the inclusions which differed from pure sulphides i.e. the oxide-rich inclusions, were identified using the elemental contrast of BSE imaging. Thus, every new oxide-rich inclusion was identified by mapping the samples as mentioned in section 5.3 earlier. The composition of these oxide inclusions was then approximated using EDS mapping. A few interesting and relevant EDS inclusion maps are shown in Figure 6.15 to Figure 6.18. The morphology and topographic appearance of a few oxide based inclusions per batch are also shown in

Appendix G.
Figure 6.15 shows the most frequent type of oxide-rich inclusion found in batches G8 and W2, with the major difference being the size and number of the inclusions as shown earlier in Figure 6.12. The approximate composition of the inclusion is [(Al,Mg)O+(Al,Ca,Si)O+(Mn,Ca)S]. This composition shown in Figure 6.15 is further confirmed by doing an EDS point analysis, which indicates that an Aluminium-Magnesium rich oxide, perhaps spinel, is formed independently, surrounded by Calcia-Alumina-Silicate (CAS) and a sulphide. Similarly, Figure 6.16 shows the most frequent oxide-rich inclusion [(Al,Mg)O+ (Al,Ca,Si)O+ MnS+ CaS] identified in P8, Figure 6.17 shows the most frequent oxide-rich inclusion [(Al,Mg)O+ (Al,Ca,Si)O+ MnS] identified in S8, and Figure 6.18 shows the most frequent oxide-rich inclusion [(Al,Mg)O+ MnS] identified in Z2.
In the case of inclusions identified in Z2, it can be observed that all the oxide-rich inclusions are composed of one Aluminium-Magnesium rich oxide surrounded by some sulphide. This is the biggest difference observed between the inclusions observed in Z2 and the different batches- wherein the other batches have complex oxide-rich inclusions containing at least two types of oxides surrounded by some sulphides. Additionally, the second oxide is usually a CAS inclusion in all the batches except batch Z2.

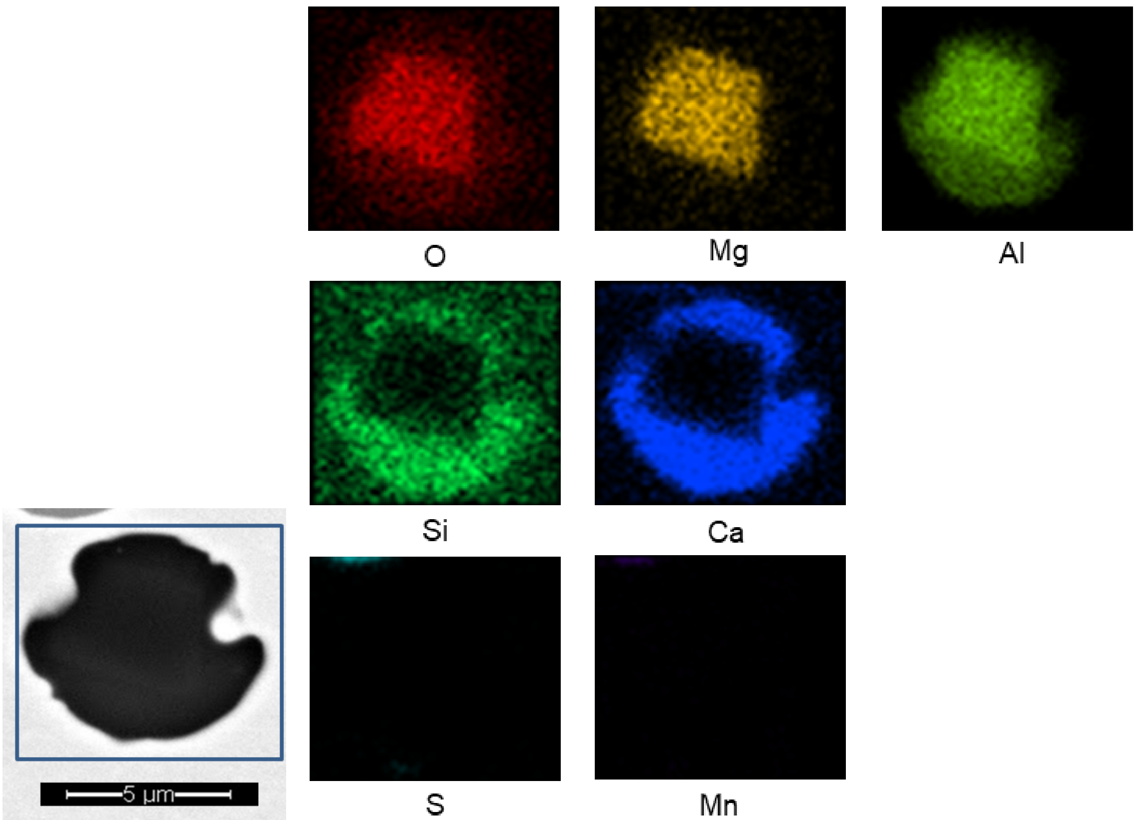

Figure 6.15: EDS Map of the most frequent type of oxy-sulphide inclusion in G8 and W2 batches. Current EDS Map from G8 batch.

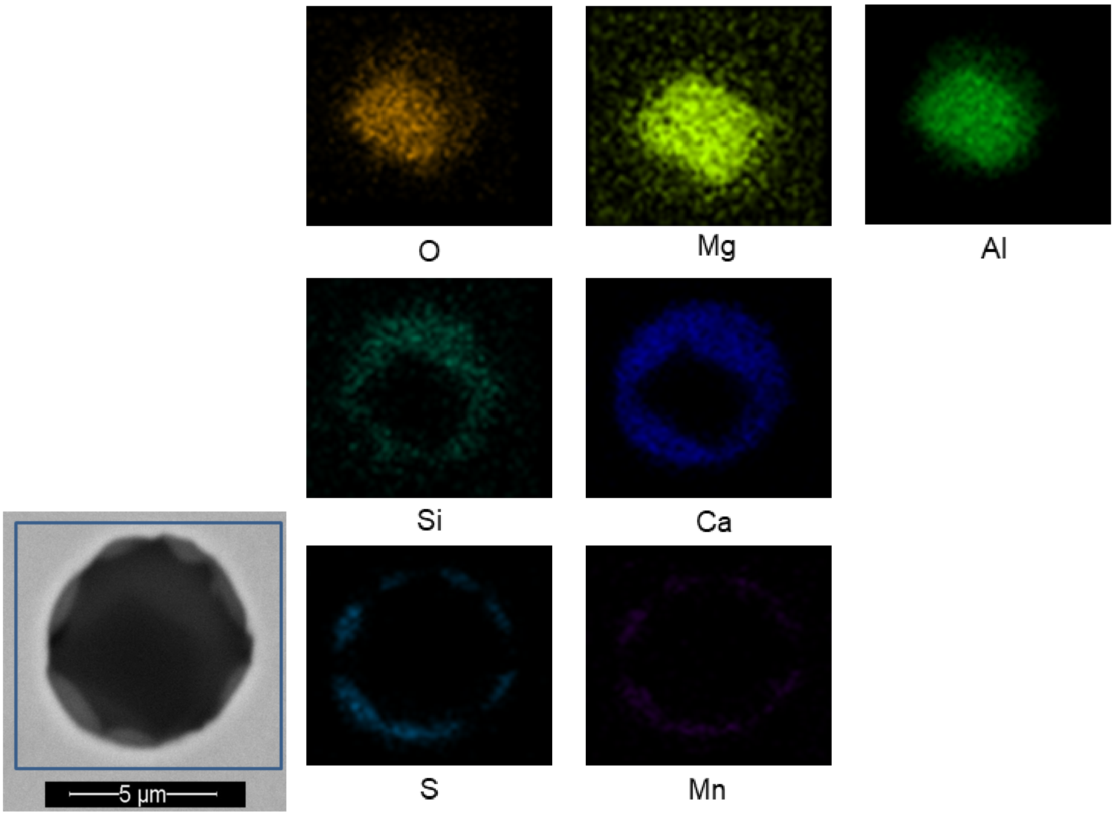

Figure 6.16: EDS map of the most frequent type of oxy-sulphide inclusion in P8 batch.

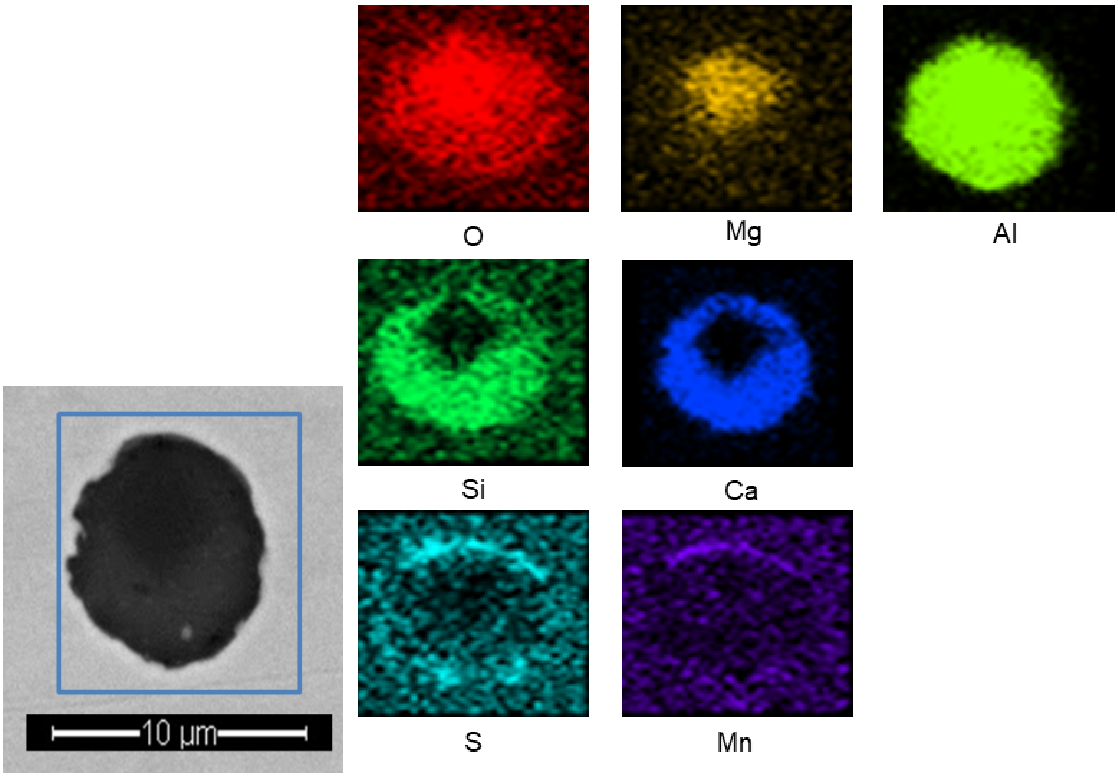

Figure 6.17: EDS map of the most frequent type of oxy-sulphide inclusion in S8 batch.

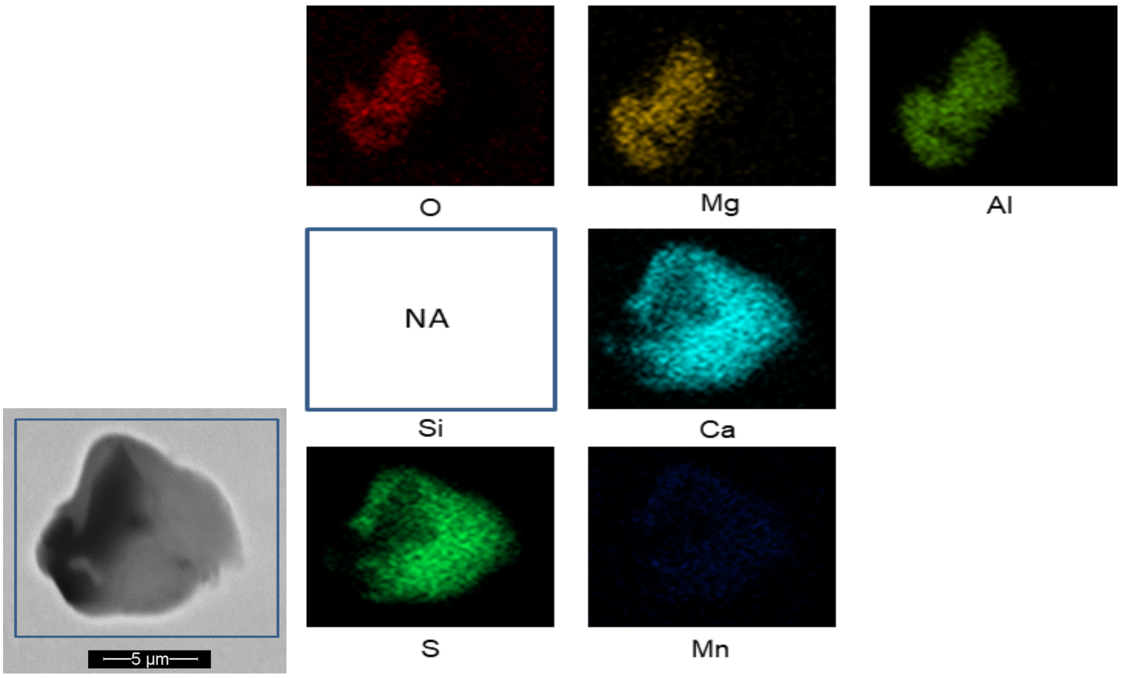

Figure 6.18: EDS map of the most frequent type of oxy-sulphide inclusion in Z2 batch.

6.3 Microstructure

The microstructure of the radial specimens was examined using Light Optical Microscopy (LOM) to assess if there are significant microstructure variations between different batches near the machined surfaces. The microstructure identified from the crankshaft samples is ferritic-pearlitic, as also mentioned in the material certificate for each batch. The microstructure of all the batches are shown in Figure 6.19.

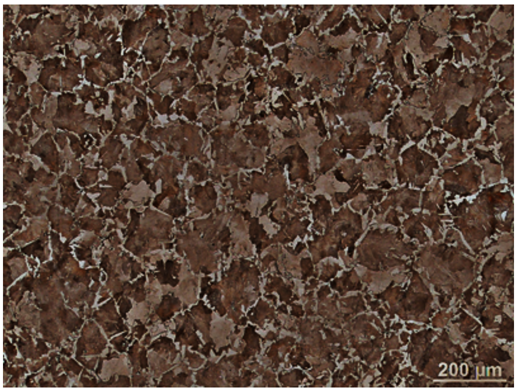

(a) Microstructure of G8

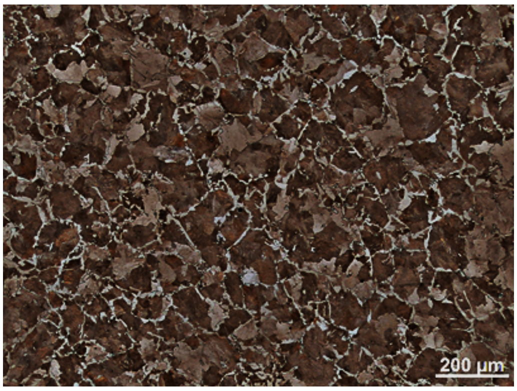

(b) Microstructure of P8

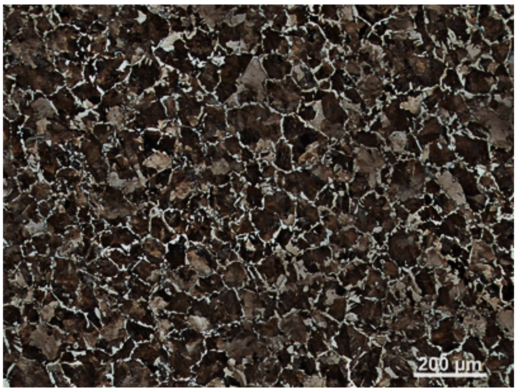

(c) Microstructure of S8

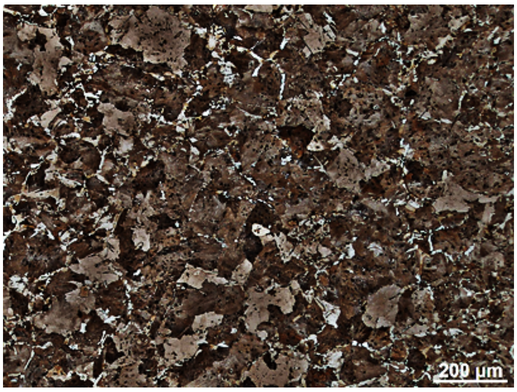

(d) Microstructure of W2

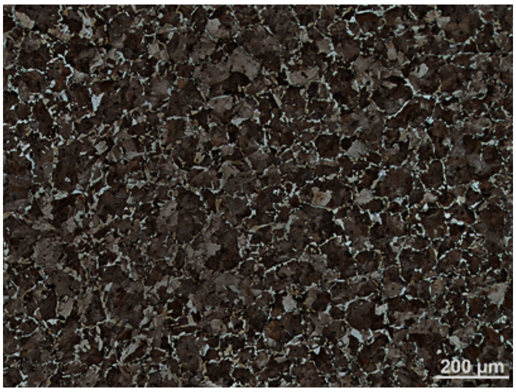

(e) Microstructure of Z2 (3mm below the surface

Figure 6.19: Microstructure of the different batches near the machined surface.

The differences between the microstructures of different batches are observed and compared only by visual comparison. Since no significant qualitative (visual) differences between samples was observed and due to the fact that the flank and nose wear of the inserts is low with minor differences between the wear of inserts from different batches, the microstructural characteristics such as the grain sizes and the pearlite-ferrite fractions were not analysed in the quantitative manner.
From Figure 6.19, it can be observed that S8 (Fig. 6.19c) and Z2 (Fig. 6.19e) have a slightly finer microstructure when compared to batch G8, P8, and S8 close to the machined surface. However, it should be noted that since the crankshaft from batch Z2 was delivered in the hardened condition, the image has been obtained at a position 3mm away from the machined surface due to the presence of martensite.

6.4 Hardness testing

Vickers Hardness test with a pyramid shaped indenter was performed on all the radial samples of the crankshaft. A total of 45 indents were made in each radial crankshaft specimen in the pattern mentioned in Figure 5.3. The values for hardness indentation have been shown as a trend for each batch in Figure 6.20 and Figure 6.21.

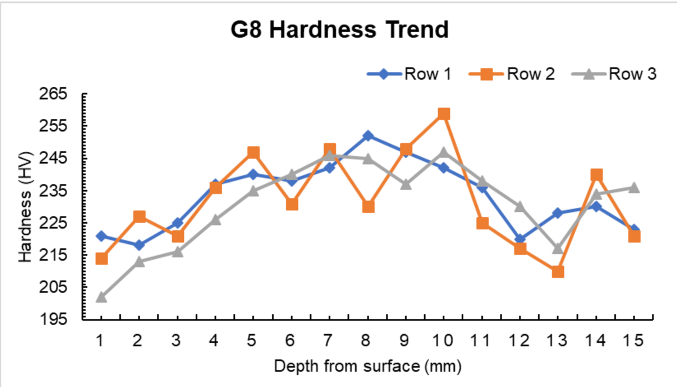

(a) G8 hardness trend

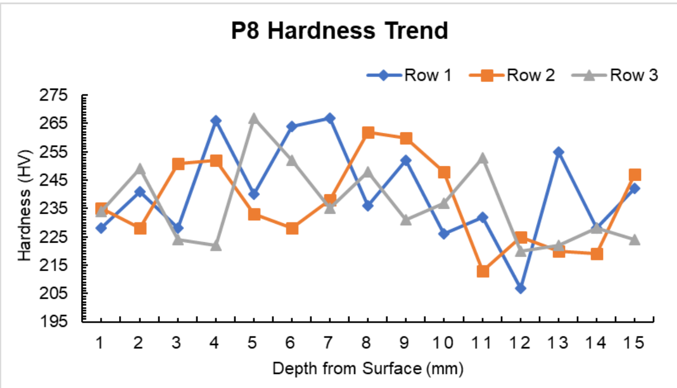

(b) P8 hardness trend

Figure 6.20: Hardness results for G8 and P8 batches- radial

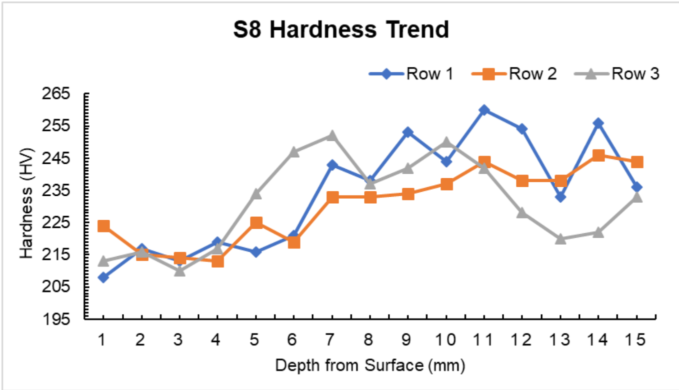

(a) S8 hardness trend

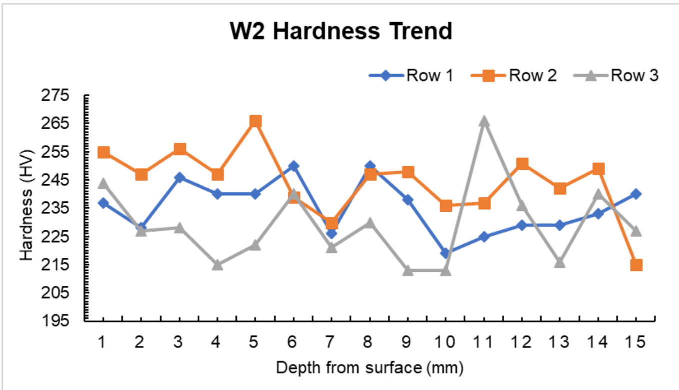

(b) W2 hardness trend

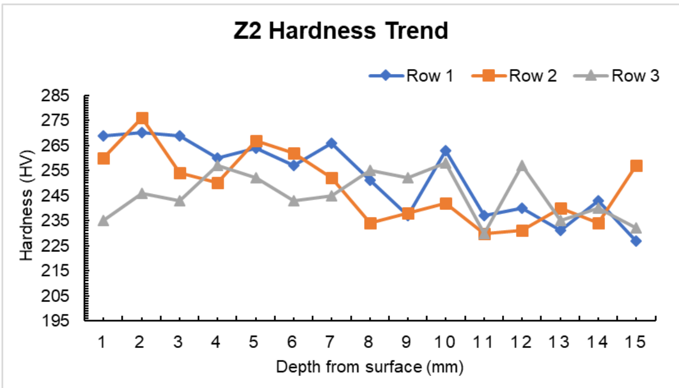

(c) Z2 hardness trend

Figure 6.21: Hardness results for S8, W2 and Z2 batches- radial

The average hardness values for the batches are as follows: G8= 232 HV, P8= 238 HV, S8= 232 HV, W2= 236 HV, and Z2= 249 HV. The hardness values were consistent with the material certificates for each batch wherein the reported hardness range for Z2 was slightly higher than the remaining batches. The few hardness values that are inconsistent with the average hardness values can be considered as scatter in the measurements.

6.5 Layer formation and plastic deformation of coatings on inserts

Different layers of NMIs were detected on the rake face of the inserts in addition to the plastic deformation of the Al_2O_3 coatings of the inserts. The layer formations and chipping of the cutting edge are shown as representative BSE images in Figure 6.22. The elements within these layers were further identified using EDS. From the contrast in each image, it can be observed that batches G8, P8, S8, and W2 had very similar layer formations as shown in Figure 6.22. However, the batch Z2 exhibited a slightly different/less layer formation as seen in Figure 6.22e. Thus, higher resolution imaging was performed to identify the differences in wear on the rake face. The indications for plastic deformation of the coatings on the inserts became visible at higher magnifications. The inserts from batches G8, P8, S8, and W2 exhibited similar layer formations and plastic deformation on the rake face while the inserts from batch Z2 exhibit slightly different layer formations when compared to the other batches at higher resolutions. Hence, only a few representative images of inserts from batches P8 and Z2 have been shown in Figure 6.23 and Figure 6.24 with images from batch W2 shown in Appendix C. Inserts from batch P8 were chosen for the comparison because:

1. These inserts had only a few chipped edges.
2. Steel from batch P8 had a relatively high total area fraction of inclusions in both, radial and transverse samples.

Inserts from batch W2 were chosen because the crankshaft samples from W2 showed the highest area fraction of MnS inclusions and the lowest area fraction of oxide-rich inclusions in both, radial and transverse crankshaft samples, with the type of inclusions being nearly the same as those in batch G8. The inserts from batch Z2 were of interest due to the different type of oxide-rich inclusions when compared to all the other batches. As can be seen, a few inserts had chipped-out edges. Chip jamming during exit of the chips or variations in mechanical loads on the inserts due to changes in the depth of cut could be possible explanations for the chipping of the inserts.

It was observed that apart from the adhered iron, inclusions from the machined crankshaft material were transferred onto the insert surfaces. The brighter contrast on the images shown from Figure 6.22 to Figure 6.23 indicate oxide-rich and MnS-rich layers that have been deposited from the crankshaft onto the insert rake faces. It should be noted that the images shown in Figure 6.23 and Figure 6.24 are obtained from approximately the same locations on the inserts. Clear differences can be observed in the formation of layers. For example, if the nose of the insert of batch P8 shown in Figure 6.23c is compared with that of batch Z2 as shown in Figure 6.24c, it can be observed that while the insert from batch P8 shows signs of superficial plastic deformation of the Al_2O_3 coating layer while the insert from batch Z2 shows a clearly different wear pattern due to perhaps the abrasive action on the Al_2O_3 coating. Similarly, the area between the nose and the chip-breaker, as shown in Figure 6.23b shows a protective layer of MnS for the insert from batch P8 while the insert from batch Z2 shows a worn-out layer of Al_2O_3 at the same location as shown in Figure 6.24b and Figure 6.25.

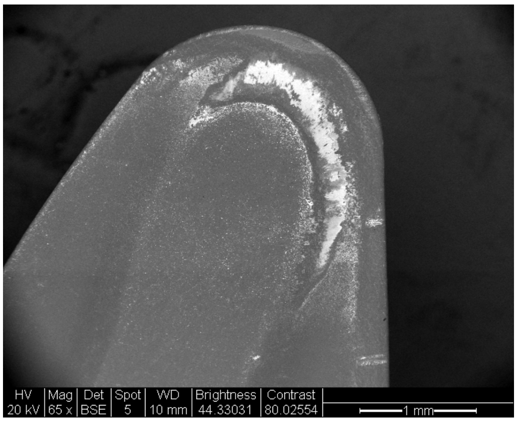

(a) G8 30:1-1

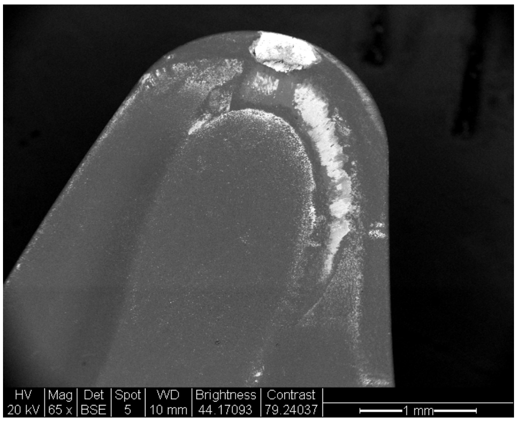

(b) P8 30:1-1

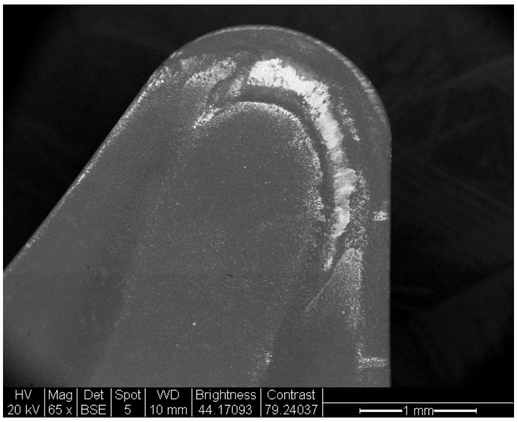

(c) S8 30:1

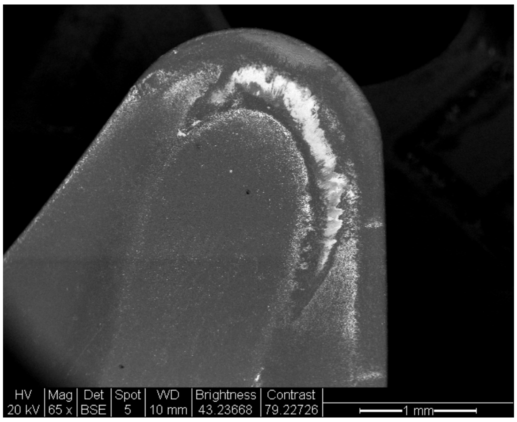

(d) W2 30:2

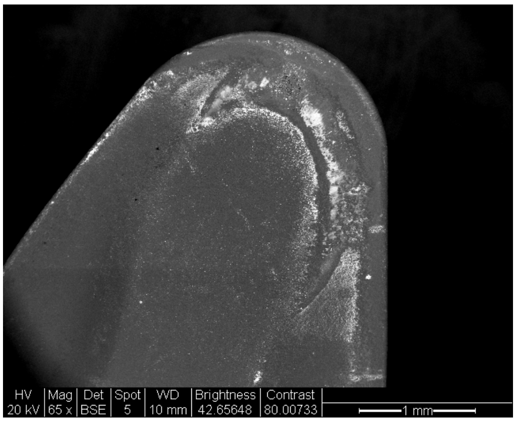

(e) Z2 30:1

Figure 6.22: Top view, 65X, BSE imaging of one insert from each batch showing the presence of transferred material from the steel onto the rake face of the inserts.

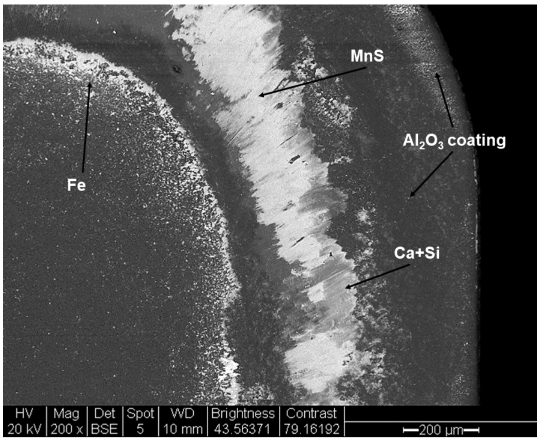

(a) P8 30:1-1, top view, between flank and chip-breaker, 200X, BSE

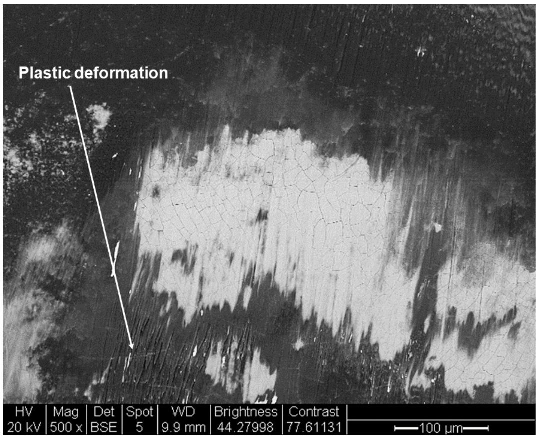

(b) P8 30:2-2, top view, between nose and chip-breaker, 500X, BSE

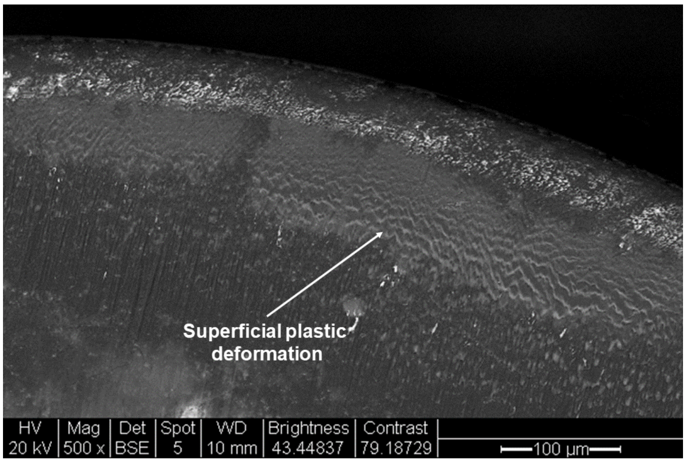

(c) P8 30:1-2, top view, nose, 500X, BSE

Figure 6.23: Layer formation and plastic deformation on the rake face of inserts from P8 batch

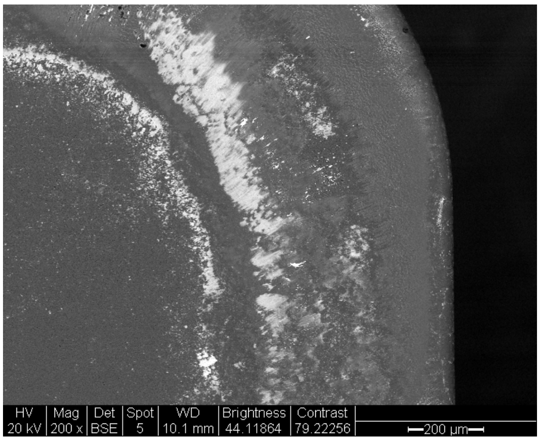

(a) Z2 30:2, top view, between flank and chip-breaker, 200X, BSE

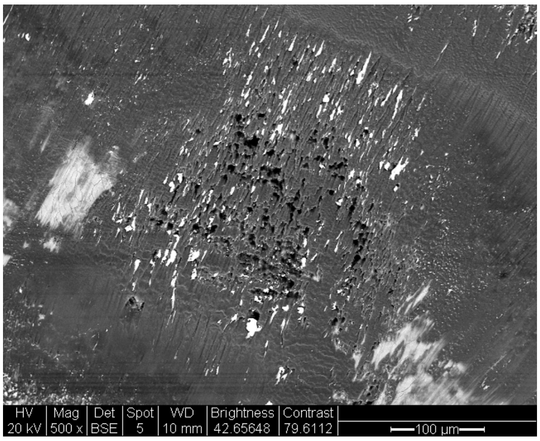

(b) Z2 30:1, top view, between nose and chip-breaker, 500X, BSE

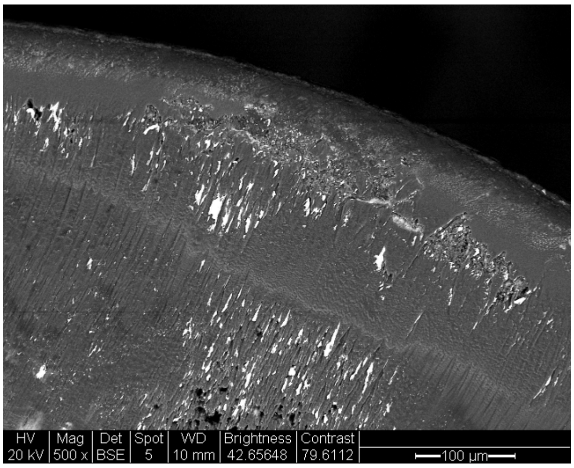

(c) Z2 30:1, top view, nose, 500X, BSE

Figure 6.24: Layer formation and plastic deformation on the rake face of inserts from Z2 batch

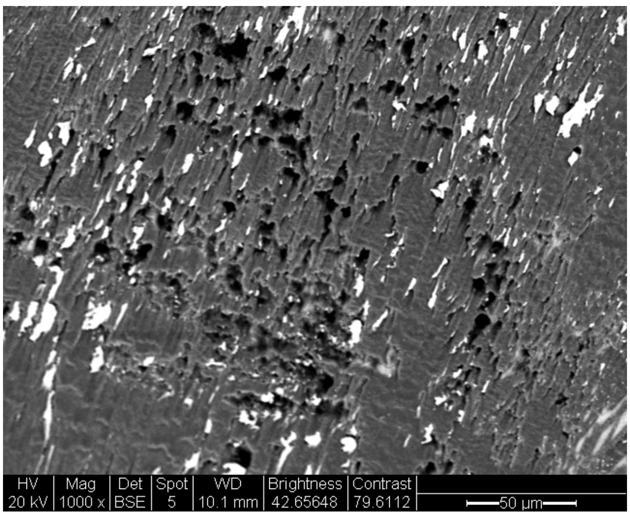

Figure 6.25: Z2 30:1, 1000X, BSE, Top View, Between Nose and Chip Breaker

These differences were further analysed using EDS. To provide a brief overview, the different layers between the nose and chip-breaker that were analysed using EDS mapping are shown in Figure 6.26 to Figure 6.28. (The results of the layers on other parts of the inserts are shown in Appendix C). As mentioned earlier, the results shown in the images are from one representative insert from the batches P8, W2, and Z2.

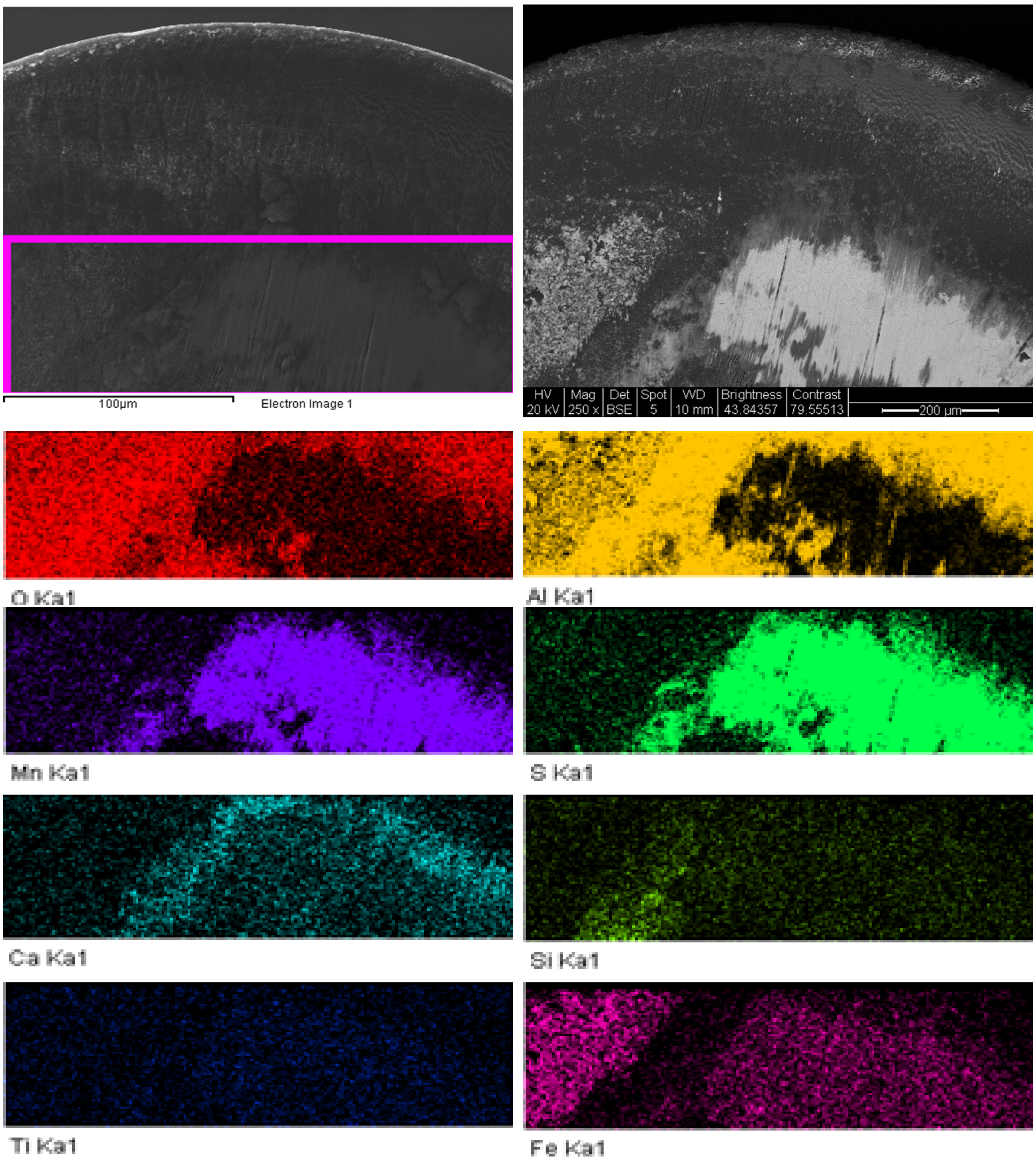

Figure 6.26: EDS map for P8 30:2-1, 250X, SE/BSE, between nose and chip breaker.

As it can be observed from Figure 6.26 and Figure 6.27, the batches P8 and W2 predominantly show the presence of MnS layer in the region between the nose and the chip-breaker, which is the region analysed in the images. Additionally, it can also be observed from Figure 6.22 shown earlier, that the thickness of the MnS layer is much larger in the region between the nose and the chip-breaker than in the pri-

mary cutting edge/ flank side of the insert.
On the contrary, it can be observed from Figure 6.28 that the insert from Z2 shows a relatively less MnS layer formation in the same region as analysed for the inserts from the other batches. Moreover, it can also be observed that the Al_2O_3 coating layer has been abraded because the EDS map shows the presence of TiC-which is the coating layer beneath the Al_2O_3 layer, in those specific regions. This wear on the rake face was observed on both the inserts of batch Z2, and on the same location of the insert, which is understandable since the process parameters and the process itself such as the tool path and cutting edge engagement remains the same for all inserts.

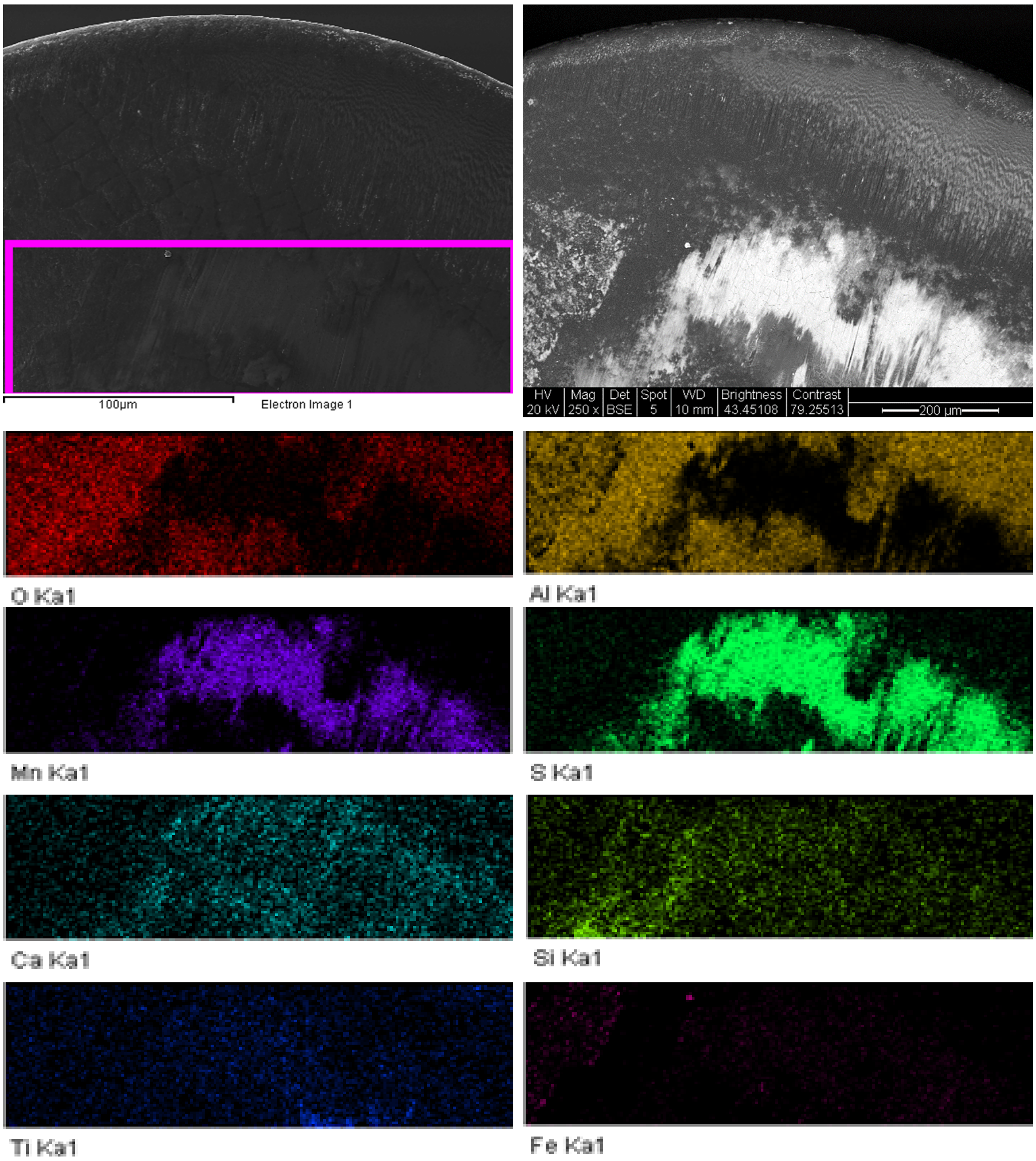

Figure 6.27: EDS map for W2 30:2, 250X SE/BSE, between nose and chip breaker.

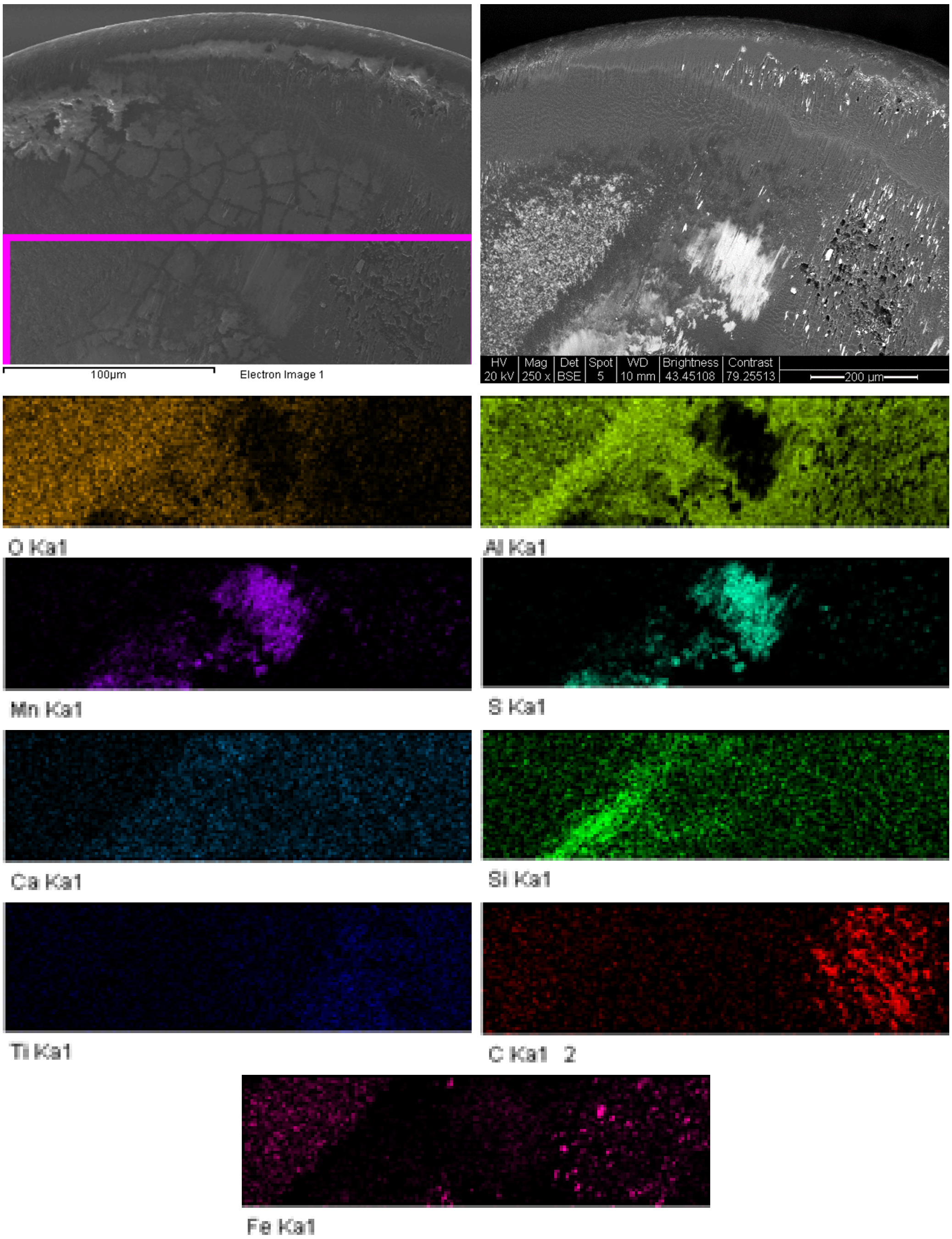

Figure 6.28: EDS map for Z2 30:2, 250X SE/BSE, between nose and chip breaker.

7 Discussion

The inserts that were analysed in this study were obtained from the regular high volume production line of crankshafts. While no significant differences in the flank and nose wear are noted between batches, the inserts from batch Z2 exhibit slightly lower wear compared to the other inserts. Ånmark et al. (2016) reported that oxy-sulphides such as (Al,Mg)O-(Mn,Ca)S can protect the insert edges at the edge-chip interface. (Al,Mg)O-(Mn,Ca)S inclusions are the most frequently identified oxide-rich inclusions in batch Z2. Moreover, both the inserts from batch Z2 showed an absence/reduced amount of MnS layers on the rake surface in addition to an abraded/worn out layer of the Al_2O_3 coating.

Based on these observations, it may be concluded that the slightly lower flank and nose wear measured on these inserts are due to the lower hardness of inclusions. However, as mentioned earlier, the depth of cut varies within specific range in production line under the operational condition. This variation comes from the allowable dimensional tolerances of the previous operations. Hence, the differences observed regarding the flank and nose wear are not solely dependent on the amount and properties of the micro-constituents in the steel, but they may also be the reflection of the process variation itself. According to Kiessling and Lange (1966), (Al,Mg)O inclusions have room temperature hardness of about 24 GPa, and are poorly deformable. The hardness of these complex inclusions as such depends on their stichometry, so depending on the Al and Mg content of the oxides, their hardness varies between Al_2O_3 (about 25-30 GPa) and MgO (about 10 GPa), see Table 7.1. Hence, they may play the abrasive and protective roles depending on their stoichiometries. In this study, on the contrary to the results presented by Ånmark et al. (2016), the (Al,Mg)O inclusions did not act as formable protective layers, see the SEM images in Figure 6.24 and Figure 6.28. Seemingly, their hardness is also within the range or less than that of Al_2O_3 coating, so they have a mild contribution to the abrasive wear.

A layer of NMIs, predominantly MnS, can be observed on the rake face of the inserts. It is well-known that MnS inclusions have a protective role, which often increases when mixed (Mn,Ca)S or (Mn,Mg)S sulphides are formed during the steelmaking process. Additionally, the wear observed on the rake face of inserts from batch Z2 is missing on all the inserts from the other batches. This could also indicate that the MnS layer may be providing protection from mechanically induced and thermally induced wear on the Al_2O_3 coating layer.

Since the machining of the crankshafts took place during regular production, it makes sense that the total number of parts machined per inserts would have been determined based on a safety buffer so that the tool does not fail prematurely, even though the tool may be good enough to machine many more components. Thus, a dedicated tool life test on each batch would have given a much clear understanding about the flank wear progression and the influence of NMIs, perhaps even leading to catastrophic failure of an insert.

Coming to the crankshaft and NMIs present within the material, it should be noted that the MnS inclusions in the transverse direction were highly elongated with some inclusions being longer than 100 µm. Nordberg and Sandström (1981) have previously suggested that inclusions above a particular size become detrimental to machinability, but the size at which they become harmful is not known. The size of these inclusions is based on 2-dimensional examination in the rolling direction. The actual real size of the inclusions examined using 3-dimensional measurement methods would be much different, usually larger than that observed by 2-dimensional examination (Du, 2016).

It should also be noted that oxide-rich NMIs have identical sizes in the radial and transverse samples, as they do not get deformed upon rolling or forging. Thus, a higher area fraction of oxide-rich NMIs in a particular batch indicate that the oxides are either higher in numbers or larger in size compared to the other batches. However, very few oxide-rich inclusions were found to have their largest dimension above 12 µm which can also be observed from the morphology of the oxide-rich inclusions shown in Appendix F. With most of the oxide-rich inclusions being very small, the area fraction also depends on the probability of finding these inclusions during inclusion mapping. As with any statistical data, a higher number of sampling points such as with the inclusion maps, will provide a better representation of the size, distribution, and type of NMIs within a material sample.

It can also be noted that the majority of oxide-rich inclusions are actually oxysulphides, i.e. the inclusions have an oxide core surrounded by sulphides. Additionally, a large proportion of these oxides are complex oxides with spinel and CAS as the major constituents. As the literature study pointed out, calcium treatment of steel is known to reduce the hardness of the pure oxides by forming softer calcium-based oxides, thereby reducing the wear during machining. Ånmark, Karasev et al. (2015) also pointed out that anorthite and gehlenite, which are CAS compounds formed by calcium treatment, improve the machinability of steel due to their lower melting temperatures of approximately 1400 °C and 1500 °C for anorthite and gehlenite respectively, which makes these inclusions much softer and malleable. The same study also found that CaS inclusions would slightly increase the tool wear when compared to the improved machinability gained by pure MnS inclusions. However, the latter observation is not always the case and it is found to depend on the cutting speed and the tool material. For instance, Kiessling and Lange (1978) reviewed the data in literature and reported an increase in tool life when (Mn,Ca)S were present, compared to the cases where only MnS was found in the steels. Comparing Figure 6.11b and Figure 6.11c, it can be observed that the batch S8 and batch Z2 have quite similar area fractions of inclusions for both the sulphides as well as oxide inclusions. The size distribution of the inclusions between these two batches is quite similar as well, as observed in Figure 6.12c and Figure 6.12e. The main differentiating factor between these two batches is the absence of CAS inclusions in batch Z2. The hardness and melting point of a few oxide inclusions are compiled in Table

7.1. In general, higher melting points and higher hardness values of the NMI lead to more detrimental effects during machinability of the steel. Hence, the difference in the wear patterns on the rake face of the inserts between batches P8-W2 and batch Z2 are most probably associated with the presence of deformable CAS inclusions in batches P8-W2 and the absence of CAS inclusions in batch Z2, while still having the presence of harder and non-deformable (Al,Mg)O inclusions.

Table 7.1: Approximate hardness and melting temperature of a few NMIs [23][29][51]

Inclusion	**Hardness (Kg/mm^2)**	**Melting temperature (°C)**
Al_2O_3	3000	2050
(Al,Mg)O	2100-2400	2135
SiO_2	1600	1720
CAS- Gehlenite	1200	1310-1590
CAS- Anorthite	850	1170-1550
MnS	<57.1	1655

Of special interest are the oxide-rich inclusions containing Magnesium, Calcium and Silicon. Du (2016) pointed out that the type of oxides and sulphides depends on the calcium content in the steel. A few other literature studies have explained the benefits of calcium treatment of steel as mentioned in section 4. However, the elements Ca, Mg, and O required to determine the type of inclusions have not been mentioned in the material certificates neither in the VCC standard. Additionally, certain available literature on the study of inclusion characteristics mention that the chemical composition of a material can provide a good understanding about the origin and type of inclusions present in steel. For example, calcium-based inclusions are generally exogenous since calcium is not soluble in the steel melt. Magnesium-based inclusions are also considered as exogenous in most cases. The most probable sources of calcium and magnesium are the refractories and ladles used during casting and secondary steel-making. However, in some modern steels, Ca and Mg are added as deoxidants to modify the inclusion properties. For example, Thunman (2009) mentions the presence of calcium aluminate inclusions formed from the ladle refining process during ladle treatment. The oxygen in the oxide-rich inclusions probably comes in from the air and reacts with the other elements during the steel-making process. The sources of these inclusions can only be traced by a detailed study. The absence of the composition of these elements in the material certificates makes it extremely difficult to predict the type, size, and/or morphology of NMIs that can be expected in the material, especially the oxide-rich NMIs.

Another important point is that the detection of NMIs within the steel without microscopic characterisation techniques is very challenging. Although, it is possible to detect larger inclusions by using non-destructive testing (NDT), they are not very accurate due to the available resolution (Silva, 2019). At the most, these methods would be useful only to detect the clustering of the inclusions and their sizes but would be unable to determine the inclusion distribution and type.

8

Conclusion

There is extensive literature on the effects of non-metallic inclusions but most of it is focused towards free machining steel and/or a comparison between different types of manufactured steels. While the effect of different inclusions on machinability has been established, there are very few studies that focus on improving the machinability from a production point of view such as predictability of the material behaviour and so on. These studies focus more towards material/steel development using inclusion engineering. Accordingly, the most prominent NMIs found in steel are sulphide and oxides wherein the NMIs with higher hardness and higher melting temperatures are considered detrimental for machinability. The formation of these inclusions in the steel and their subsequent properties are influenced by the process parameters involved in steelmaking. Sulphide inclusions such as MnS, CaS, and (Mn,Ca)S are considered good for machinability as they form protective layers on the different cutting surfaces of the tool, thereby reducing tool wear. On the other hand, oxide inclusions are considered detrimental for machinability (due to higher hardness or chemical affinity with the coating). However, these oxide inclusions can be modified to form different complex oxy-sulphide inclusions, which are softer than the pure oxides and as a consequence can be less detrimental to machinability and may even improve machinability in some cases such as when Calcium-Alumina-Silicates (CAS) are formed, as suggested by some studies.

In this study, a difference in the wear patterns on the cutting edges of the inserts was observed with each changing batch, although the actual differences in wear among the different inserts were within the allowances for depth of cut variations. This can be attributed to the fact that these inserts were obtained from a regular production process where surface roughness of the machined crankshaft was the criterion for tool change. In terms of the crankshaft materials, the key difference between the batches was that the area fraction of the inclusions was different for each batch, with the exception of batch S8 and Z2 having quite similar area fractions. The key difference between batch Z2 and S8 (even other batches), was that the CAS inclusions were missing in the batch Z2. Thus, the rake surface of inserts from Z2 exhibited lesser NMI layer deposition on all the inserts of Z2, thereby exhibiting a significantly different wear of the Al_2O_3 coating wherein the Al_2O_3 coating layer was eroded/damaged. On the other hand, all the inserts from other batches had the presence of CAS inclusions and exhibited the presence of a protective layer on the rake surface of the inserts at the same location where the inserts from batch Z2 showed a damaged Al_2O_3 coating layer. This perhaps indicates the beneficial protective and lubricative effects of layers formed on the tool surfaces due to presence of soft and chemico-physically stable inclusions. This observation also validates

the conclusions of some previous studies which highlight the importance of certain inclusions in protecting the cutting tools during machining.
The majority of the analysed oxide-rich NMIs were complex oxy-sulphides with an oxide core which was surrounded by sulphides. The elements Ca and Mg which were not reported in the material certificate of any batch, formed most of the oxide-rich NMIs. Almost all the complex oxides identified in this study had the presence of a magnesium-aluminum based oxide constituent followed by a calcium-silicon-aluminum based oxide, except for batch Z2 which had no calcium-silicon-aluminum based oxide constituent. Elements such as calcium, magnesium and oxygen were not reported in the chemical certificates of the material. Moreover, the current VCC standard does not require the material manufacturer to report these elements (Ca, Mg, and O) in the chemical certificates. Additionally, the microstructure of the material and the tested hardness is consistent with the material certificate for each batch. This indicates that there are batch variations occurring with respect to the presence of different non-metallic inclusions within the steel. And as observed with the layer formation on the cutting tools from different batches, these batch variations influence the type of wear occurring on the surface of the cutting tools. Thus, the current results indicate the presence of batch variations which affect the cutting tools differently based on the type of NMIs present in the crankshaft material. However, prediction of the material behaviour and tool wear during machining would require additional work.

8.1 Future work and recommendations

- The surface of the inserts below the MnS inclusion layers should be examined by removing the MnS layer. This would provide a good understanding of the condition of the Al_2O_3 coating layer below the inclusion layer.
- The interlamellar spacing among the pearlite colonies should be measured to examine if there are any differences between the batches as some studies indicate that the lamellar spacing affects the strength of the material which may also affect machinability.
- The current EDS analysis on its own is inadequate to understand the exact composition of the NMIs. Thus, additional experimentation such as electrolytic extraction and Auger Electron Spectroscopy (AES) could be performed to understand and confirm the composition and morphology of the NMIs. The composition of the NMIs can give a rough indicator on where to concentrate the improvement efforts, for example, material development or machining process optimisation.
- Dedicated tool life tests with flank wear as a wear criterion would enable an easier comparison and understanding of the actual effects of NMIs on the tool life.

Bibliography

[1] Alessandro, Paolo C., and Millefanti, Giorgetti U. (2017). *Current challenges in material choice for high-performance engine crankshaft.* DOI: 10.1016/j.prostr.2017.12.048 [Accessed 07 March 2019]

[2] ASM Handbook (1990). *Properties and Selection: Irons, Steels, and High-Performance Alloys.* ASM Handbook Committee, 1990, Volume 1. DOI: 10.31399/asm.hb.v01.9781627081610 [Accessed 11 April 2019]

[3] Bielefeldt, Wagner V., Vilela, Antonio Cezar F. (2015). *Study of inclusions in high sulfur, al-killed ca-treated steel via experiments and thermodynamic calculations.* Steel Research International. April 2015, Vol. 86 Issue 4, p375, 11 p. DOI: 10.1002/srin.201400112 [Accessed 19 March 2019]

[4] Bhadeshia, H., and Honeycombe, R. (2017). *Steels: microstructure and properties, fourth edition.* [Accessed 07 March 2019]

[5] Brandaleze, E., Hereñu, S., Tormo, J., and Alvarez, I. (2013). *Characterisation of inclusions in resulphurised microalloyed steel.* Ironmaking and Steelmaking 40(3):216-220 · April 2013. DOI: 10.1179/1743281212Y.0000000031 [Accessed 02 April 2019]

[6] Bryson, William E. (2015). *Heat Treatment - Master Control Manual.* Hanser Publishers. [Accessed 28 February 2019]

[7] Chen, Y., Bao, Y., Wang, M., Cai, X., Wang, L. and Zhao, L. (2014). *Basic research on mechanism of BN inclusion in improving the machinability of steel.* REVISTA DE METALURGIA. 50(4):e028, 2014. DOI: 10.3989/revmetalm.028 [Accessed 16 August 2019]

[8] Chen, Y., Bao, Y., Wang, M., Cai, X., Wang, L. and Zhao, L. (2016). *Superior machinability of steel enhanced with BN and MnS particles.* International Journal of Minerals, Metallurgy, and Materials. Volume 23, Issue 3, pp 276–282, March 2016. DOI: 10.1007/s12613-016-1236-x#citeas [Accessed 16 August 2019]

[9] *CHEMICAL COMPOSITION.* (n.d.). Available from https://www.materials.sandvik/en/products/trademarks/sanmac/chemical-

composition. [Accessed 20 January 2019]

[10] Dovebro, M. (2012). *Correlation between material properties, grinding eects and Barkhausen noise measurements for two crankshaft steels.* Master's Thesis in Applied Physics, Chalmers University of Technology. Available from http://publications.lib.chalmers.se/records/fulltext/164652.pdf [Accessed 07 March 2019]

[11] Du, H. (2016). *The evaluation of non-metallic inclusions in calcium-treated steel by using electrolytic extraction.* Degree project in materials science and engineering, KTH Royal Institute of Technology. Available from: https://kth.diva-portal.org/smash/get/diva2:957615/FULLTEXT01.pdf [Accessed 06 June 2019]

[12] Fulemova, J., Janda, Z. (2014). *Influence of the Cutting Edge Radius and the Cutting Edge Preparation on Tool Life and Cutting Forces at Inserts with Wiper Geometry.* Procedia Engineering Volume 69, 2014, Pages 565-573 open access. DOI: 10.1016/j.proeng.2014.03.027 [Accessed 02 April 2019]

[13] Gassner, M., Schalk, N., Tkadletz, M., Czettl, C., Mitterer, C. (2019). *Thermal crack network on CVD TiCN/*α*-*Al_2O_3*coated cemented carbide cutting tools.* International Journal of Refractory Metals and Hard Materials. Volume 81, pages 1-6. DOI:10.1016/j.ijrmhm.2019.02.006 [Accessed 30 May 2019]

[14] Hashimura, M., Mizuno, A., and Miyanishi, K. (2009). *Effect of MnS distribution on machinability in low carbon free-cutting steel.* Iron and Steel Technology, September 2009, 6(9), 45-51. [Accessed 05 April 2019]

[15] Helle, A. (1995). *On the interaction between inclusions in steel and the cutting tool during machining.* Acta Polytechnica Scandinavica: Chemical Technology Series, 1995, Ch 228. [Accessed 08 April 2019]

[16] Hoier, P., Malakizadi, A., Friebe, S., Klement, U., Krajnik, P. (2019). *Microstructural variations in 316L austenitic stainless steel and their influence on tool wear in machining.* DOI: 10.1016/j.wear.2019.02.024 [Accessed 16 June 2019]

[17] Jamshidi, A., Cave, J., Maropoulos, P., Ansell, M. (2014). Manufacturing process challenges when machining Superalloys. [Accessed 27 March 2019]

[18] Jiang, L., Cui, K., and Hfinninen H. (1996). *Effects of the composition, shape factor and area fraction of sulfide inclusions on the machinability of re-sulfurized free-machining steel.* Journal of Materials Processing Technology, 58, 1996, 160-165. [Accessed 03 April 2019]

[19] Jung, I., Decterov, S., and Pelton, A. (2004). *A thermodynamic model for deoxidation equilibria in steel.* Metallurgical and Materials Transactions B. Volume 35, Issue 3, pp 493–507. June 2004. DOI: 10.1007/s11663-004-0050-4 [Accessed 16 August 2019]

[20] Kiessling, R. and Lange, N. (1964). *Non-Metallic Inclusions in Steel- Part-I.* [Accessed 28 January 2019]

[21] Kiessling, R. and Lange, N. (1966). *Non-Metallic Inclusions in Steel- Part-II.* [Accessed 28 January 2019]

[22] Kiessling, R. and Lange, N. (1978). *Non-Metallic Inclusions in Steel- Part-IV.* [Accessed 28 January 2019]

[23] Klocke, F. (2011). *Manufacturing Processes 1.* Springer Berlin Heidelberg, Berlin, Heidelberg. DOI:10.1007/978-3-642-11979-8 [Accessed 08 March 2019]

[24] Lam, P. (2016). *Three-dimensional Investigations of Different Sulfides in Steels by Using Electrolytic Extraction.* Master Thesis. KTH Royal Institute of Technology. Available from: http://www.diva-portal.org/smash/get/diva2:1044324/FULLTEXT01.pdf [Accessed 14 July 2019]

[25] Liu, H. and Chen, W. (2012). *Effect of total oxygen content on the machinability of low carbon resulfurized free cutting steel.* Steel Research International 2012; 83(12): 1172–1179. DOI: 10.1002/srin.201200053 [Accessed 18 March 2019]

[26] *Machining success requires a productive balance.* (n.d.) Available from https://www.secotools.com/#article/21477?language=en [Accessed 22 January 2019]

[27] Mahmutović, A., Nagode, A., Rimac, M., and Mujagić, Derviš. (2017). *Modification of the inclusions in austenitic stainless steel by adding tellurium and zirconium.* Materiali in tehnologije. 51. 523-528. DOI: 10.17222/mit.2015.297 [Accessed 14 March 2019]

[28] Mandal, S. K. (2015). *Steel Metallurgy: Properties, Specifications and Applications, Ch 1-3.* [Accessed 01 July 2019]

[29] *MATERIAL CONSISTENCY.* (n.d.). Available from https://www.materials.sandvik/en/products/trademarks/sanmac/material-consistency/ [Accessed 11 March 2019]

[30] Matsuno, F., Nishikida, S., and Ikesaki, H. (1985). *Mechanical Properties of Manganese Sulphides in the Temperature Range between Room Temperature*

and 1000 °C. Transactions ISIJ, Vol. 25, 1985, pp 989-998. [Accessed 14 July 2019]

[31] Nordberg, H. and Sandström, R. (1981). *Swedish Symposium on Non-Metallic Inclusions in Steel.* [Accessed 15 January 2019]

[32] NPTEL (2015). Available from https://nptel.ac.in/courses/113104059/2 [Accessed 28 February 2019]

[33] Ruppi, S., Högrelius, B., and Huhtiranta, M. (1998). Wear characteristics of TiC, Ti(C,N), TiN and A12O3 coatings in the turning of conventional and Ca-treated steels. International Journal of Refractory Metals and Hard Materials 16(4-6):353-368. December 1998. DOI: 10.1016/S0263-4368(98)00039-0 [Accessed 03 April 2019]

[34] Sandvik (2017). *Metal Cutting Handbook.* Available from https://www.sandvik.coromant.com/en-us/services/education/pages/e-learning.aspx. [Accessed 13 February 2019]

[35] Scurria, M., Emre, S., Möller, B., Wagener, R. et al. (2017). *Evaluation of the Influence of MnS in Forged Steel 38MnVS6 on Fatigue Life.* SAE Int. J. Engines 10(2): 366-372. DOI: 10.4271/2017-01-0353 [Accessed 11 March 2019]

[36] Sinha, N. (2011). *Machining.* Lecture notes. Available from: http://home.iitk.ac.in/ nsinha/Machining%20II.pdf. [Accessed 13 February 2019].

[37] Silva, André L. V. (2018). *Non-metallic inclusions in steels – origin and control.* [Accessed 28 February 2019]

[38] Silva, André L. V. (2019). *The effects of non-metallic inclusions on properties relevant to the performance of steel in structural and mechanical applications.* [Accessed 09 July 2019]

[39] Surreddi, Kumar B., Björkeborn, K. and Klement, U. (2013). *Effect of heat treatment on chip formation in a case hardening steel.* Journal of Materials and Chemical Engineering. 1.1-7. [Accessed 28 March 2019]

[40] Tanaka, R., Yamane, Y., Sekiya, K., Narutaki, N. and Shiraga, T. (2007). *Machinability of BN free-machining steel in turning.* International Journal of Machine Tools and Manufacture. 47(12), pp 1971-1977, October 2007. DOI: 10.1016/j.ijmachtools.2007.02.003 [Accessed 16 August 2019]

[41] Thunman, M. (2009). *Formation of Inclusions and their Development during Secondary.* Doctoral Thesis. KTH Royal Institute of Technology. Available from: https://www.diva-portal.org/smash/get/diva2:217063/FULLTEXT01.pdf [Ac-

cessed 06 June 2019]

[42] Verma, N., Pistorius, P., Fruehan, R., Potter, M., Oltmann, H., and pretorius, E. (2012). *Calcium Modification of Spinel Inclusions in Aluminum-Killed Steel: Reaction Steps.* Metallurgical and Materials Transactions B.Volume 43, Issue 4, pp 830–840. August 2012. DOI: 10.1007/s11663-012-9660-4 [Accessed 16 August 2019]

[43] Volvo Car Corporation. (2018). *Crank shaft quality control in Volvo Cars' engine factory in Skövde, Sweden.* Available from: https://www.media.volvocars.com/se/sv-se/media/photos/219342/crank-shaft-quality-control-in-volvo-cars-engine-factory-in-skovde-sweden [Accessed 16 August 2019]

[44] Wang, YN., Yang, J. and Bao, Y.P. (2014). *Effects of Non-metallic Inclusions on Machinability of Free-Cutting Steels Investigated by Nanoindentation Measurements.* Metallurgical and Materials Transactions A (2015) 46: 281. DOI: 10.1007/s11661-014-2596-3 [Accessed 02 April 2019]

[45] Wente, Edward F., Nutting, J. and Wondris, E.F. (2017). *Steel-Encyclopaedia Britannica.* [Accessed 28 February 2019]

[46] Xia, X., Zhang, J. and Zou, Y. (2015). *An investigation on the machinability of newly developed low-carbon sulphurised free-cutting steels.* Proceedings of the Institution of Mechanical Engineers, Part B: Journal of Engineering Manufacture, 1 September 2016, 230(9):1592-1599. DOI: 10.1177/0954405415599944 [Accessed 18 March 2019]

[47] Yang, S., Li, J., Zhang, L., Peaslee, K. and Wang, Z. (2010). *Evolution of $Mgo \cdot Al_2O_3$ Based Inclusions in Alloy Steel During the Refining Process. Steel Making.* Metallurgical and Mining Industry, 2010, Vol. 2, No. 2. [Accessed 14 July 2019]

[48] Yaguchi, H. (1986). *Effect of MnS inclusion size on machinability of low-carbon, leaded, resulfurized free-machining steel.* Journal of Applied Metalworking, Jul1986, Vol. 4 Issue 3, p214-225. [Accessed 05 April 2019]

[49] Zhang, G.L., An, Q.L., Chen, M., Zhang, Y.S. and Liu, G. (2009). *8th CHINA-JAPAN International Conference on Ultra-Precision Machining, CJICUPM2008.* Advanced Materials Research, 2009, 69-70:510-514 Language: English. DOI: 10.4028/www.scientific.net/AMR.69-70.510 [Accessed 05 April 2019]

[50] Zumdahl, S. (2009). *Carbide-Encyclopaedia Britannica.* [Accessed 28 February 2019]

[51] Ånmark, N., Karasev, A. and Jönsson, Pär G. (2015).*The Effect of Different Non-Metallic Inclusions on the Machinability of Steels.* [Accessed 22 January 2019]

[52] Ånmark, N., Lövquist, S., Vosough, M., Björk, T. (2015). *The Effect of Cleanliness and Micro Hardness on the Machinability of Carburizing Steel Grades Suitable for Automotive Applications.* Steel Research International; 2016: 87 (4); p403-p412. DOI: 10.1002/srin.201500243 [Accessed 18 March 2019]

[53] Ånmark, N., Björk, T., Karasev, A. and Jönsson, Pär G. (2015). *Effect of different inclusions on mechanical properties and machinability of 20NiCrMo carburizing steels.* [Accessed 02 April 2019]

[54] Ånmark, N., Karasev, A. and Jönsson, Pär G. (2016). *The Influence of Microstructure and Non-Metallic Inclusions on the Machinability of Clean Steels.* Steel Research Institute 88(1), 2017. DOI: 10.1002/srin.201600111 [Accessed 14 March 2019]

[55] Ånmark, N. and Björk, T. (2016). *Effects of the composition of Ca-rich inclusions on tool wear mechanisms during the hard-turning of steels for transmission components.* Wear, Volumes 368–369, 2016, Pages 173-182, ISSN 0043-1648. DOI: 10.1016/j.wear.2016.09.016 [Accessed 02 April 2019]

A

Topographic images of inserts

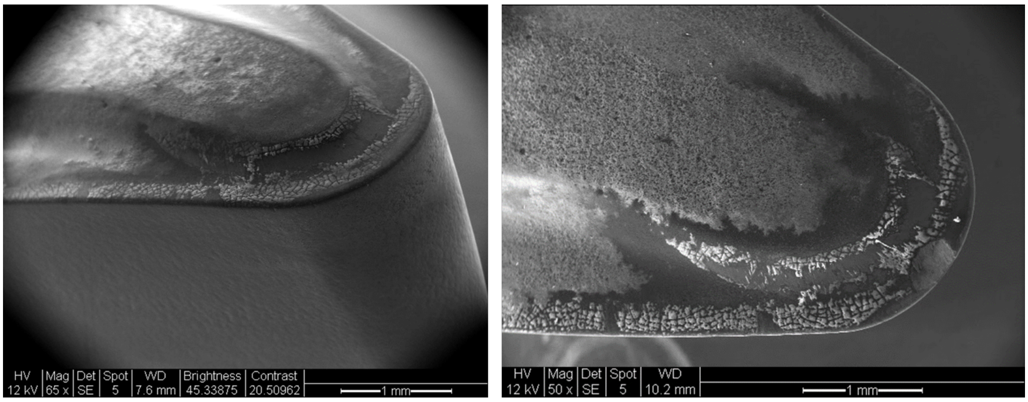

Figure A.1: G8- Left: 30:1-2 Isometric View, Right: 30:2-1 top view

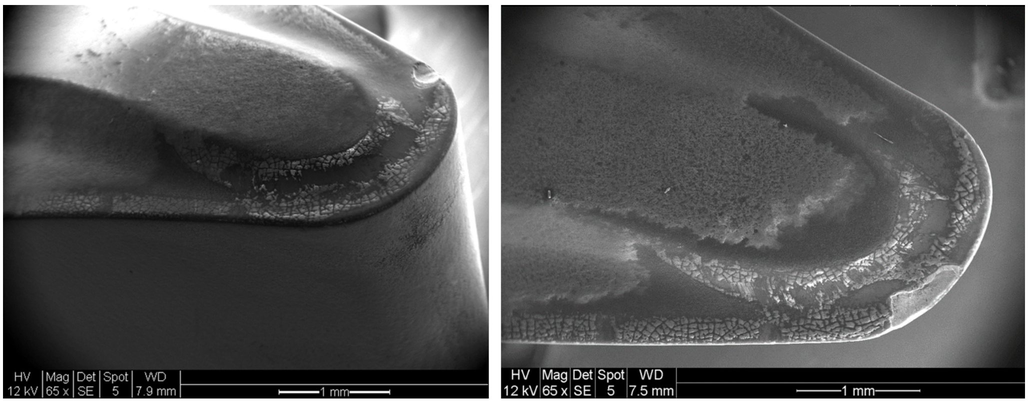

Figure A.2: P8- Left: 30:1-2 isometric view, Right: 30:2-2 top view

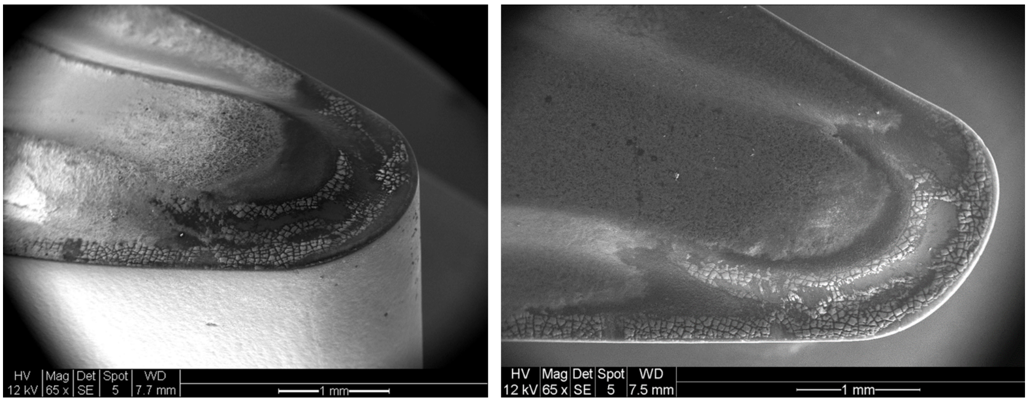

Figure A.3: S8- Left: 30:2 isometric view, Right: S8 30:1 top view

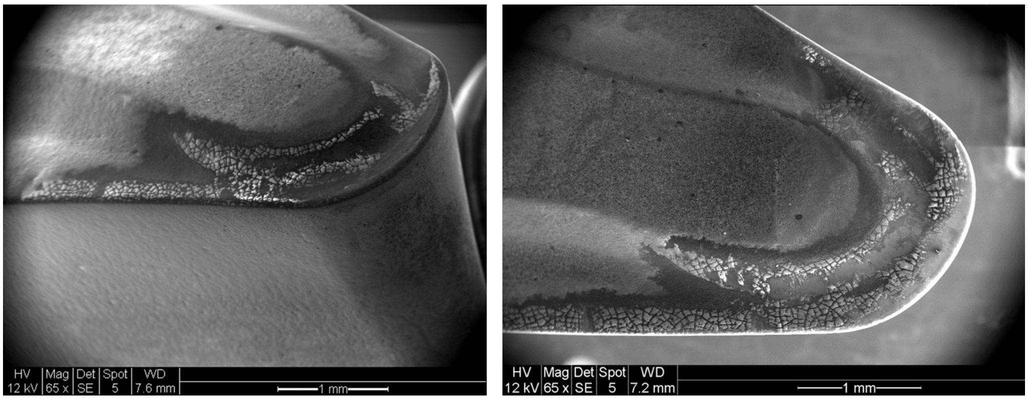

Figure A.4: Left: Z2-30:1 isometric view, Right: W2-30:1 top view

B

Images for flank and nose wear on inserts

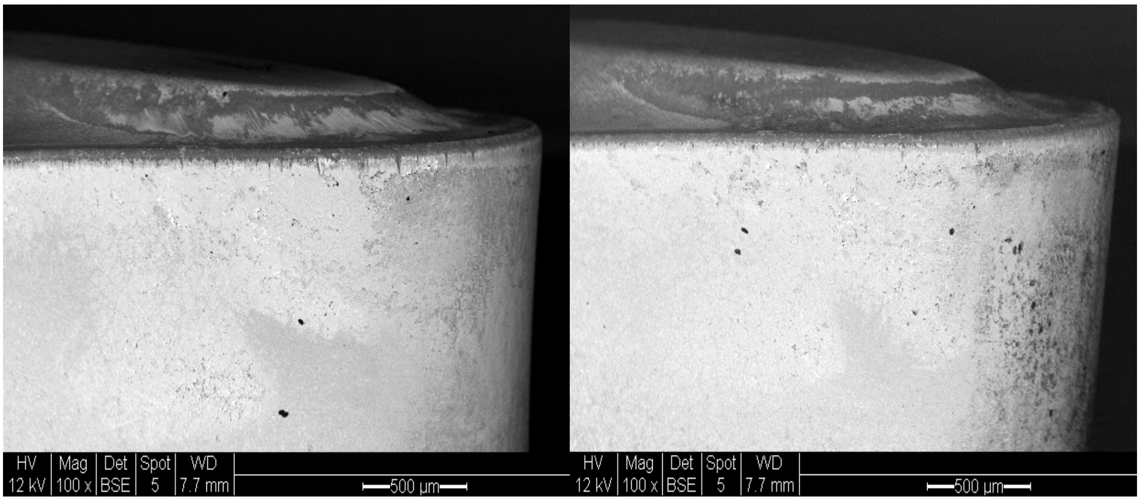

Figure B.1: Flank wear- Left: W2 30:1, VB_{BMax}= 52.9 µm VB_C=97µm. Right: Z2 30:1, VB_{BMax}= 37.5 µm VB_C=85.2µm

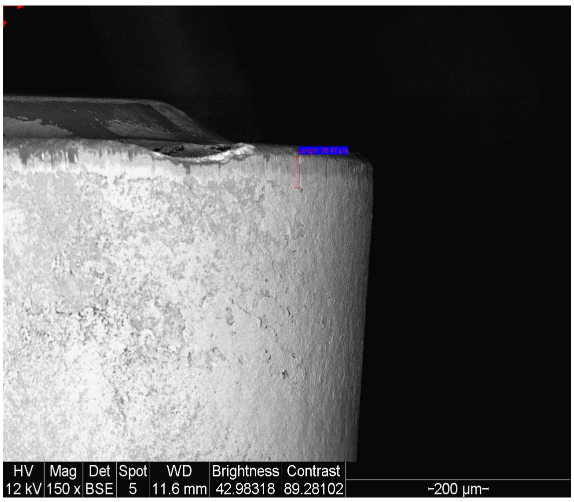

Figure B.2: Nose wear for P8 30:1-1, VB_C=98µm

C

Layer formation and plastic deformation on the rake surface of inserts

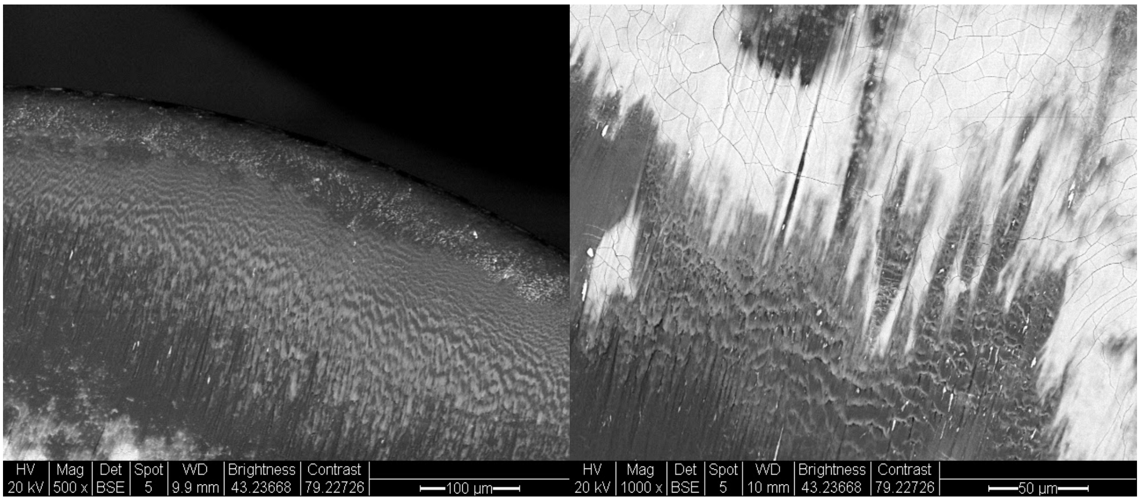

Figure C.1: W2- 500X BSE. Left: 30:2 top view, nose. Right: 30:1 top view, between nose and chip breaker.

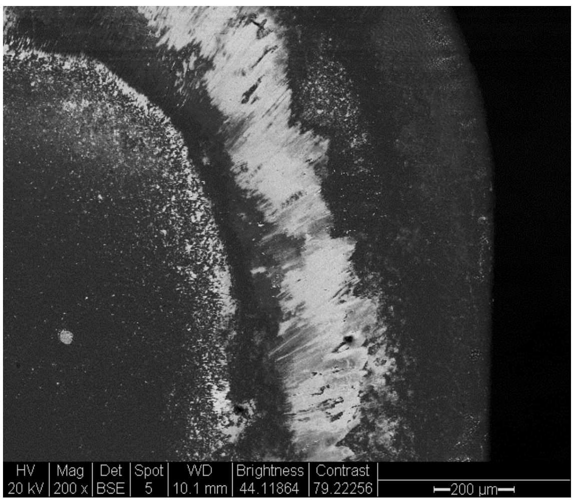

Figure C.2: W2- 200X, BSE, 30:1 top view, between flank and chip-breaker

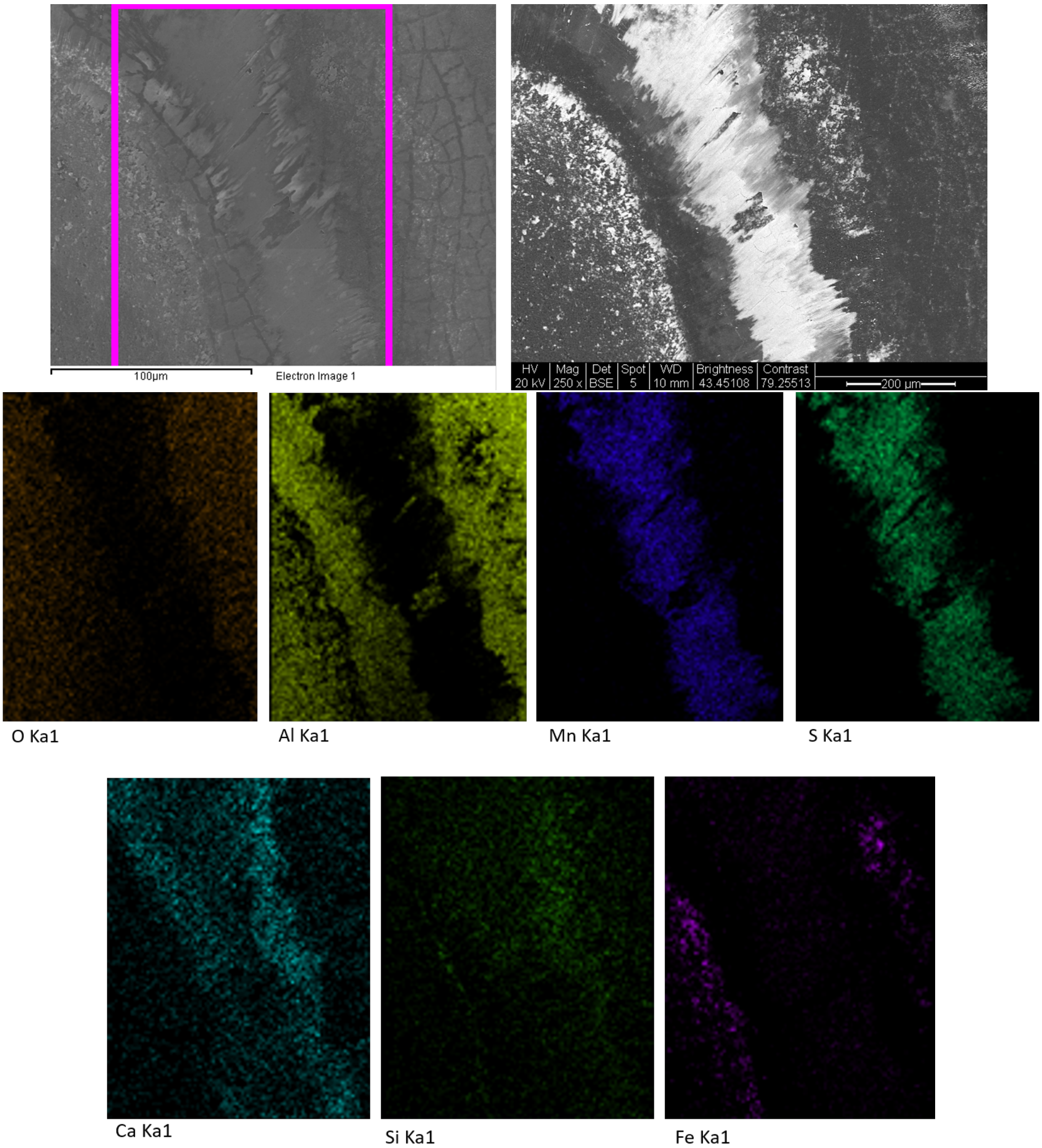

Figure C.3: EDS map for P8 30:2-1, 250X SE/BSE, between flank and chip breaker

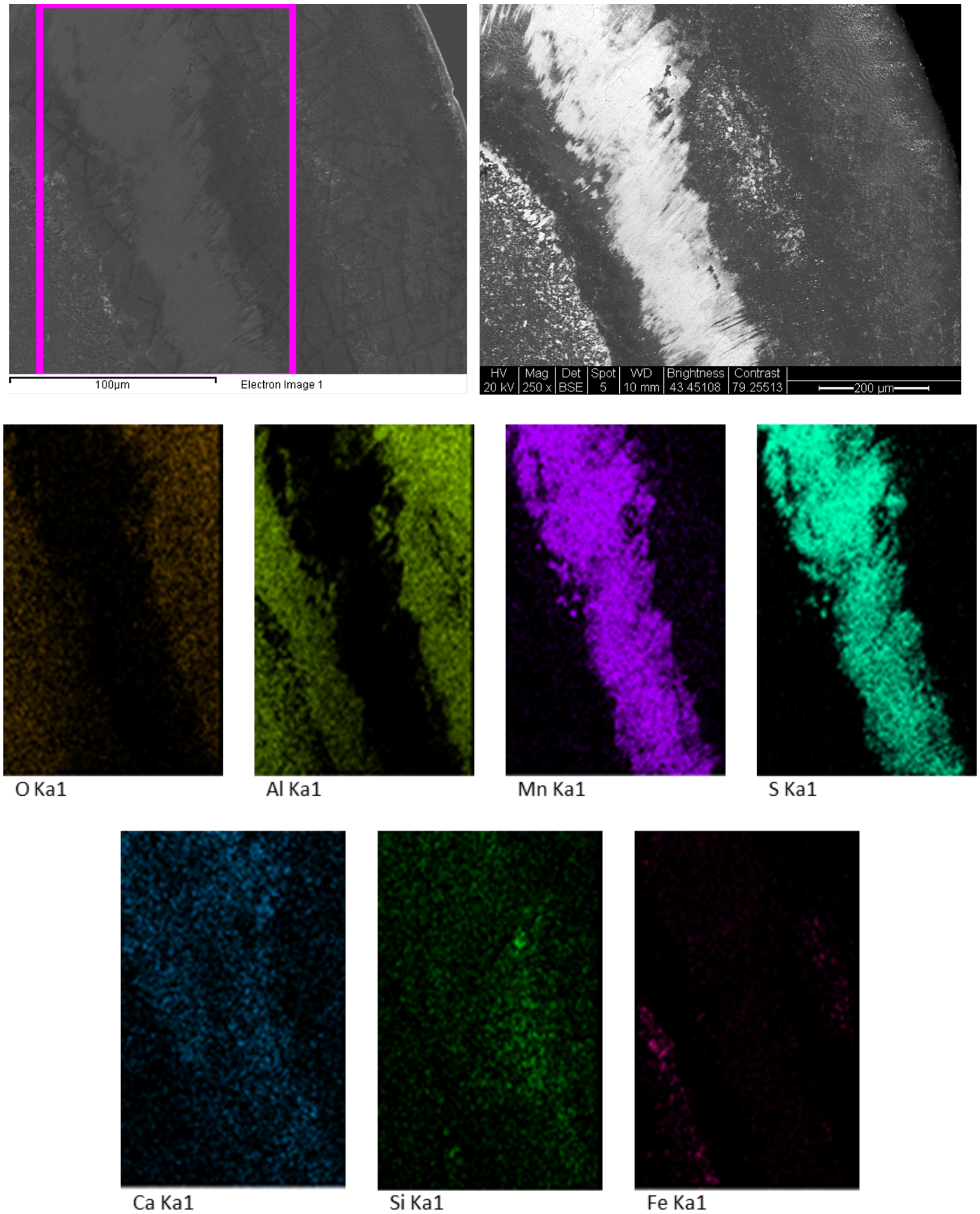

Figure C.4: EDS map for W2 30:2, 250X SE/BSE, between flank and chip breaker

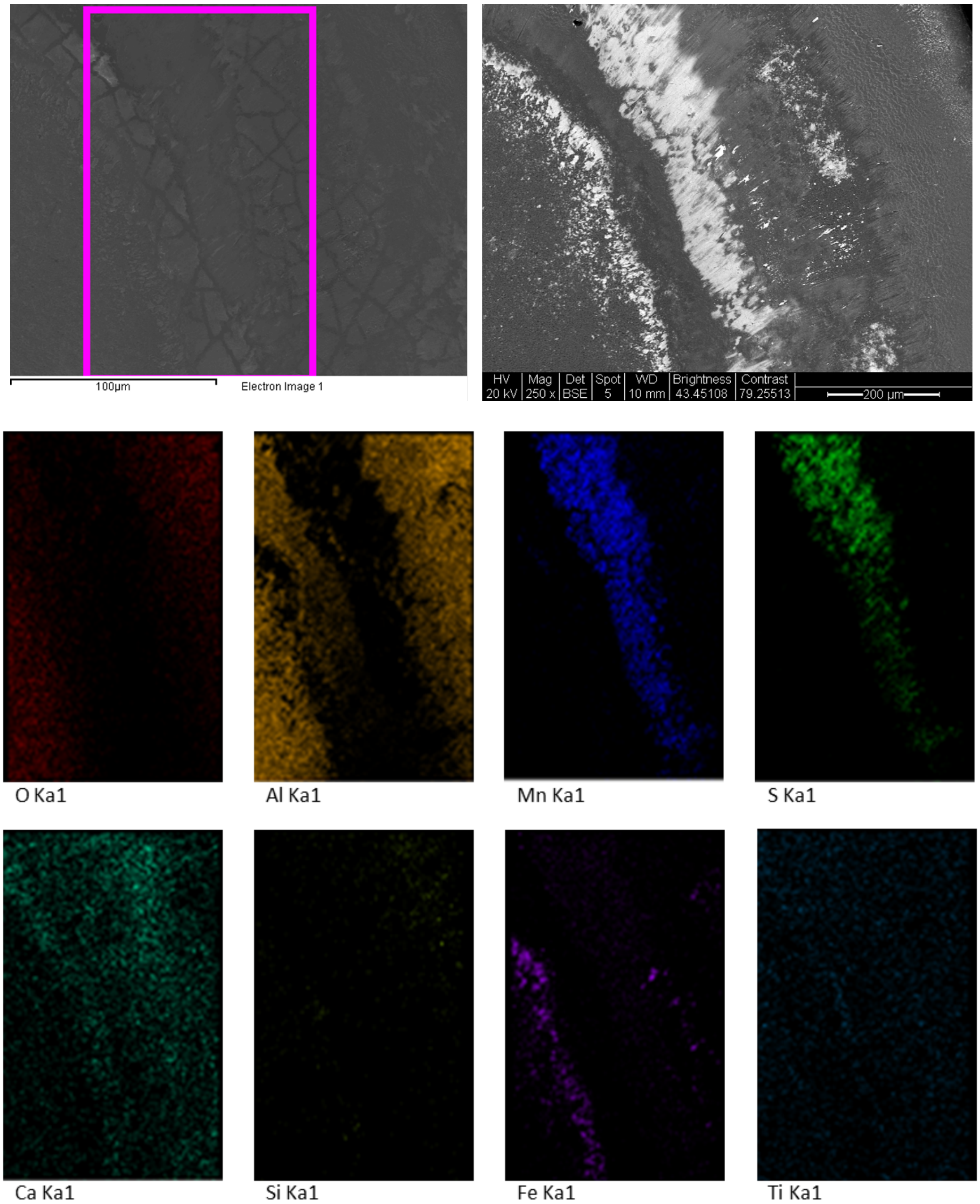

Figure C.5: EDS map for Z2 30:2, 250X SE/BSE, between flank and chip breaker

D
Inclusion mapping

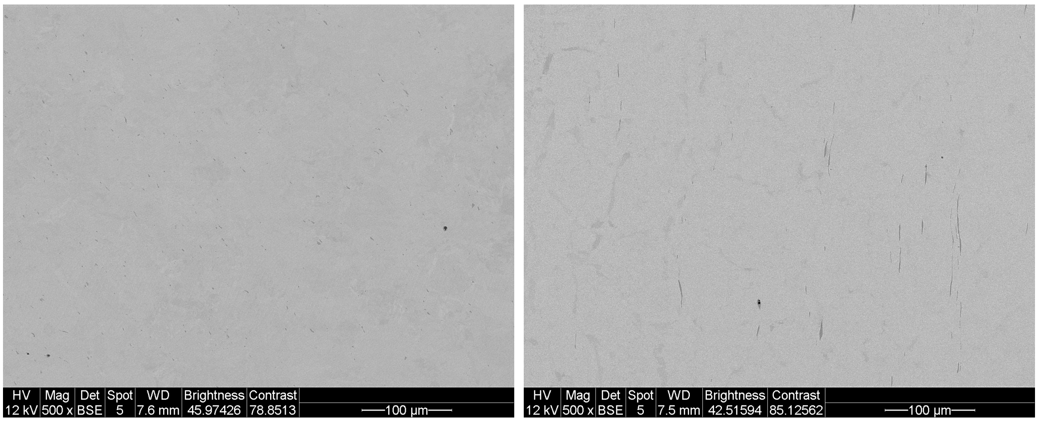

Figure D.1: Z2 inclusion map- Left: Radial cross-section, Right: Transverse cross-section

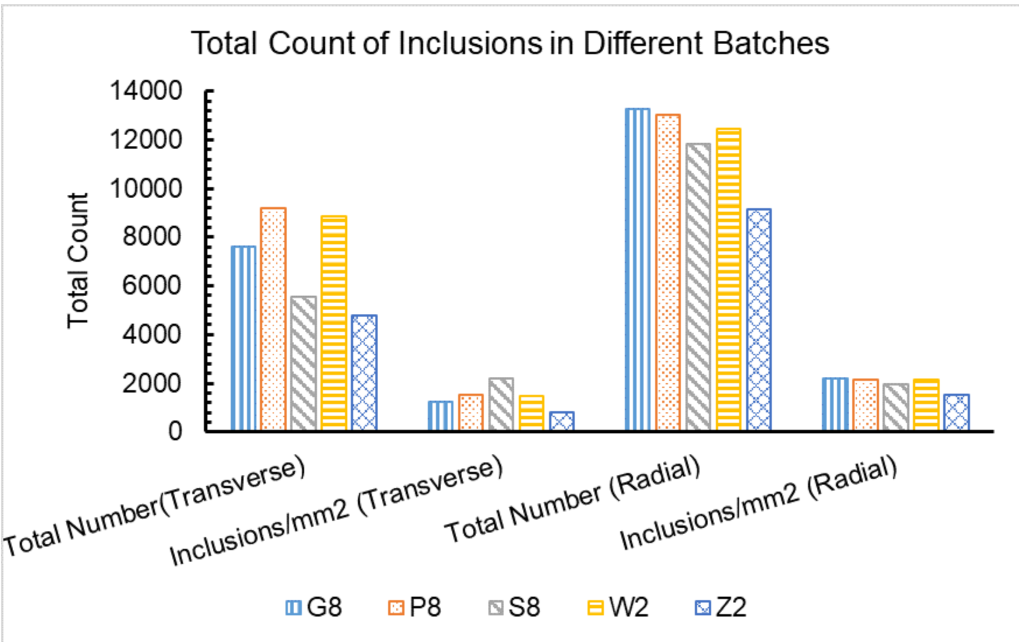

Figure D.2: Total count of inclusions in different batches

E

Normal distribution of inclusions based on area

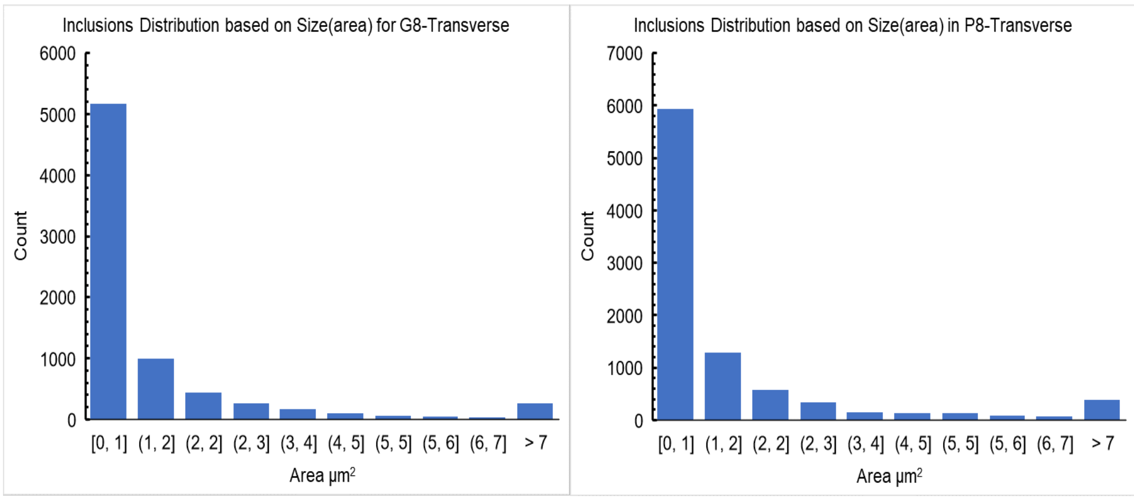

Figure E.1: Distribution of inclusions for transverse samples. Left: G8, Right: P8

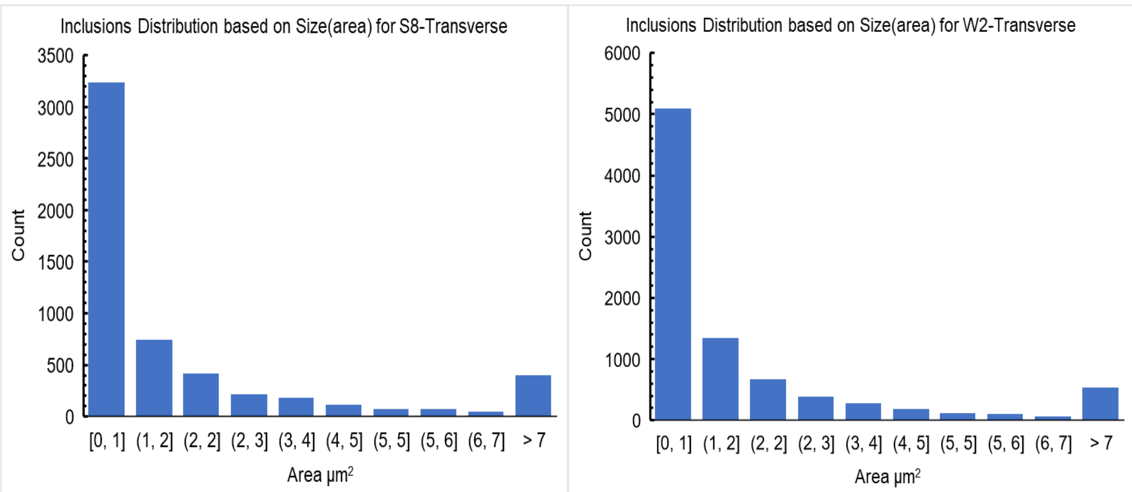

Figure E.2: Distribution of inclusions for transverse samples. Left: S8, Right: W2

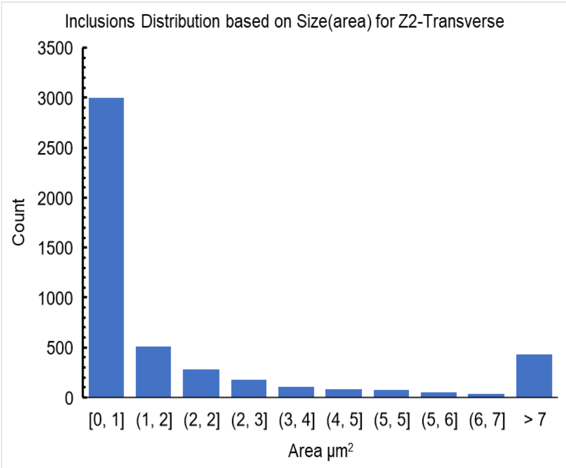

Figure E.3: Distribution of inclusions for transverse sample. Z2

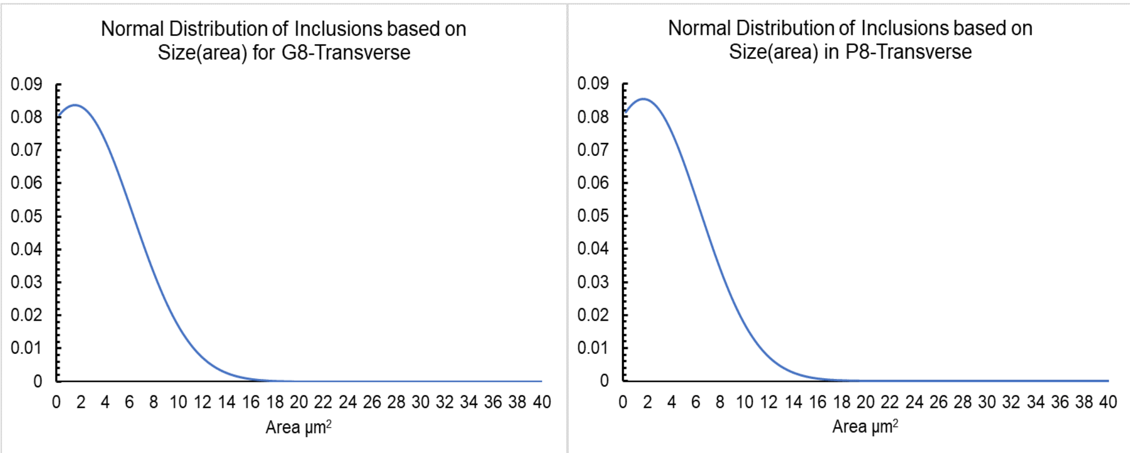

Figure E.4: Normal distribution of inclusions for transverse samples. Left: G8, Right P8

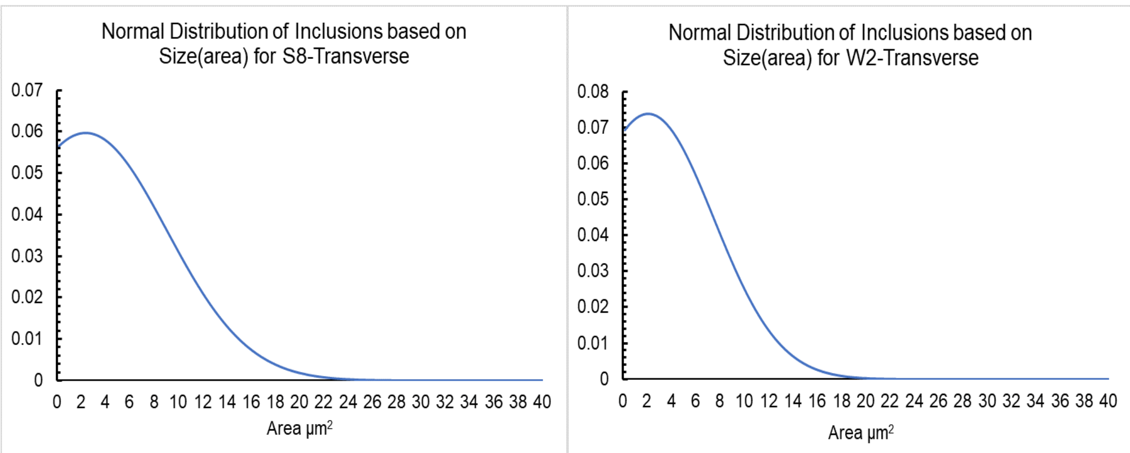

Figure E.5: Normal distribution of inclusions for transverse samples. Left: S8, Right W2

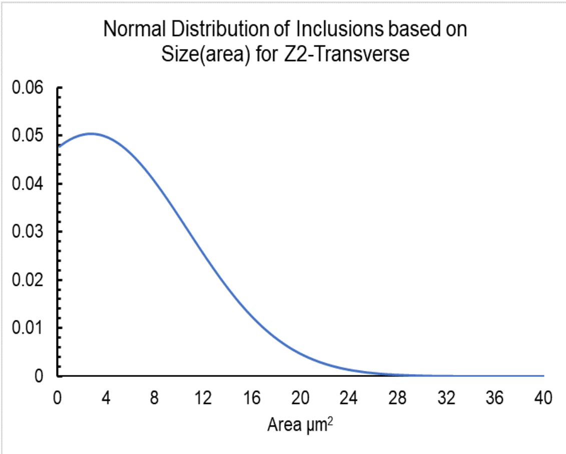

Figure E.6: Normal distribution of inclusions for transverse sample. Z2

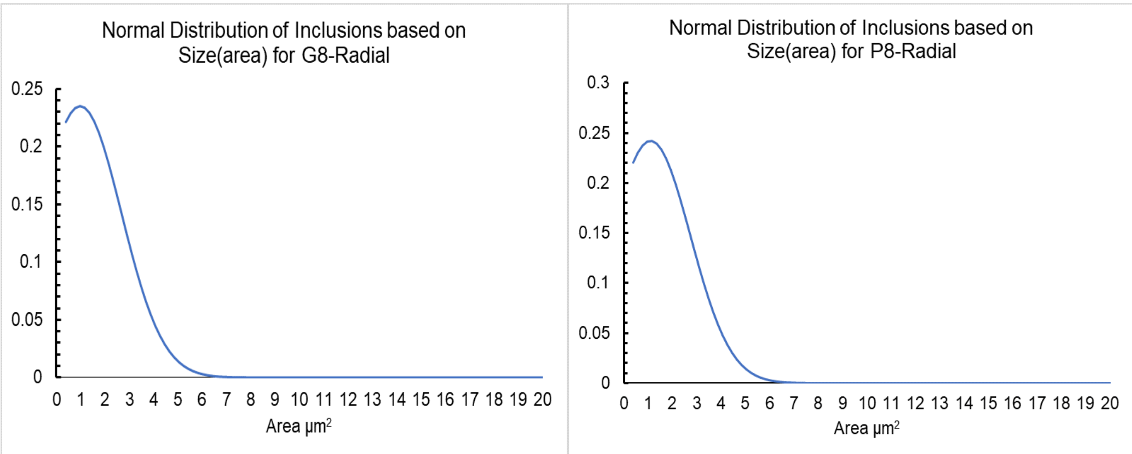

Figure E.7: Normal distribution of inclusions for radial samples. Left: G8, Right P8

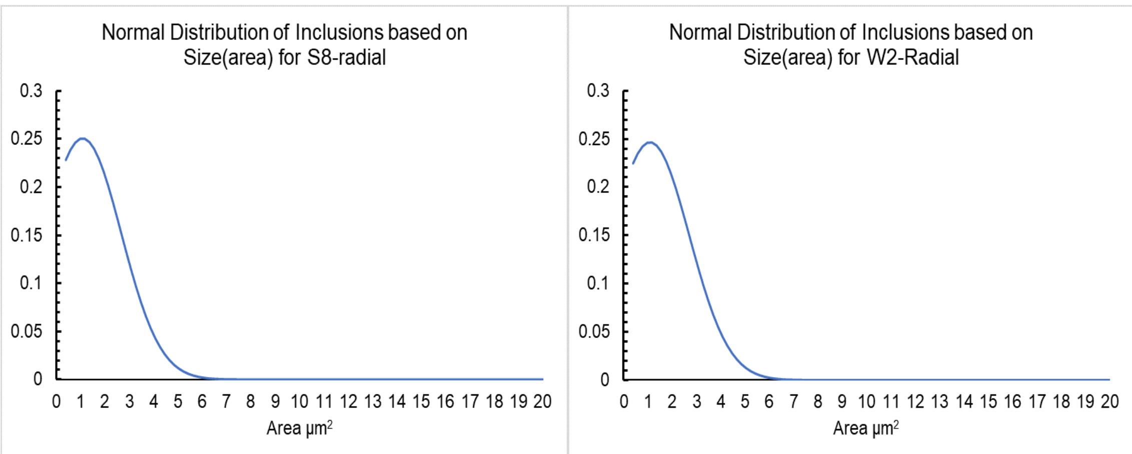

Figure E.8: Normal distribution of inclusions for radial samples. Left: S8, Right W2

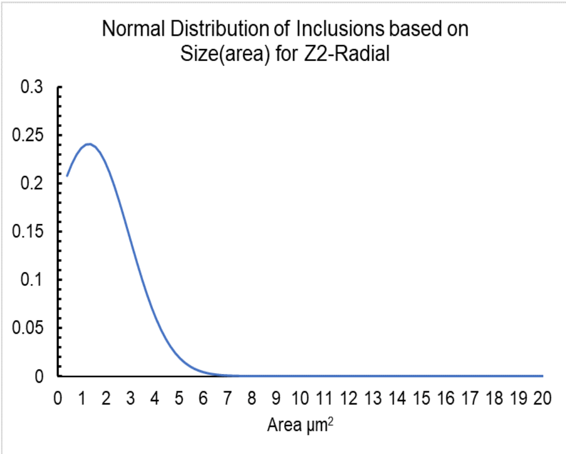

Figure E.9: Normal distribution of inclusions for radial sample. Z2

F

Composition of oxy-sulphide inclusions

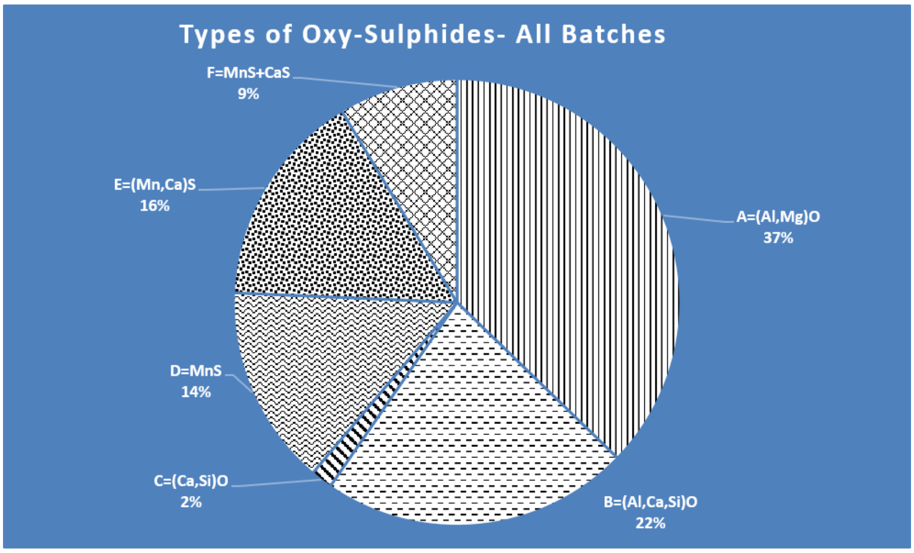

Figure F.1: Amount and type of oxy-sulphides in all batches combined

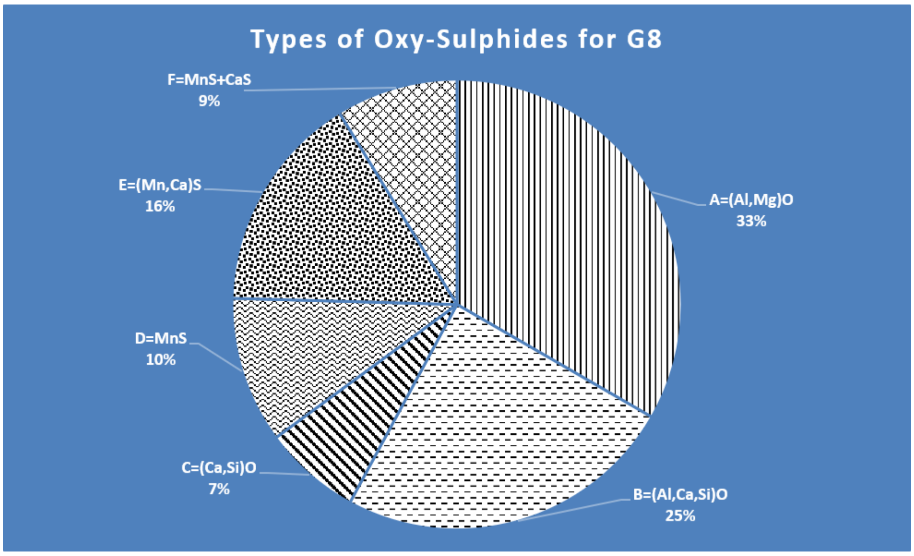

Figure F.2: Amount and type of oxy-sulphides in G8

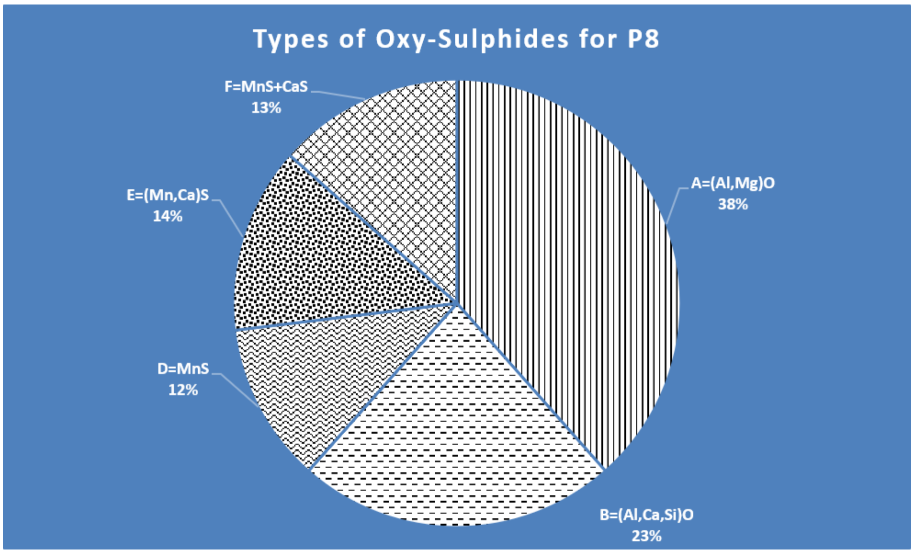

Figure F.3: Amount and type of oxy-sulphides in P8

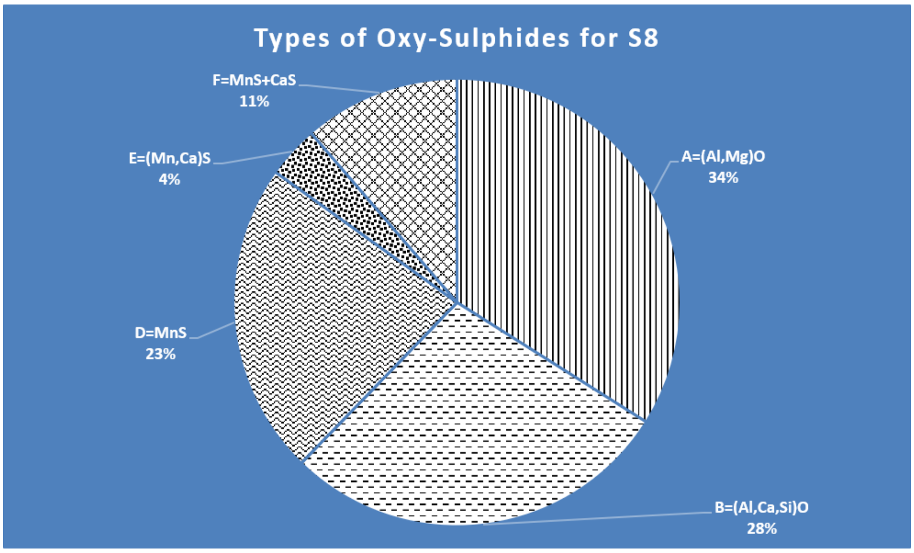

Figure F.4: Amount and type of oxy-sulphides in S8

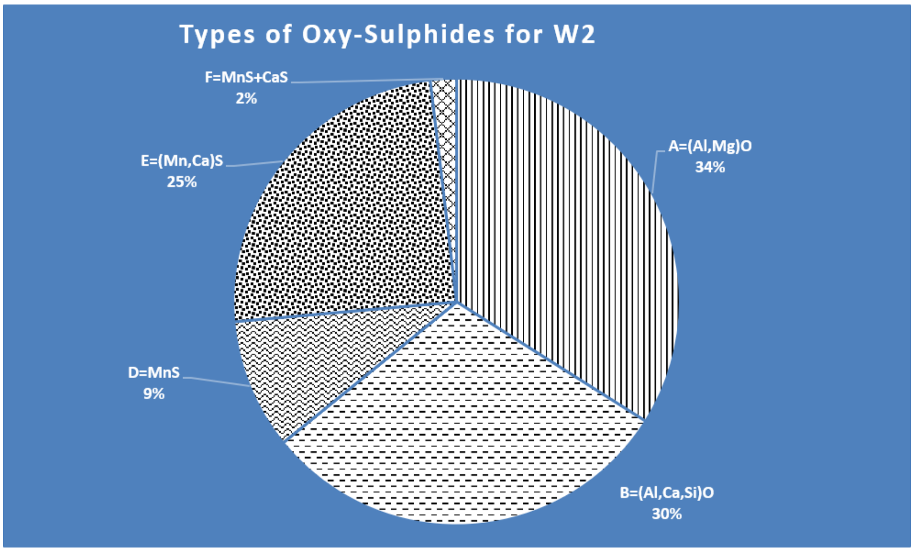

Figure F.5: Amount and type of oxy-sulphides in W2

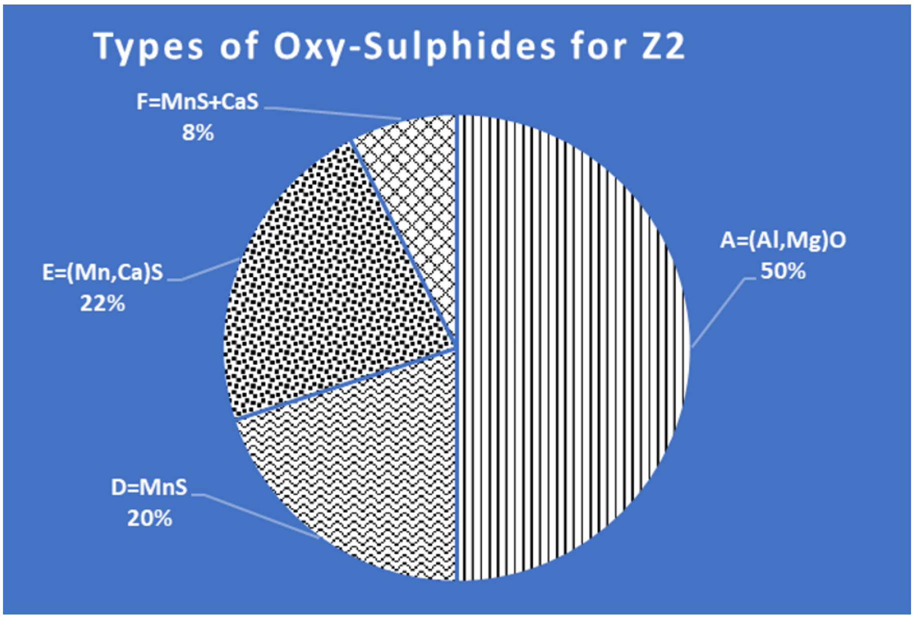

Figure F.6: Amount and type of oxy-sulphides in Z2

G

Morphology of inclusions from different batches

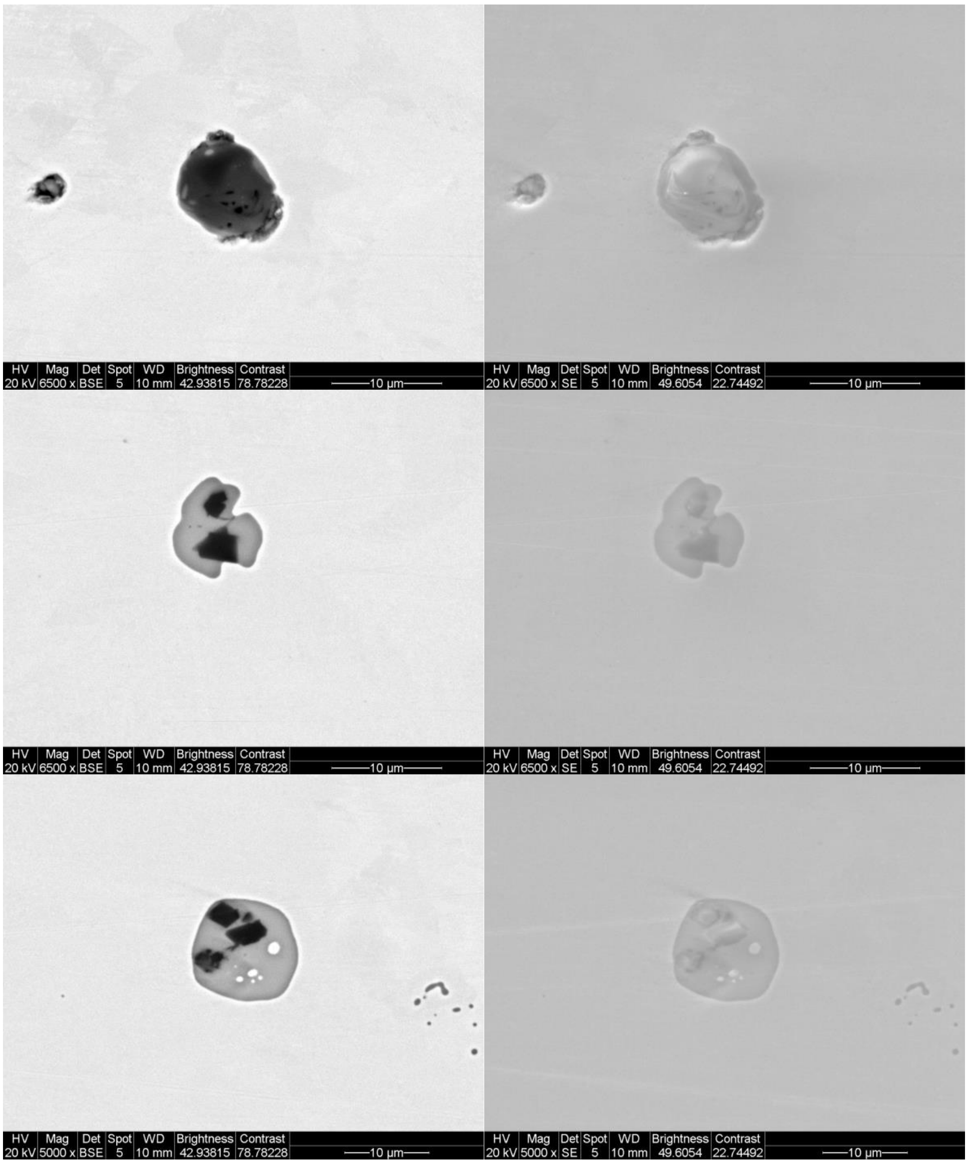

Figure G.1: BSE(left)/SE(right) micrographs of oxy-sulphide inclusions from G8

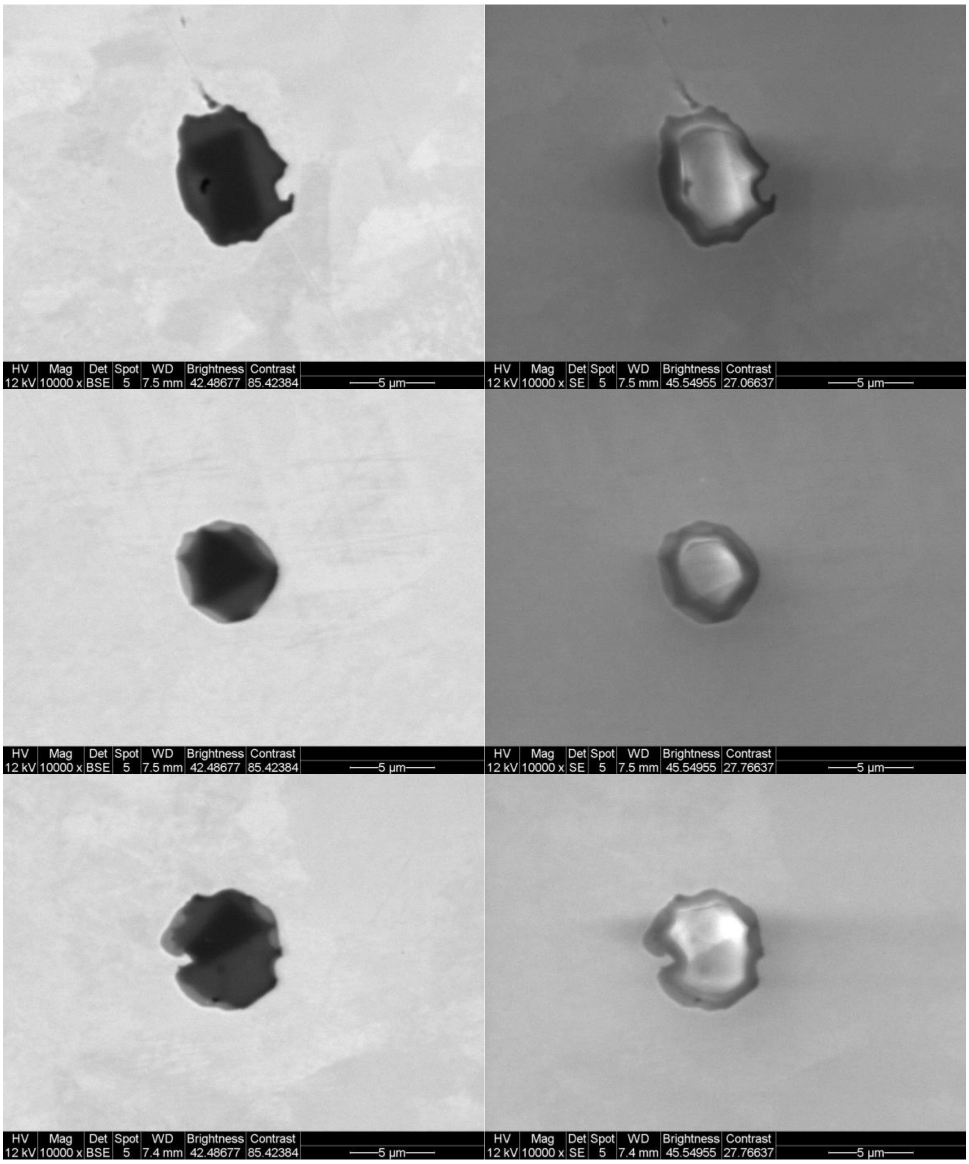

Figure G.2: BSE(left)/SE(right) micrographs of oxy-sulphide inclusions from P8

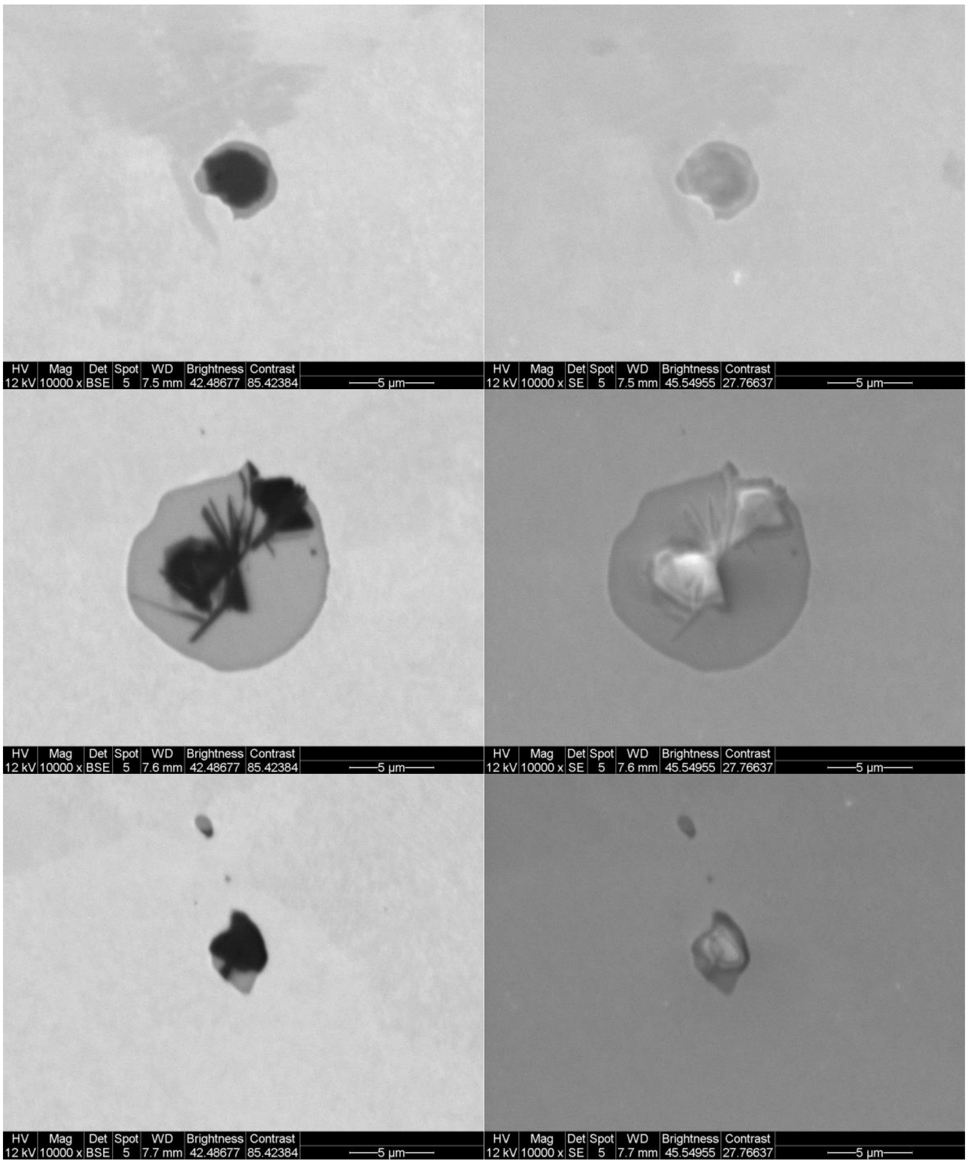

Figure G.3: BSE(left)/SE(right) micrographs of oxy-sulphide inclusions from S8

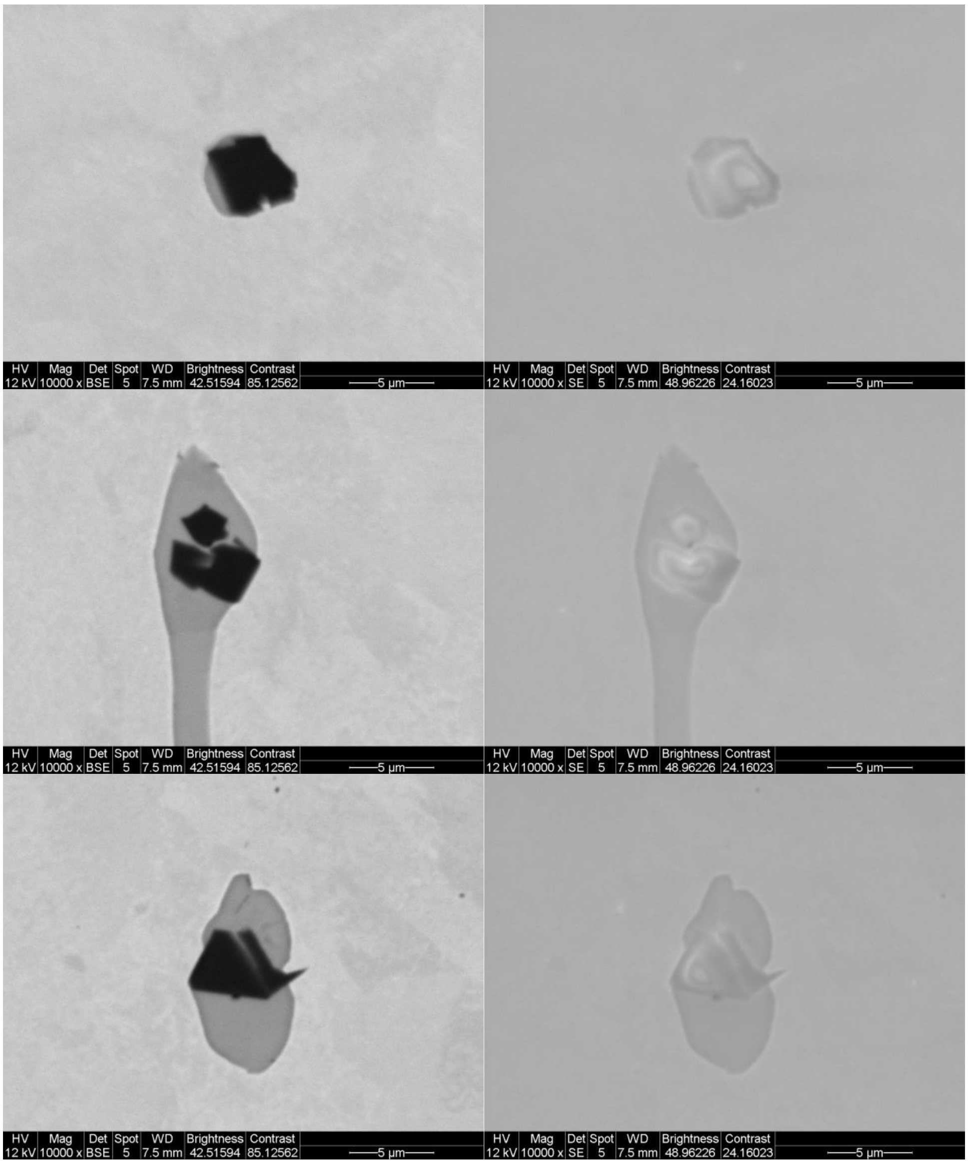

Figure G.4: BSE(left)/SE(right) micrographs of oxy-sulphide inclusions from W2

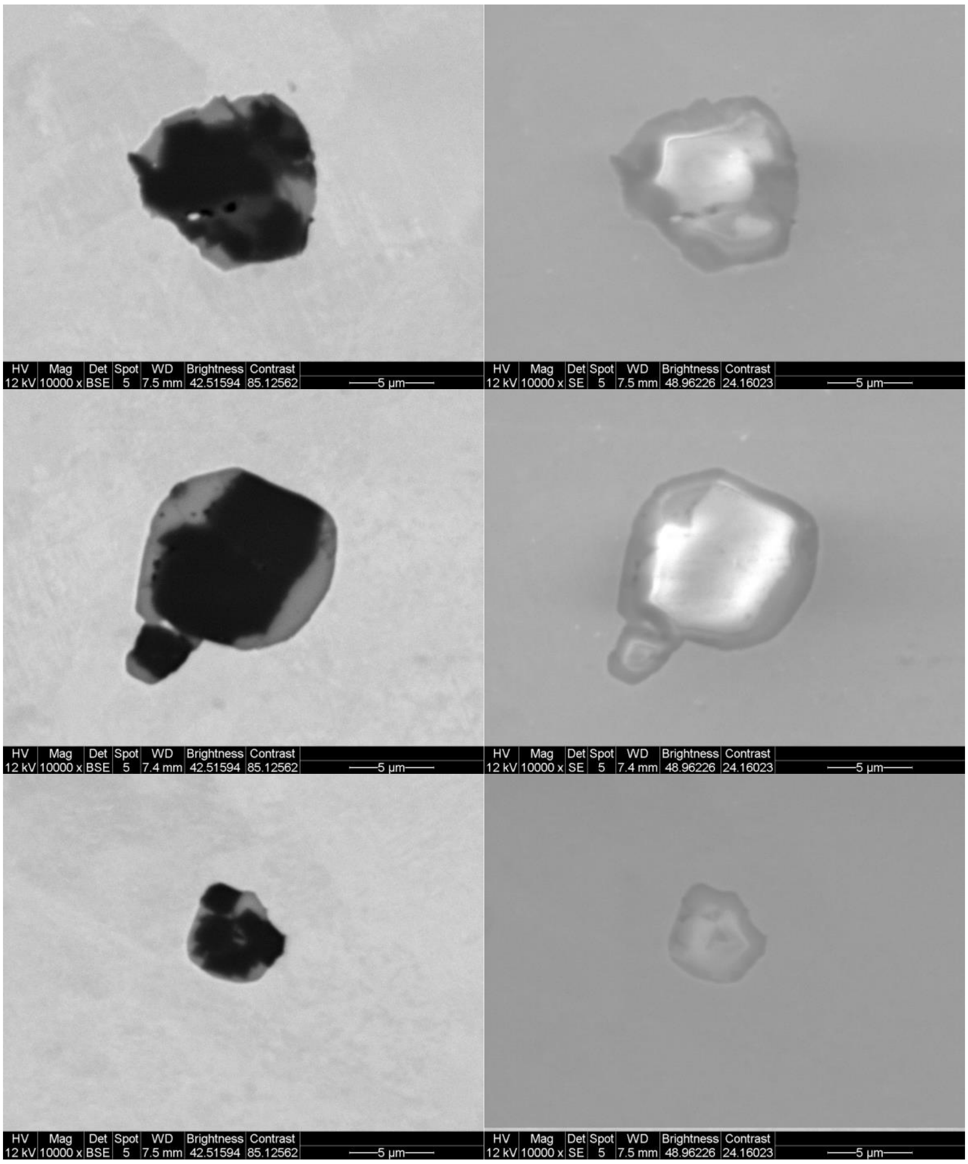

Figure G.5: BSE(left)/SE(right) micrographs of oxy-sulphide inclusions from Z2